Bacteria-Enabled Autonomous Drug Delivery Systems: Design, Modeling, and Characterization of Transport and Sensing

Mahama Aziz Traore

Dissertation submitted to the faculty of the Virginia Polytechnic Institute and State University in partial fulfillment of the requirements for the degree of

Doctor of Philosophy
In
Mechanical Engineering

Bahareh Behkam
Stanley A. Hefta
Donald J. Leo
Mark R. Paul
Birgit Scharf

May 06, 2014
Blacksburg, VA

Keywords: Tumor targeting bacteria, Cancer therapy, Microfluidics, Bio-hybrid microrobotics

Bacteria-Enabled Autonomous Drug Delivery Systems: Design, Modeling, and Characterization of Transport and Sensing

Mahama Aziz Traore

Abstract

The lack of efficacy of existing chemotherapeutic treatments of solid tumors is partially attributed to the limited diffusion distance of therapeutics and the low selectivity of anti-cancer drugs with respect to cancerous tissue, which also leads to high levels of systemic toxicity in patients. Thus, chemotherapy can be enhanced through improving anti-cancer drug carrier selectivity and transport properties. Several strains of gram positive (e.g. *Clostridium* and *Bifidobacterium*) and gram-negative (e.g. *Salmonella* Typhimurium and *Escherichia coli*) bacteria have been shown to possess the innate ability to preferentially colonize tumor tissues. The overall goal of this dissertation is to characterize the transport and sensing of Bacteria-Enabled Drug Delivery Systems (BEADS) in select relevant environments and to investigate the associated underlying principles. BEADS consist of an engineered abiotic load (i.e. drug-laden micro or nano-particles) and a living component (i.e. bacteria) for sensing and actuation purposes. Findings of this dissertation work are culminated in experimental demonstration of deeper penetration of the NanoBEADS within tumor tissue when compared to passively diffusing chemotherapeutic nanoparticles. Lastly, the transport mechanisms that *Salmonella* Typhimurium VNP20009 utilize to preferentially colonize solid tumors are also examined with the ultimate goal of engineering intelligent and more efficacious drug delivery vehicles for cancer therapy.

Acknowledgements

Foremost, I am very grateful to my advisor and mentor Dr. Bahareh Behkam for her constant and relentless support of my Ph.D. work, her patience, understanding and enthusiasm. Over the past five years, she has become more than an advisor to me; I have learned and grown both professionally and personally. I would also like to thank my committee members; Dr. Birgit Scharf deserves special recognition, her advices and support has contributed greatly to my work and experiences. Dr. Stan Hefta, Dr. Mark Paul and Dr. Donald Leo deserve many thanks for their insightful comments, support and encouragement along the way.

On a more personal note, I would like to thank my family for their unwavering support, encouragements and above all their unconditional love. I owe them everything; Mom and Dad have sacrificed so much for me and have always believed in me. I am also indebted to very special friends, who have helped me along the way, some of whom I consider more than friends; Preston Pinto, Dragan Avirovik, and Meghan Canter. I am grateful for their friendship and moral support throughout all these years in graduate school and away from home.

I also would like to thank all the members of the MicroN BASE laboratory, especially Ali Sahari, Brian Geuther, Chris Suh, Ahram Kim, Zhou Ye, Evan Smith, Eric Acome and Carmen Damico, all of whom I have spent a large amount of time with over the past five years. They have all been great colleagues, their friendship, their intellectual and technical support has been instrumental in creating an environment that has helped me excel.

This work has become possible with the help of a large number of people. I would like to specifically acknowledge Katherine Broadway (Ph.D.'19), Benjamin Webb (Ph.D.'15), Kevin Sheets (Ph.D.'14), and Puja Sharma (Ph.D.'15). I am also very thankful to Dr. Pitchumani and his students Karthik Nythianandam (Ph.D.'13) and Atul Verma (Ph. D. '15) for helpful

discussions and insights on certain complex COMSOL simulations I conducted. I also would like to thank Dr. Amrinder Nain and Dr. Shiv Kale for generously sharing their mammalian cell culturing facility as well as Dr. Daniela Cimini for generously donating the human colon carcinoma HT-29 cells used in this work. I am also grateful to Dr. Brooks Low from the therapeutic radiology department at Yale school of medicine.

I would like to also thank Mr. Donald Leber, manager of the Micro and Nano fabrication laboratory at Virginia Tech for being so helpful for all microfabrication need during my Ph.D. I would also like to recognize Mrs. Kathy Lowe for all the help, training and protocols she provided for carrying out the scanning electron microscopy of hydrogel specimens.

I am very grateful to Dr. Sally E. Johnson and Jennifer Bradley in the Department of Animal and Poultry Sciences for being accommodating and sharing their cryotome for tumor slicing experiments. I also would like to thank Dr. Kristi DeCourcy and Ms. Kate Schallhorn for all their help on standard and confocal microscopy and tissue imaging.

I am extremely grateful to the staff over at the Virginia Bioinformatics Institute for their dedication, friendship, support and great discussions (especially during coffee breaks). Special thanks go to Jason Rodriguez and all members of Dr. Biswarup Mukhopadhyay's lab, Linda Correll, Susan Stevens-Mauldon, David Gibbs, and Traci Roberts.

The entire Mechanical Engineering department has been terrific, especially Ben Poe and Jamie Archual for always being there to fix all IT related issues; they have been fantastic over the past five years. I am also grateful to Cathy Hill for answering every administrative-related question I came up with. Special thanks to Dr. Srinath Ekkad and Dr. Robert West for their support, advices and mentorship over the years.

Virginia Tech has been a wonderful place for me to complete my graduate studies. I have immensely profited from this rich and safe environment to conduct my Ph.D. research. I will always be a Hokie at heart. This work would not have been possible if it was not for the funding source provided by Mechanical Engineering Department and National Science Foundation (IIS-117519).

Table of contents

List of Figures

List of Tables

Chapter 1: Introduction

1.1 Motivation and problem statement

Malignant neoplasm (cancer) is a leading cause of death and is responsible for about 25% of all deaths in the United States [1]. This year alone in the U.S., 1,660,290 new cases of cancer are expected to be diagnosed and among those 580,350 deaths are expected [2]. There has been a concerted effort over the past 80 years, and more so recently, to provide answers to this devastating disease, as evident by the improvements in early cancer detection, treatment and reduced mortality rates [3], [4]. There is however more that needs to be achieved to both improve the early detection of cancer and the efficacy of existing treatment methods to minimize the side effects in patients.

Existing chemotherapeutic treatments of cancer are not fully effective partly because the anti-cancer drugs passively penetrate (diffuse through) the tumor tissue and in the process the drugs do not reach all tumor cells [5–7]. The low selectivity of anti-cancer drugs with respect to cancerous tissue is also problematic due to systemic exposure of healthy cells to anti-cancer drugs. Chemotherapy can be enhanced through both better anti-cancer drugs cargo targeting towards cancerous cells.

An ideal drug delivery vehicle for chemotherapeutic purposes should be able to evade the immune system and specifically targets its delivery site. A large number of pathogens have developed the ability to effectively do just that. This pathogenic faculty to evade the innate immune system and to selectively target a host cell has fueled an interest for the development of attenuated pathogenicity in certain bacterial strains for therapeutic usage [8],[9]. Some bacterial strains have been identified to possess the ability to target and preferentially colonize and grow

within tumor tissues [10–14]. A large body of work has already proven the high selectivity towards tumor regions as well as colonization within the tumors by some bacterial strains [15–17].

We hypothesize that tumor-targeting bacteria (*Salmonella enterica serovar* Typhimurium and *Escherichia coli*) can be coupled with engineered nano-systems (drug loaded and surface modified nano-particles) to serve as intelligent bio-hybrid bacteria-enabled autonomous drug delivery systems (BEADS). Here, we propose to exploit the innate motility (locomotion) and chemotaxis (sensing) attributes of bacteria to carry nanoparticles and/or nanoparticles loaded drugs to selectively target tumor sites (Figure 1. 1). This dissertation is centered on three main objectives:

1) Construction and characterization of BEADS:
    - Construction of Nanoscale Bacteria Enabled Autonomous Drug Delivery Systems (NanoBEADS)
    - Construction of Microscale Bacteria Enabled Autonomous Drug Delivery Systems (MicroBEADS)
2) Understanding the mechanism of chemotaxis (biased locomotion in response to select chemical gradient) behavior that BEADS utilize to sense and respond to their microenvironment:
    - Development and characterization of a microfluidic device for quantification of the BEADS behavior in well-defined chemical environments
    - Study of chemotactic behavior of free swimming bacteria
    - Computational modeling and experimental study of chemotactic behavior of BEADS.

3) Characterization of BEADS performance:

- Development of an in-vitro tumor model for the transport studies of bacteria and BEADS within the tumor.
- Investigation of the penetration and distribution of BEADS within tumor spheroids.
- Investigation of the penetration and distribution of *S.* Typhimurium VNP20009 and its relevant non-motile, non-chemotactic mutants within tumor spheroids.

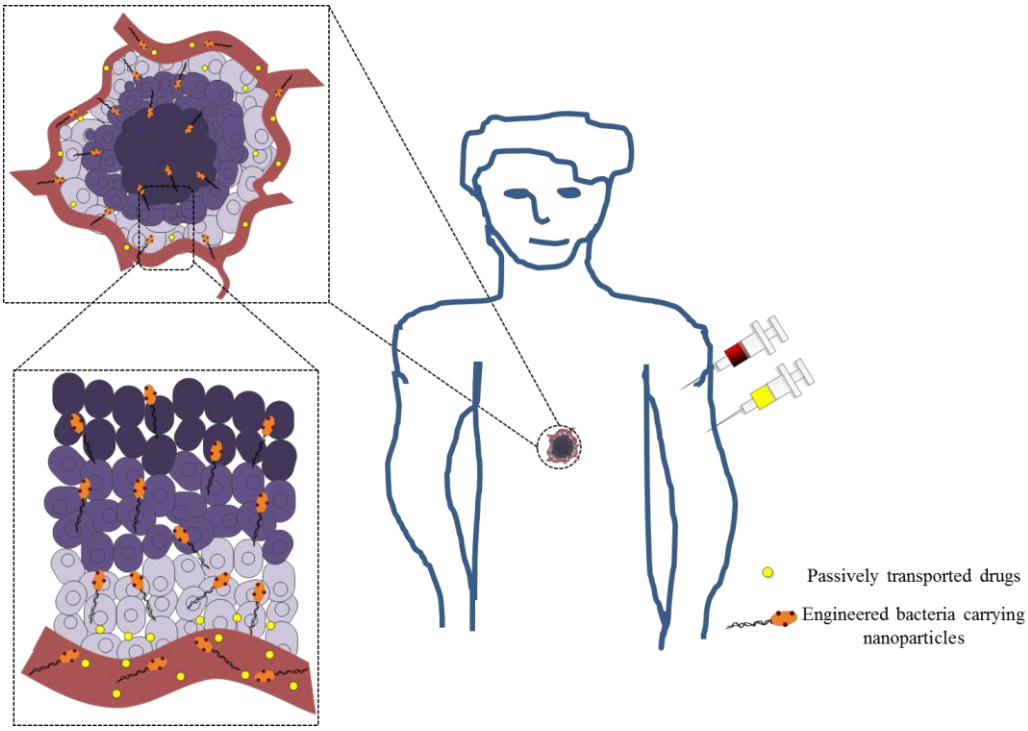

Figure 1. 1. After intravenous injection, the penetration of passively transported drugs is primarily limited to the proliferative region of the tumor. On the other hand, particles carried by engineered bacteria can penetrate deeper within the tumor and as a consequence are well distributed in the tumor.

1.2 Background

a. The cancerous tumor microenvironment and the challenges of chemotherapy

Cancer is a group of diseases that is characterized by the uncontrolled growth of abnormal cells within the body [2], [18]. There are over 100 known distinct types of cancer found in different organs that affect humans. The physiology of cancerous cells that eventually lead to the malignant growth of tumors has known characteristics: 1) Self-sufficiency in growth signals, 2) Insensitivity to growth-inhibitors, 3) Evasion of the apoptosis (programmed cell death), 4) Limitless replicative potential, 5) Sustained angiogenesis, 6) Tissue invasion and metastasis [19]. If left untreated, cancer can lead to death.

Most human cancerous tumors are solid in nature; they are made up of cells that are continually expanding due to uncontrolled growth and division. The effective delivery of drugs within the whole tumor can improve the therapy of most solid tumors. Most anticancer drugs are small molecules, and when administered to a patient, they follow a well-known process: 1) the drug is transported within the circulatory system, 2) the drug is transported across the vasculature walls into the surrounding tissue, and finally 3) the drug is carried through the interstitial space into the tumor [7].

As in any organs, tumor microregions are heterogeneous in nature. They are composed of tumor cells, stromal cells, fibroblasts and inflammatory cells. They present gradients of acidity and regions of hypoxia towards the center (see Figure 1. 1). The acidic property of the necrotic core of tumors originates from the fact that tumor cells perform glycolysis, which is the conversion of glucose into lactate to produce ATP for energy, survival and proliferation purposes. Tumor microregions are also supported by the tumor stroma (altered extracellular matrix (ECM) with

increased number of fibroblasts) [5], [20]. The tumor stroma contributes to an increase in interstitial pressure (adverse pressure), which in turn handicaps the penetration of drugs within the tumor [20], [21].

Cells residing in the hypoxic region may be viable [5]; the limited penetration of anticancer drugs can kill proximal cells to blood vessels. This process leaves cells in the hypoxic region with enough nutrients to regenerate therefore making it impossible to eliminate all cells in the tumor. This is a major issue with current chemotherapeutics because cells that are in the hypoxic region of the tumor can regenerate between treatments. Cells in necrotic regions of tumors are generally nutrient deprived, mainly they lack compounds such as glucose and amino acids.

Also, the adverse pressure within the tumor may prevent the passive penetration (through diffusion) of drugs. Some drugs have been shown to have limited transport properties in tumors [5].

For an anticancer drug to be effective, it must reach all cells within the tumor to prevent clonogenic tumor stem cells from regeneration. There are many factors that play a major role in carrying drugs into the tumor [20]. There are among others: the physicochemical properties of the drugs (molecular weight, size, chemical composition and conformation, diffusivity, etc.), the microenvironment of the tumor (the interstitial fluid pressure (IFP), the cell density of the tumor, cell-cell contact and the ECM,

Figure 1. 2).

Tumors with a diameter of 2 mm or less are usually perfused by the vasculature present in surrounding tissues through diffusion [22]. Larger tumors start to create their own blood supplies through angiogenesis. The microvessels that originate from angiogenesis are leaky and have pore sizes varying from 100 nm to 780 nm. In contrary, the junction between endothelial cells of the

lining of blood vessels is very tight in normal tissue with a spacing of less than 2 nm [7]. Also, compared to normal tissue, tumors show higher amounts of growth factors such as VEGF (vascular endothelial growth factor also known as the vascular permeability factor).

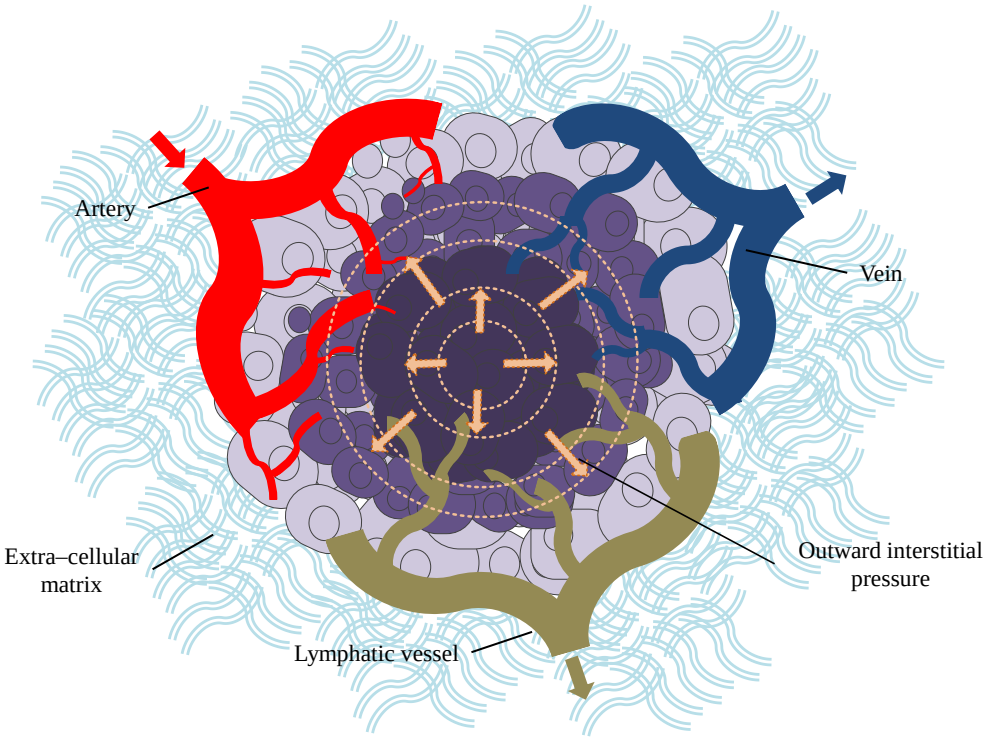

Figure 1. 2. Microenvironment of the tumor. Outward pointing arrows signify the elevated interstitial fluid pressure.

The blood flow rate in the vascular space near a tumor site is on average lower than the blood flow in normal tissue. This is due to the higher flow resistance in tumor blood vessels from the increased blood viscosity, which emanates from the presence of tumors cells, large molecules and proteins [7].

Another important factor to take into consideration in understanding tumors is the lymphatic system. In the human body, lymphatic vessels are distributed throughout and their main role is to

push the interstitial fluid back into the blood vessels. Lymphatic vessels are highly permeable, thus in normal and inflammatory tissues, larger particles and macromolecules are cleared from the tissues through the lymphatic vessels (Figure 1. 3).

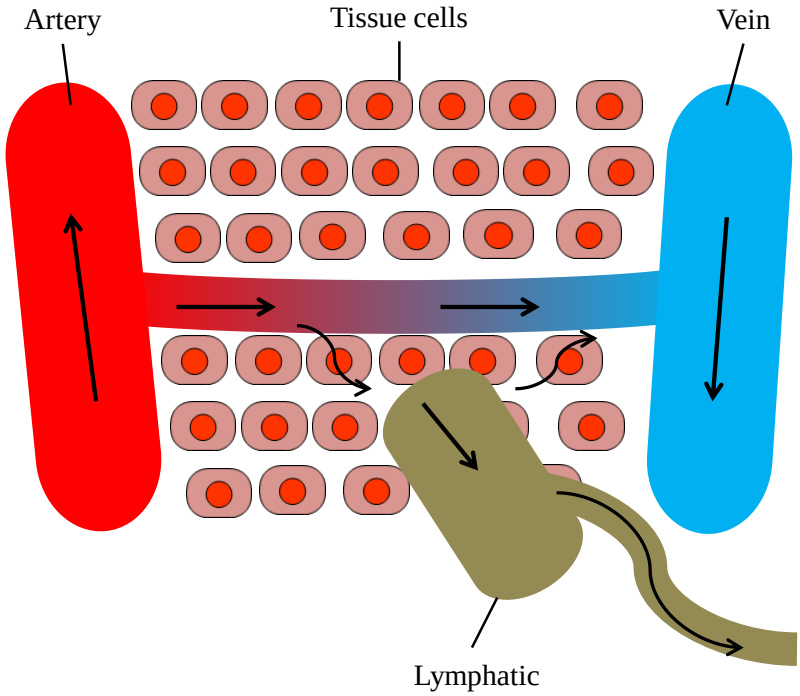

Figure 1. 3. Vascular transport at the tissue level. In normal tissue, the lymphatic system works to clear macromolecules and other large particles. In tumor tissues, the lymphatic system is often dysfunctional.

Drug molecules are transported across the vasculature walls through fluid movement caused by the pressure gradient between the blood vessels and the interstitial space. This pressure difference namely the microvascular pressure (MVP) is a crucial component of drug transport into tumor sites. Drug transport occurs across the tumor microvascular wall due to diffusion and convection through the pores of the endothelial layer. Once a drug molecule exits the vasculature, it must travel about 100 μm or more to reach all viable cells, because the maximum distance between two near blood vessels is about 200 μm in the human body. The relatively high

interstitial pressure found in most tumors is responsible for the absence of penetration and distribution of drugs within tumors [20]. The poor blood supply to tumors can also favor the lack of penetration and distribution of drugs within tumors.

Macromolecules and other components present in blood vessels are drained into the lymphatic system or venous end of the vascular system through the interstitium. The lack of a functional lymphatic system observed in tumors contributes highly to the increase of the interstitial fluid pressure [7]. This is a major deterrent to the extravasation of macromolecules and particles into the tumor interstitial space. Smaller molecules transport within the interstitial space is dependent on diffusion whereas larger molecules depend on advection. The pure diffusion of larger macromolecules or nanoparticles into tumors is compromised due to lower diffusion coefficients for larger molecules or particles.

The higher IFP (up to 60 mmHg) contributes to an outward convective flow, away from the center of the tumor, which prevents the penetration of smaller molecules and to that effect larger molecules as well [21], [23–26]. This can be explained by understanding the balance of pressures in the transcapillary transport in tissues (Figure 1. 4). In normal tissues, where the lymphatic system is functional, there is an overall outward filtration pressure from the blood vessels. However, in tumor tissue where the lymphatic vessels are abnormal, there are inconsistencies in the balance of pressure across the blood vessels.

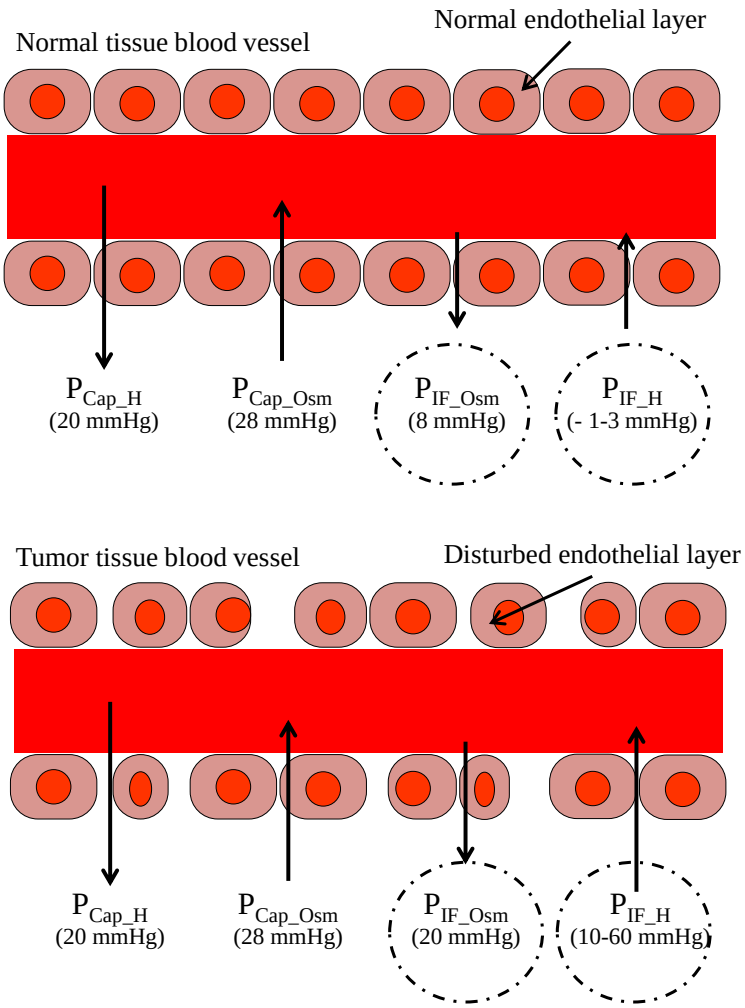

Figure 1. 4. Diagram showing the balance of pressures that occur in transcapillary transport in tissue. In tumor tissue the pressure that originates from the interstitium changes dramatically. Also, it can be noted that the endothelial cell layer is disorganized.

b. Current state of the field on cancer targeting and drug delivery

Cancer can be targeted using a variety of treatments such as chemotherapy, radiotherapy, surgery, immunotherapy, gene therapy, and hormone therapy. There is a tremendous need for more targeted drug therapies and delivery against cancer. Targeted therapies using drugs are also considered as chemotherapy but have the ability to take on cancerous cells while having less damage to healthy/normal cells in the body. They are used towards the prevention of the spread of cancer cells and growth of solid tumors.

A number of targeted therapies [4], [27] have been developed to disrupt the process through which cancer cells rapidly reproduce in the body and initiate tumors. Most of the targeted therapies can be grouped based on their working principles:

1) Enzyme inhibitors: enzymes are catalyst usually composed of proteins [28] that help control what cells in our body do on a daily basis. Certain targeted drug therapies work by interacting with enzymes that are signals for cancerous cells to grow, effectively preventing the enzyme from working properly. Some known enzymes inhibitors are tyrosine kinase inhibitors, growth factor-inhibitors, and signal transduction inhibitors.
2) Apoptosis-inducing drugs: these types of targeted therapies work by affecting proteins within cancer cells and cause them to die.
3) Angiogenesis inhibitors: these drugs help block the VEGFs. Angiogenesis is the process through which solid tumors recruit new blood vessels from preexisting vessels. It is the result of a number of interactions between different molecules (regulators, mediators and stimulants). Examples of prominent angiogenesis proteins are VEGF and platelet derived growth factor (PDGF).

4) Monoclonal antibodies: Targeting cancerous sites can be made possible through tumor-specific targeting mechanisms. These types of targeting methods use tumor-activated drugs that are inactive until they reach the cancer sites. Examples of these types of targeting mechanisms are monoclonal antibodies. Antibodies are large molecules that bind with high affinity to a specific protein called antigen. Once attached to their target, they can destroy the cells containing the antigen.

These targeted therapies can become very successful and efficient through better delivery methods. A number of targeted delivery routes have been explored to improve the selectivity of anti-cancer agents. Anti-cancer agents can target cancerous sites by avoiding the reticuloendothelial system (RES). In general, hydrophobic nanoparticles and other drugs carriers are cleared to the liver, spleen and other organs of the RES. For instance, hydrophilic poly (vinyl pyrrolidone) particles with average diameter of 35 nm have a 1% uptake by the liver and spleen, and are still present in the circulation 8 hours after injection. Better targeting can be achieved using particles that have longer circulation time; particle carriers with average diameter below 100 nm with hydrophilic surfaces can be used for that purpose.

Improvement in cancer targeting can also be realized by exploiting the enhanced permeability and retention (EPR) effect, which is a byproduct of the disorganized vasculature found in solid vascularized tumors. It has previously been shown that nanoparticles accumulate in cancerous tissues because of the EPR effect [3], [29–31].

c. Bacteria targeting and preferential growth within tumors

For about two centuries live infectious bacteria have been identified to naturally target and replicate within tumors [11], [32], [33]. Researchers started to think about the use of bacteria as a cancer therapeutic agent back in the nineteenth century. In the early 1800’s, a French researcher

named Vaultier, had already hypothesized a link between bacterial infection and cancer regression in patients [13]. In the late 1860's, a first case of tumor regression was reported when a patient who had an inoperable neck tumor had a bacterial infection. In the United States, William Coley, a surgical oncologist, used to purposefully induce bacterial infection in patient with the goal of reducing the tumor size. This prompted researchers to identify several bacterial species that have tumor-targeting abilities as well as therapeutic effects in mouse models: obligate anaerobes (*Clostridia* and *Bifidobacteria*) and facultative anaerobes (*Salmonella* Typhimurium, *Escherichia coli* and *Listeria monocytogenes*). Successful cancer treatment using facultative anaerobic bacteria has been so far limited to animal models. The human trials that have taken place thus far were inconclusive as none of the patients experienced objective tumor regression even for patients with tumors that were colonized by bacteria [9], [34]. There is however hope in using bacterial strains for targeting and possibly helping in curing cancer. For example, the Bacille-Calmette Guerin (BCG), which is used as vaccine against tuberculosis, is commonly used in clinical settings to decrease the recurrence of tumors by about 70% [35].

In summary, bacteria are an attractive option in the fight against cancer because they have the capability to evade the innate immune system and target cancerous cells [8], [13], [36]. They can access regions of tumors that are inaccessible through passive means (drug diffusion). A considerable body of work has shown that bacteria can target a tumor, penetrate and colonize it [10–12], [14], [32], [33], [37]. Genetic engineering and synthetic biology has provided scientists the necessary tools to engineer bacteria; facultative anaerobe *Salmonella enterica serovar* Typhimurium was engineered to attenuate its toxicity when introduced in the human body [17]. To that end, clinical experiments have demonstrated that intravenous introduction of a bacterial suspension of a maximum of 3×10^8 colony forming units per meter squared (CFU/m^2) was safe

and would not cause a septic shock [9] in patients. It is however important to note that bacteria alone have not been shown to be efficacious in full treatment of tumors. In this work, we hypothesize that the coupling of tumor-targeting bacteria and engineered spherical nano/micro-particles (model drug particles) will enhance the efficacy of bacteria-based therapies

1.4 Organization of the Thesis

The overarching goal of this thesis is to develop a bacteria-based live autonomous drug delivery system and to characterize its extravascular transport within an in-vitro multicellular tumor spheroid model. Our focus is on demonstrating that bacteria can carry micro and nanoscale loads in a controlled manner and deliver them deep within the tumor despite the fluid pressure exerted constantly outward. In this system, bacteria are viewed as microrobotic systems capable of sensing, controlled actuation, and communication among themselves and with their immediate environment. To better understand the sensing mechanism bacteria use to naturally move towards a target (i.e. chemotaxis), we have conducted chemotaxis assays under well-defined chemical attractant gradients using a hydrogel-based microfluidic device. The characterization of the transport of particles in aqueous environments was achieved through the development of a computational model for the propulsion of bacteria and bacteria propelled particles in a fluidic milieu. Using our understanding of chemotaxis of bacteria and bacteria-propelled particles, we study the extravascular transport of NanoBEADS (Nanoparticles Bacteria-Enabled Autonomous Delivery Systems) within an in-vitro tumor. The remaining part of this document is organized as follows:

Chapter 2: In this chapter, two types of microfluidic platforms, flow-based and diffusion-based, were introduced and discussed. We designed, fabricated and characterized both type of devices. The bulk of the chapter is dedicated to a microfluidic device for quantitative study of bacterial response (e.g. chemotaxis) in well-defined and controllable chemical environment was designed and developed. The advantages of the diffusion-based device are

demonstrated and discussed. This chapter illustrates how microfluidic tools can be designed and implemented towards generating the types of conditions needed to conduct extensive quantitative studies that further elucidate the behavior of bacteria. At the end of this chapter, the versatility of the diffusion-based device for study of other prokaryotic and eukaryotic cells is discussed. In the appendix of this chapter, the flow-based device design, characterization and fabrication is briefly discussed.

Chapter 3: In this chapter, using the diffusion-based device developed in chapter 2, the behavior of *Escherichia coli* under known chemical gradients was studied. We were able to determine the smallest chemical attractant gradients that prompted a chemotactic response from the bacteria. We were also able to determine experimentally the most favorable chemical attractant gradient bacteria migrated towards. In this study, we attempted to decouple the effects of absolute chemical concentration and chemical concentration gradient on bacterial response. We were able to show that bacteria can exhibit a negative chemotactic response even in the presence of a favorable chemical gradient when the limit absolute chemical concentrations are high.

Chapter 4: In this chapter, the synthesis of MicroBEADS (i.e. bacteria coupled with microparticles) is briefly discussed. Subsequently, we developed a computational model that will capture and describe the trajectory of a single bacterium in a fluidic milieu. The knowledge gained from this computational model can be directly applied to the modeling of the chemotactic behavior of a single bacterium carrying nanoparticles (NanoBEADS) towards an in-vitro tumor spheroid.

Chapter 5: In this chapter, biorobotic systems consisting of spherical polystyrene nanoparticles attached to the body of bacteria are developed. The construction and dynamics of these nanoparticle bacteria enabled autonomous delivery systems (NanoBEADS) are studied in isotropic fluidic environments. We show that the 3D motion of NanoBEADS is dependent upon the nanoparticle size, number of nanoparticles attached and their attachment sites. These bio-based micromachines can be utilized as single agent or as a swarm in order to carry out specific tasks that have a wide range of applications.

An autonomous microfluidic sorting platform is also described in the appendix section of this chapter. Using the platform discussed, we can autonomously separate motile NanoBEADS constructs from non-motile ones.

Chapter 6: In this chapter, we first briefly demonstrate that multi-cellular tumor spheroids (in-vitro tumor model) are valid representations of in-vivo tumor due to the similarities in their microenvironment. We have generated in-vitro multicellular tumor spheroids using human colon carcinoma cells and mammary breast cancer cells. The transport of bacterial mutants known to preferentially colonize tumors is also discussed. NanoBEADS transport and distribution in the interstitial space of the tumor spheroid is also presented.

Chapter 7: The original contributions of this Ph.D. dissertation as well as concluding remarks are offered in this chapter. Some of the most complex problems in the bioengineering require a multidisciplinary approach towards applicable solutions. The research experience acquired in engineering (microfluidics, mathematical modeling, etc.) and biology during this

Ph.D. work can be used towards further explorations of contemporary challenges in bioengineering. Future directions pertaining to this goal are also addressed in this final chapter

Chapter 2: A PEG-DA microfluidic device for cell chemotaxis studies

Abstract

The study of cells in a well-defined and chemically programmable microenvironment is essential for a complete and fundamental understanding of the cell behaviors with respect to specific chemical compounds. Flow-free microfluidic devices that generate quasi-steady chemical gradients (spatially varying but temporally constant) have been demonstrated as effective chemotaxis assay platforms due to dissociating the effect of chemical cues from mechanical shear forces caused by fluid flow. Here, we demonstrate the fabrication and characterization of a flow-free microfluidic platform made of polyethylene glycol diacrylate (PEG-DA) hydrogel. We have demonstrated that the mass transport properties of these devices can be customized by fabricating them from PEG-DA gels of four distinct molecular weights. In contrast to microfluidic devices developed using soft lithography; this class of devices can be realized using a more cost-effective approach of direct photopolymerization with fewer microfabrication steps. This microfluidic platform was tested by conducting a quantitative study of the chemotactic behavior of *Escherichia coli* (*E. coli*) RP437, a model microorganism, in presence of the chemo-effector, casamino-acids. Using the microfabrication and characterization methodology presented in this work, microfluidic platforms with well-defined and customizable diffusive properties can be developed to accommodate the study of a wide range of cell types.

2.1 Introduction

Chemotaxis or directed motility of cells towards the source of chemical attractants is an essential attribute of both eukaryotic and prokaryotic cells. Understanding all the contours of chemotaxis in general and bacterial chemotaxis specifically can shed more light on a number of important biological processes and practical applications. As such, numerous assays and devices have been introduced throughout the years which aim to understand both qualitatively and quantitatively how given bacteria strains perform chemotaxis in the presence of a chemo-effector.

The Pfeffer assay [38] also known as the capillary assay which was enhanced by Adler [39] can be used to quantify the chemotactic behavior of bacteria in response to a chemo-effector. In such assays, a capillary filled with a chemo-effector is immersed in an enclosure containing the bacteria suspension. The chemo-effector diffuses in the enclosure and the bacteria respond by collecting in and around the mouth of the capillary. The chemotactic behavior of the bacteria is quantified by counting the number of bacteria cells inside the capillary. The strength of the Pfeffer assay resides in its ease of implementation and quick qualitative demonstration of chemotaxis of a bacterial strain towards a chemo-attractant. A major drawback for quantification of chemotactic response originates from the fact that this assay works primarily with chemo-attractants. In the case of a chemo-repellent inside the capillary, it is impossible to quantify the chemotactic behavior of the bacteria.

Swim plate assay has also been used to study the chemotactic behavior of bacteria [40]. In this method, a semi-solid agar plate containing a metabolizable chemo-attractant is inoculated with bacteria. Over time, the bacteria grow and migrate outwards forming a ring. The diameter change

of the ring is used to determine the strength of the bacteria chemotactic response towards a chemo-attractant. This method enables rapid evaluation of both attractants and repellents; however, it is limited to metabolizable chemo-attractants only and also cannot be used to quantify the chemotactic behavior of the bacteria in the presence of a chemo- repellent.

A number of other useful assays have also been developed to study the chemotactic behavior of bacteria. These assays include the tethered cells assay [41], the stopped-flow diffusion chambers (SFDC) [42], the temporal gradient assay, and the automated tracking of single cells [43].

The previously described methods do not allow for accurately quantifiable and spatially or temporally controllable chemical gradients within which the chemotactic behavior of bacteria can be studied. With the advent of microfluidic devices, a much-improved level of control of chemical cues for the study of cells has been accomplished. Microfluidic devices have been extensively used for the study of both prokaryotic and eukaryotic cells under well-defined chemical and mechanical conditions. Most microfluidic devices developed for the study of cells and bacteria can be broadly divide into two categories of flow-based microfluidic devices and flow-free microfluidic devices. An extensive review of both kinds of microfluidic devices has been recently presented [44].

In a flow-based microfluidic device, the generation of a linear chemical gradient relies on the laminar flow and slow mixing of two chemical sources downstream [45–47]. This method has many advantages such as relative ease in the fabrication and assembly of the device. One major drawback however is the presence of fluid flow in the main channel where the cells are studied. The flow-induced shear forces may alter cell behavior or the flow itself may interfere with the studied phenomena (such as cell motility) and affect experiment outcome. Also, the presence of

fluid flow within the channel of interest will generate spatial variations in the linear gradient profiles along the length of the channel.

Another type of devices used for the study of bacterial cells operates according to the principle of diffusion and does not generate any fluid flow in the main channel. In many cases, the establishment of steady-state (temporally invariant) spatially varying chemical gradients within which cells can be studied over extended periods of time and in the absence of any fluid flow is highly important. In a flow-free microfluidic device, the chemical gradient establishment relies solely on the diffusion of chemicals from two outer channels through the walls of the device to a center channel [48–51]. This type of devices present the advantage of elimination of the flow-related undesired effects in the channel of interest [52], [53].

In this chapter, we introduce a polyethylene glycol diacrylate (PEG-DA) hydrogel microfluidic device for the establishment of customizable spatially varying chemical gradients, based on the flow-free microfluidic assay devices, as shown in Figure 2. 1. This platform, which works based on the principle of diffusion, allows for the establishment of controllable chemical concentration gradients for different chemo-effectors in the center channel for the study of cells. The unique advantages of the photopolymerizable hydrogel based devices introduced in this work include ease of fabrication and assembly of the device and generation of controllable and distinct chemical concentration gradients for different molecular weight hydrogels.

The fabrication of existing flow-free devices [48], [49], [51] involves the conventional soft lithography method of template microfabrication followed by pouring, curing, and peeling of select thermosets to form a polymeric device. The requisite template microfabrication increases the cost of the device and the molding steps may limit the feature sizes that can be achieved

given the fragility of polymers (*i.e.* hydrogels) used in flow-free devices. Fabrication of the PEG-DA microfluidic platform introduced in this work does not require a microfabricated template and is based on one essential step transfer of a mask design pattern to the PEG-DA hydrogel. The relatively facile fabrication process is based on a one-step UV photopolymerization of the hydrogel and excludes additional processes such as template fabrication followed by hydrogel molding and peeling used in fabrication of microfluidic devices based on soft lithography. As demonstrated in this work, the wide range of molecular weights of the PEG-DA polymer used here enables us to achieve different diffusive properties with respect to the specific chemical compound-cell type to be studied.

We have fabricated and characterized a PEG-DA hydrogel-based microfluidic device for the study of cells. The PEG-DA platform was tested by studying the chemotactic behavior of *Escherichia coli* (*E. coli*) RP437 in presence of the chemo-effector casamino acids. The goal of this case study is to demonstrate that the microfluidic platform developed can be used for biological experiments to study the behavior of prokaryotic and eukaryotic cells under well-defined and customizable chemical environments.

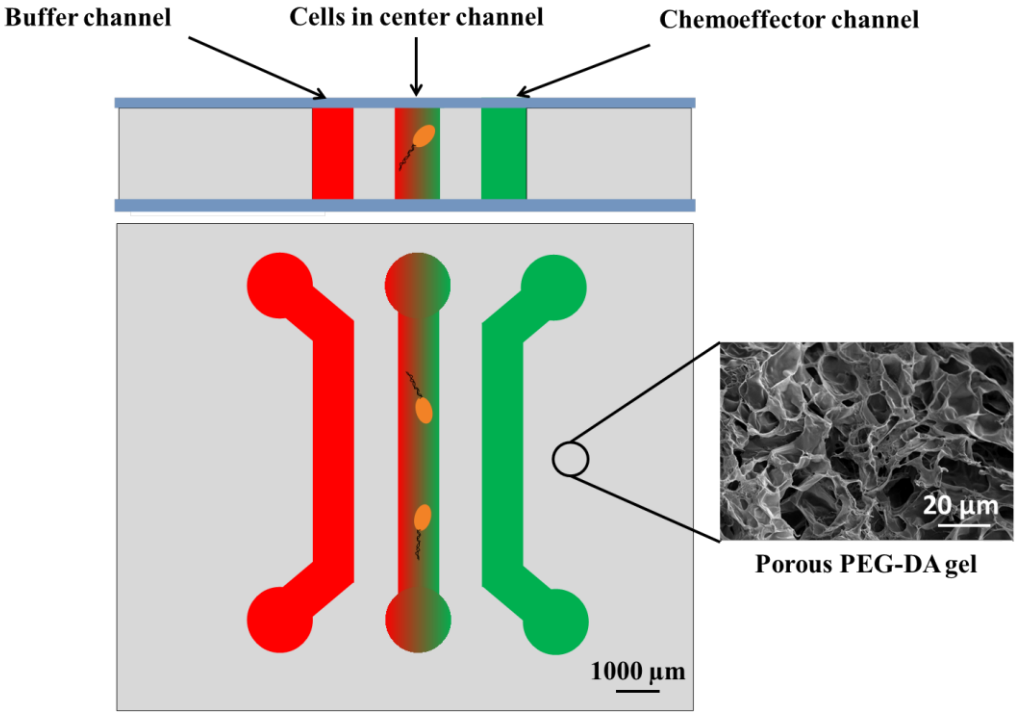

Figure 2. 1. Schematic shows the cross-sectional view and the top view of a flow-free microfluidic device. The inset depicts a scanning electron microscopy (SEM) image of the porous polyethylene glycol diacrylate (PEG-DA) gel that the device is made of. [124]

2.2 Materials and methods

a. Bulk PEG-DA gel polymerization and mass transport characterization

PEG-DA of molecular weights 700, 2000, 6000, and 10000 Da were purchased from Sigma-Aldrich (St. Louis, MO) and mixed in phosphate buffered saline (1× PBS (phosphate buffered saline: 150 mM NaCl, 2 mM $Na_2HPO_4.7H_2O$, 1.9 mM KH_2PO_4; 1L H_2O, pH adjusted to 7.4) at 10% (w/v) concentration to form the precursor solution. The photoinitiator solution was prepared by mixing Irgacure® 2959 (Sigma-Aldrich) in 70% ethanol at 10% (w/v). The hydrogel solution was obtained by adding 50 µL of the photoinitiator solution to 1 mL of the precursor solution. The hydrogel solution was photopolymerized using UV light (365 nm, 0.78 mJ/cm^2, and exposure time: 5 minutes). The gels are then soaked in PBS overnight to remove any excess photoinitiator.

A Franz diffusion cell, shown in Figure 2. 2, was used to quantify the mass transport through the hydrogels. The Franz diffusion cell is composed of two compartments separated by a PEG-DA gel membrane of known thickness. One of the compartments is filled with the chemo-effector of interest (i.e. 10% (w/v) casamino acids in PBS) and the other is filled with the buffer solution (i.e. PBS). The chemo-effector solution in the donor chamber diffuses through the separating PEG-DA membrane over time. At given time intervals, a sample volume is withdrawn from the acceptor chamber and used as an indicator of the casamino acids amount that has diffused through the separating membrane. In order to quantify this amount, sample volumes withdrawn at known time intervals are analyzed using a UV spectrophotometer (DU-800, Beckman-Coulter, Brea CA) at the wavelength of 238 nm. Each compartment contains a small magnetic stir bar used to ensure that the solutions are well mixed throughout the measurement.

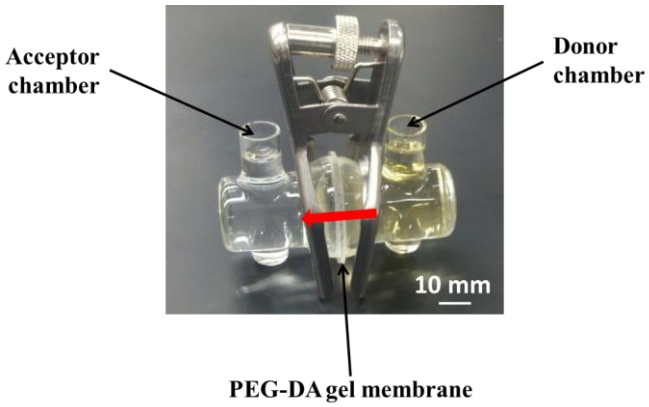

Figure 2. 2. The Franz diffusion cell used to characterize diffusion coefficients through PEG-DA gel membranes as a function of the diffusing chemical and the gel molecular weight. The red arrow indicates that diffusion occurs from the donor chamber to the acceptor chamber. [124]

b. Scanning electron microscopy (SEM) of the PEG-DA gels

The internal structure of the fabricated PEG-DA gel membranes was visualized using a SEM (EVO 40, Carl Zeiss Inc., Oberkochen, Germany) [54]. The gels were first allowed to swell in deionized (DI) water and reach equilibrium. They were then flash frozen in liquid nitrogen and immediately fractured. The fractured samples were then dried using a freeze-dryer, sputter-coated with gold for 30 s (SPI Module Sputter Coater System, SPI, West Chester, PA) and then imaged.

c. Fabrication of the microfluidic device

A one-step photolithography process was used to fabricate the microfluidic device. A rectangular PDMS enclosure of thickness of ~220 μm is first bonded to a glass slide using oxygen plasma (PDC-32G, Harrick Plasma, Ithaca, NY) for 30 s at 18 W. To ensure good sealing between the PEG-DA device and the underlying glass substrate, the glass surface was functionalized using a

TPM (3-(Trichlorosilyl) propyl methacrylate) solution (Sigma-Aldrich, St. Louis, MO). The glass surface was first rendered hydrophilic using oxygen plasma (200 mTorr, 18 W, 5 minutes). This step is important as it removes all inorganic compounds and promotes hydroxylation of the surface. A 1% (v/v) TPM solution dissolved in paraffin oil (Sigma-Aldrich) was prepared. The silane solution was poured in the enclosure and incubated at room temperature for 10 minutes [55], [56]. After incubation, the enclosure was thoroughly rinsed with ethanol and hard baked at 95 °C. Subsequently, the liquid PEG-DA was poured within the enclosure until it was completely filled. A glass mask was placed on the PDMS enclosure containing the liquid hydrogel. The photopolymerization was carried out by UV light exposure (365 nm, 18W/cm^2, Omnicure S1000, Vanier, Quebec) for a duration of 15 seconds. The areas of the PEG-DA solution exposed to the UV light cure due to the photopolymerization process. The non-polymerized regions are removed by rinsing the device.

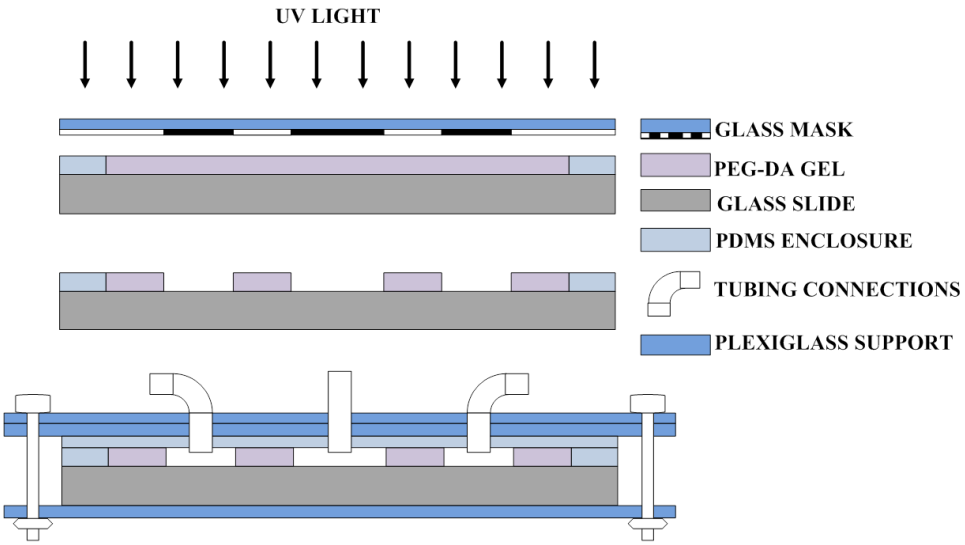

Figure 2. 3. Process flow for the fabrication and assembly of the PEG-DA microfluidic platform. [124].

Figure 2. 3 shows the process flow for the fabrication and assembly of the device. A PDMS layer is placed directly over the PEG-DA device layer to provide enough lateral support for the connectors to deliver the fluid inside the channels without leaking. Two plexiglass support layers are used to provide the necessary pressure required for the assembly of the device.

2.3 Results and discussions

a. Diffusion coefficient characteristics of the PEG-DA gels

The chemical diffusion of casamino acids, the chemo-attractant used in this study, through PEG-DA gels as a function of gels' concentration and molecular weight was determined using a Franz diffusion cell as described in section 2.1. The knowledge of the diffusion characteristics of the chemo-effector through the PEG-DA gel will enable the establishment of customizable chemical gradients in the center channel of the device and provides critical insights about the dimensions and the time needed to establish the gradient. At known time intervals, samples were withdrawn from the acceptor compartment. The absorbance values for the withdrawn samples were then measured using a UV spectrophotometer at 238 nm wavelength. The absorbance in this specific study is a measure of the amount of chemical that has diffused through the gel over time; it is directly related to the amount of chemo-attractant in the measured sample. The permeated amounts of chemo-attractant are plotted over time and the diffusion coefficient of the chemo-attractant through the gel is determined from this plot in conjunction with (2.1) [57]. Knowing the lag time t_L, at which the linear regime of the permeation curve intersect the x-axis as well as h the thickness of the gel membrane used, the diffusion coefficient is calculated from:

$$D = \frac{h^2}{6t_L} \tag{2.1}$$

Using this method, the diffusion coefficients of the PEG-DA gels used in this study were measured. The result is presented in Table 2. 1.

Table 2. 1. Casamino acids diffusion coefficients for all the PEG-DA gels used in this study.

PEG-DA (Da)	Diffusion coefficients (10^{-6} cm^2/s)
700	1.50 ± 0.50
2000	2.66 ± 0.53
6000	3.61 ± 0.90
10000	5.19 ± 0.98

It can be seen from Table 2. 1 that as the molecular weight of the gel increases, so does the diffusion coefficient through the gel. This trend is due to the larger mesh size of the higher molecular weight gels for the same initial concentration of PEG-DA and no cross-linker. This observation is validated by the SEM micrographs that qualitatively demonstrate that the average mesh size increases with the molecular weight of the gels (Figure 2. 1).

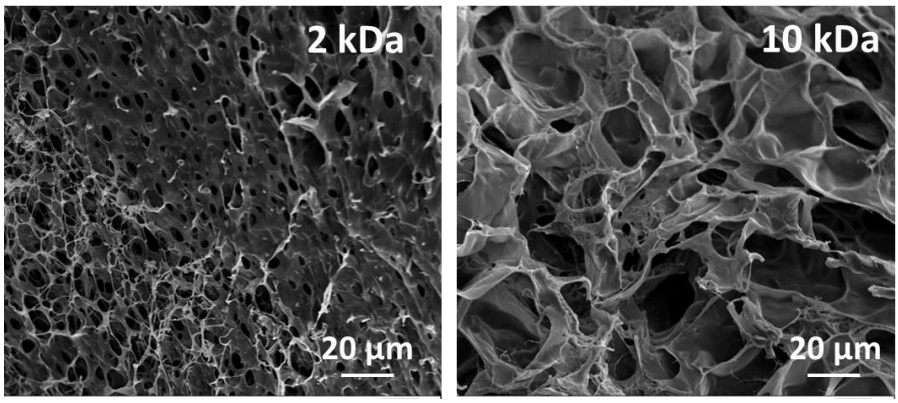

Figure 2. 4. Representative SEM micrographs qualitatively demonstrate the mesh size increase from a lower molecular weight PEG-DA gel (2 kDa) to a higher molecular weight PEG-DA gel (10 kDa). [124]

b. Swelling characteristics of PEG-DA gels

The swelling kinetics of the different molecular weight PEG-DA gels were studied over a time periods of 2 days at room temperature. The different molecular weight gel samples were immersed in DI water and allowed to swell over time. The samples were then removed from the DI water, carefully and quickly blotted to remove the water on the surface of the gel and then weighed. The swelling ratio (*SR*) of the gel is determined using the equation below:

$$SR = \frac{W_S - W_0}{W_0} \tag{2.2}$$

where W_S is the swollen weight and W_0 the dry weight of the gel.

A plot of the swelling ratio for all molecular weight samples is shown in Figure 2. 5. The molecular weight of the gel is an important factor in the swelling characteristics of the gels. As illustrated in the plot, higher molecular weights PEG-DA gels have larger swelling ratio values. Quantification of the swelling ratio of each hydrogel is critical to the design and successful assembly of the microfluidic device by forecasting the final dimensions of the gel-based device in the swollen state.

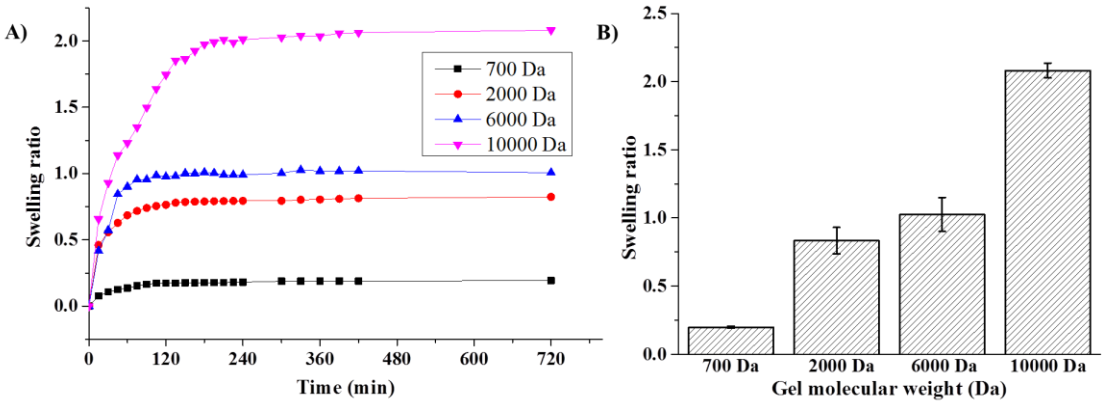

Figure 2. 5. A) Swelling ratio curves for all molecular weights of the PEG-DA gels used in this study as a function of time. B) Final swelling ratio for each of the gels. [124]

c. Chemical gradients characterization

The chemical concentration established in the center channel of the microfluidic device was simulated using the finite element analysis software package COMSOL® for the experimentally determined chemical diffusion coefficients. The simulations were run for all microfluidic devices using all four molecular weight PEG-DA gels. For all simulations, channel lengths and widths were respectively 8 mm and 1 mm. The gel walls that separate the channels are 1 mm thick. The following initial and boundary conditions

were imposed: (1) The diffusion coefficient through PDMS is assumed to be zero given its non-permeable nature to the chemicals of interest (casamino acids, PBS) when cured; (2) The chemical flux at the PDMS interface is also zero since there is no chemical input into the system from the PDMS; (3) The chemical concentrations in both outer channels are maintained constant.

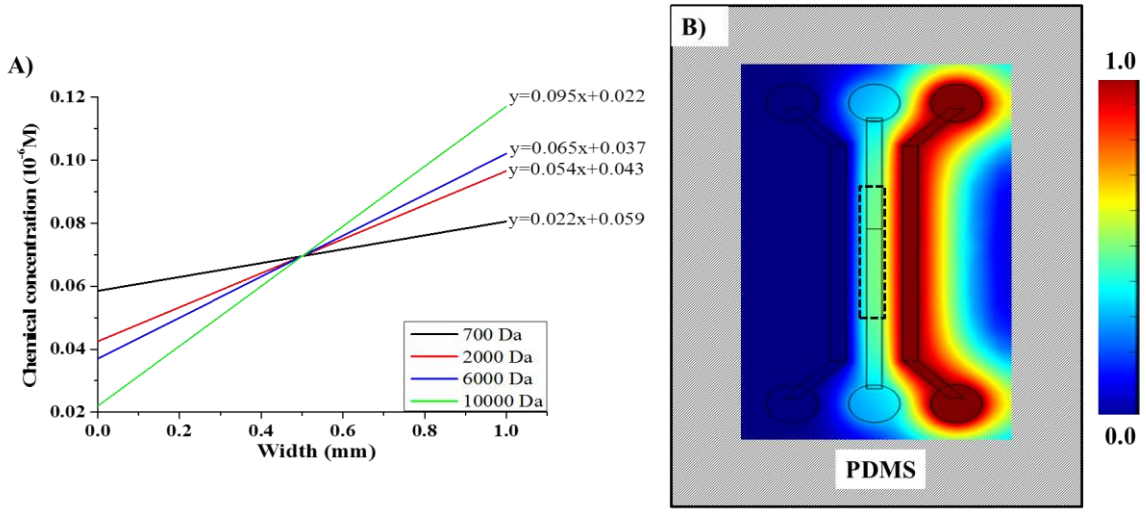

Figure 2. 6. A) Numerically modeled quasi-steady chemical concentration profiles in the center channel of the microfluidic device after one hour. B) Schematic showing the three channels in PEG-DA and PDMS enclosure (hatched area). The chemical concentration profiles shown in (A) are representative of the concentration profiles within the dotted rectangular region of the center channel. [124]

In practice, this is accomplished by continuous flow of the chemo-effector and the buffer solutions respectively in the right and the left outer channels at 5 μL/min. Simulation results suggest that the quasi-steady concentration gradient is achieved in 45 minutes. The established linear chemical concentration gradient in the center channel over the width of the center channel for all molecular weights used in the study is demonstrated in Figure 2. 6. The gradients shown in Figure 2. 6.A were obtained one hour after the introduction of the chemoeffector and the buffer solution in the three channels. The chemical gradients obtained can reasonably be maintained for hours as long as the chemoeffector solution and buffer solution are constantly flowed in the outer channels.

The chemical gradient profiles obtained from the simulations were validated against the gradient profiles determined experimentally. A fluorescein solution (MW 332 Da, Invitrogen, Grand

Island, NY), with a molecular weight close to that of the casamino acids (250 Da), was used to experimentally determine the chemical concentration profile in the center channel. A fluorescein solution of known concentration was continuously flowed in the chemo-effector channel and similarly the buffer solution was continuously flowed in the buffer channel at a rate of 5 µL/min. Fluorescent images of the center channel for each molecular weights were obtained (Figure 2. 7) and analyzed according to the method explain in section 2.2.d.

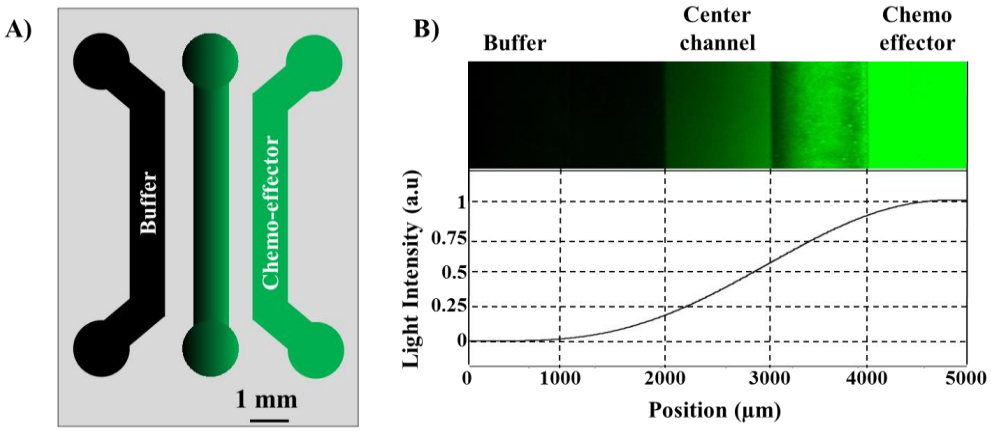

Figure 2. 7 (A) Schematic of microfluidic device. (B) Chemical gradient profile in center channel of the device obtained through fluorescent imaging and light intensity analysis. [124]

The analysis of the fluorescent images was performed and the linear chemical gradient in the center channel for each molecular weight was plotted over the width of the center channel once the system reached a quasi-steady state (Figure 2. 7).

A comparison of the linear chemical gradient obtained using the simulations done in COMSOL® and the experiments using fluorescein is shown in Table 2. 2.

Table 2. 2. Summary of the results comparing the fluorescein concentration gradients obtained in simulations and experiments for all PEG-DA gel devices.

	Gradient in center channel (10^{-6} M/mm)			
MW (Da)	700	2000	6000	10000
Simulations	0.022	0.054	0.065	0.095
Experiments	0.024	0.051	0.071	0.097
Difference (%)	8.3	3.9	8.5	5.2

As seen in Table 2. 2, there is a close agreement between the experimental results and the COMSOL simulations for all molecular weights of the PEG-DA gel. The difference in values between experiments and simulations may originate from photo-bleaching of the fluorescein over the time of exposure. The 700 Da molecular weight based microfluidic device was chosen to demonstrate the efficacy and compatibility of this class of devices for biological experiments. In particular, we conducted a study of the chemotactic behavior of *E. coli* RP437 under known gradients of the chemo-attractant casamino acids.

2.4 Conclusions

In this work, we have developed and characterized microfluidic platforms using photopolymerizable hydrogel (PEG-DA) of different molecular weights. Using this fabrication method, other platform designs for the study of cells can be realized as well. The ease of fabrication of the PEG-DA based device (due to elimination of standard steps such as template fabrication, molding and peeling of the hydrogel, etc.) compared to other flow-free devices makes this class of devices unique and advantageous. The fabrication method presented here also allows for the realization of small feature sizes generally attainable through conventional microfabrication processes but are more challenging to achieve using hydrogels in conjunction with soft lithography based methods.

We demonstrated the efficacy of this platform by conducting a study of the chemotactic behavior of *E. coli* RP437 when challenged with casamino acids gradients (Chapter 3). The microfluidic device platforms presented here can be used to generate controllable and quasi-steady chemical concentration gradients for studying other prokaryotic or eukaryotic cells as well. As demonstrated, the wide range of molecular weights of the PEG-DA polymer used here enables us to achieve customizable diffusive properties with respect to the specific chemical compound-cell type to be studied. This will enable the investigation of the response of cells to a wide range of chemical cues.

The knowledge of the diffusion characteristics and swelling ratios of the PEG-DA gels ensures that the chemical environment can be accurately simulated and used to better explain the experimental results obtained in the study. Also, the design of the device allows for the addition

of mechanical cues on the glass surface to generate well-defined physicochemical microenvironments. This will enable the investigation of the response of cells to a wide range of combined chemical and mechanical cues within a single device.

Appendix A: Convective flow-based microfluidic device for chemotaxis studies

Fabrication of the chemical gradient generator

The chemical gradient generator was fabricated using standard photolithography. Briefly, polydimethylsiloxane (PDMS) was poured onto a SU-8 master and cured at 125 °C on a hot plate for 20 minutes. The cured PDMS mold was peeled off, inlet and outlet holes were punched and the mold was bonded to a glass slide using air plasma.

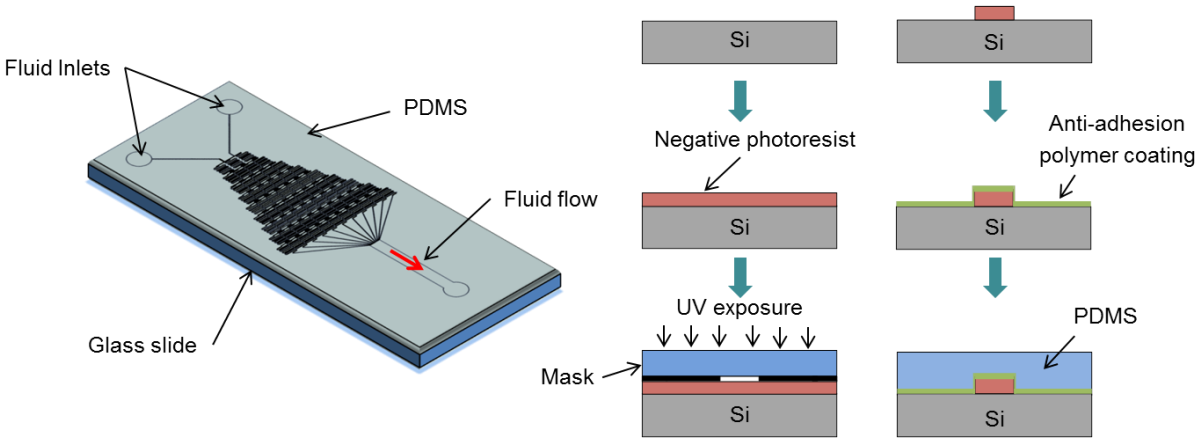

Figure 2. 8. Diagram of convective flow-based microfluidic device and fabrication process flow.

The device consists of 2 inlets divided into 11 branches to generate 11 streams with different chemical concentrations as seen in Figure 2. 9. The streams of fluid are then reconstituted into one main channel for the gradient generation.

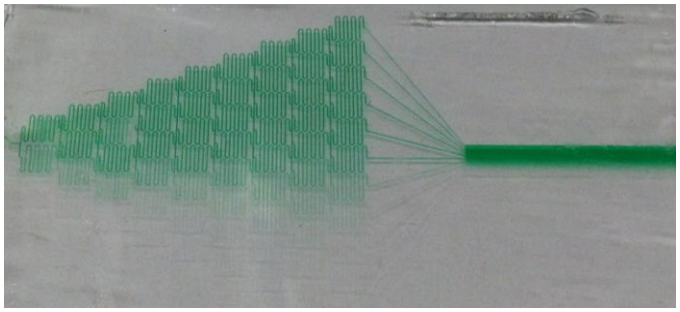

Figure 2. 9. Image representative of a flow-based microfluidic setup

Figure 2. 9 illustrates the design of the PDMS gradient generator. When the fluids enter in the inlets of the device, they are repeatedly split and mixed until they reach the main channel. In the main channel, the flow is laminar and diffusive mixing occurs between the streams. The diffusion between each stream is dictated by the following equation:

$$\frac{\partial c}{\partial x} = \frac{D}{v(y)}\left(\frac{\partial^2 c}{\partial y^2}\right) \tag{2.3}$$

Where c is the concentration as a function of x and y, D is the diffusion coefficient of the solute of interest in the buffer; v is the velocity of the fluid stream. The diffusion of the solute occurs along the y-axis across the width of the channel.

Numerical simulation and device characterization:

The chemical concentration within the main channel was simulated in Matlab for different flow rates and compared against experiments. A fluorescein solution was used to fluorescently visualize the generated chemical gradients.

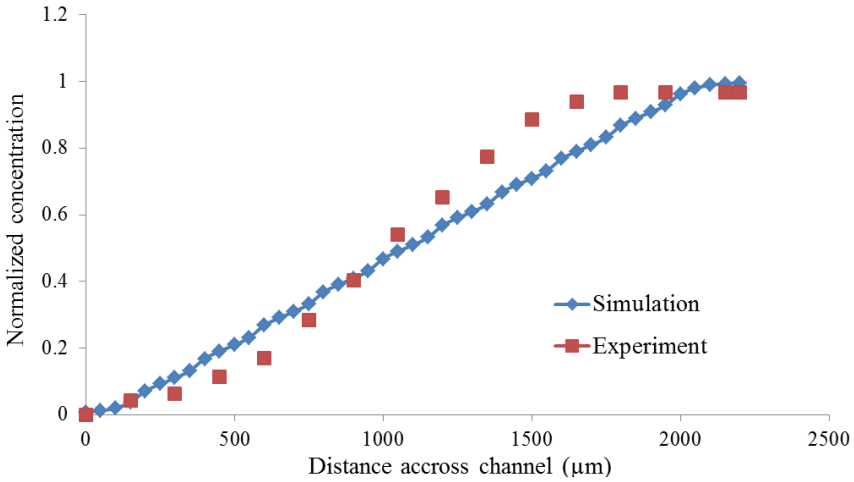

Figure 2. 10. Concentration gradient characterization using a flow rate of 0.5 µL/min at a 1 mm down the channel length.

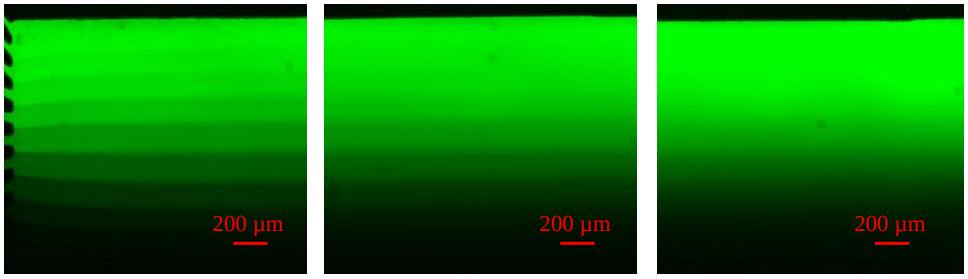

Figure 2. 11. Fluorescein gradient within channel

Chapter 3: Chemotaxis study of *Escherichia coli* under varying chemo-attractant gradients

Abstract

Bacteria move toward or away from a chemo-effector by sensing temporal gradients of the chemical substance in a process known as chemotaxis. A deep understanding of bacterial chemotaxis appears crucial due to the major role it plays in human diseases. The chemotactic behavior of *Escherichia coli* has been the subject of many qualitative and quantitative studies over the past forty years. In this chapter, *E. coli* strain RP437 was exposed to steady, linear, and controllable concentration gradients of the chemo-effector casamino acids and the cells chemotactic behavior was quantified. We have determined: (i) the threshold chemical concentration gradient needed for the bacteria to exhibit a chemotactic response is between $0.25\text{-}1.25\times10^{-7}$ g/mL/mm, (ii) the gradient at which bacteria no longer show a positive chemotactic response towards the chemo-effector is at or above 2.5×10^{-3} g/mL/mm and (iii) the most favorable chemo-effector concentration gradient is approximately 1.25 to 2.5×10^{-4} g/mL/mm. Moreover, we have investigated the chemotactic behavior of the cells in a spatiotemporally varying concentration field and have demonstrated that bacterial chemotaxis is dependent upon the absolute chemical concentration sensed by the bacterium even in an environment where the chemical concentration gradient is most favorable.

3.1 Introduction

Most flagellated bacterial cells move in fluidic and semi-solid environments by alternating run and tumble motions. Hence, in a chemically isotropic environment, the bacterial motion has characteristics of a random walk. In presence of a chemical attractant gradient, bacteria extend their run periods through reduction of their tumbling frequency and move toward the chemical source in a biased random walk [58]. This biased motion of bacteria towards or away from a chemo-effector source is known as bacterial chemotaxis.

The chemotactic response of bacteria towards or away from chemical attractants or repellents is mediated by the intracellular signal transduction that is unique to bacteria. *E. coli* bacteria have five chemical receptors located within the periplasmic membrane. The five receptors are Tar for aspartate, Tsr for serine; Trg for galactose and ribose; Tap for peptides and Aer which may be a redox detector.

The chemotactic response is achieved through sensing by the receptor complex which is mainly found at the pole of the bacterium's body and the flagellar-motor assembly complex which is distributed around the body of the bacterial cell. Between these two major complexes, a two-component "signal transducer system" (CheA and CheY) serves as a trigger for the response. When an attractant molecule binds to a receptor, the CheA is inhibited which in turns favors the decrease in phosphorylation and blocks the interaction between the response regulator and the motor.

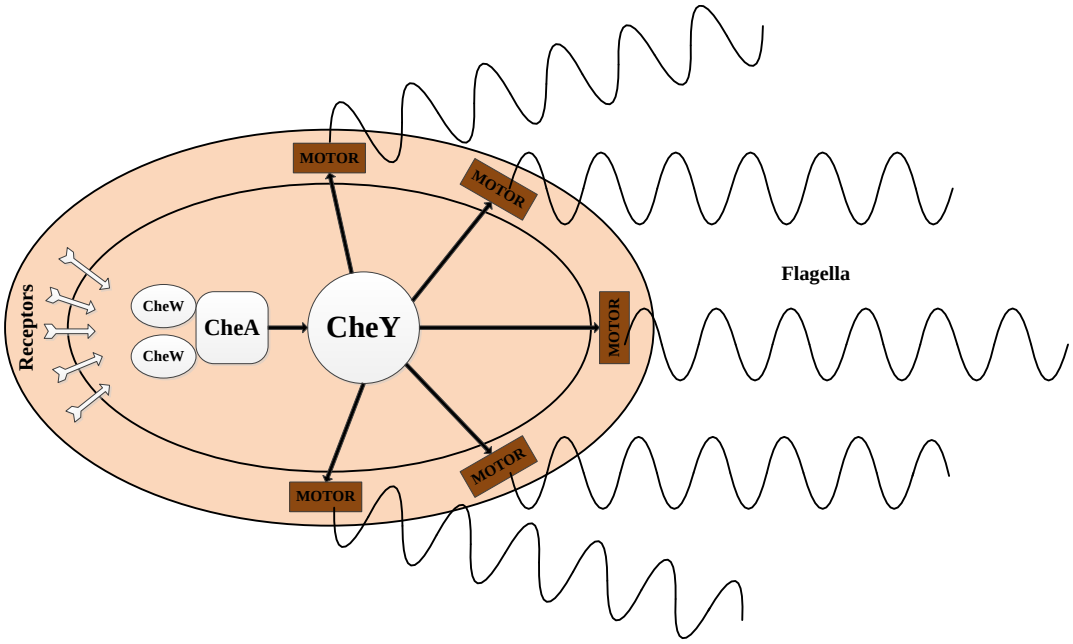

Figure 3. 1. Schematic showing the chemotactic system of most flagellated bacteria

Bacterial chemotaxis is a phenomenon prevalent in a variety of processes and applications. The range of applications of bacterial chemotaxis varies from purely biological processes to actuation control of bio-hybrid engineered systems [59], [60]. Bacterial chemotaxis is an essential trait for pathogenic bacteria to find and colonize specific host tissues [10]. It has also been reported that chemotactic sensing of the chemicals released by cancer tumors may be responsible for targeted colonization of bacteria such as *Salmonella enterica serovar* Typhimurium in tumors [10], [33]. Therefore, bacterial chemotaxis can be tailored towards targeted delivery of drugs to cancer tumor sites.

It is evident that bacterial chemotaxis is an essential component of a wide range of processes and can be used towards applications such as sensing and targeting. Therefore, it is crucial to advance our quantitative understanding of the role of absolute chemical concentration and concentration gradient range on bacterial chemotactic behavior. Previous research has shown that

microfluidic assays in conjunction with population scale dynamic metrics can be used to shed some light on different aspects of bacterial chemotaxis [45], [61–64]; however a quantitative study of the role of absolute chemical concentration values versus chemical concentration gradient values is still missing.

Here, *Escherichia coli* cells were introduced in a steady (time-invariant), well-defined chemical microenvironment and their responses were recorded and quantified. The choice of chemical attractant used in this study (casamino acids, i.e. CAA) was motivated by the fact it is a complex chemical that better emulates compounds found outside of controlled experimental settings. More importantly, a chemical attractant that indirectly plays a role in human diseases would be best suited for the application explored in this work. Hence, CAA was selected as the chemical attractant given its impact on the formation of quorum sensing dependent biofilms for multiple bacterial strains [65]. The chemotaxis partition coefficient (CPC) and the chemotactic migration coefficient (CMC) of *E. coli* RP437 for concentrations gradients of casamino acids ranging from 1.25×10^{-10} g/mL/mm to 2.5×10^{-2} g/mL/mm were calculated. Intrinsic properties such as the threshold chemical concentration gradient needed for bacteria to exhibit a chemotactic response and the concentration gradient at which the chemotactic response transitions from positive to negative were determined for casamino acids. Moreover, the effects of the concentration gradient and the absolute chemical concentration were dissociated by establishing the most favorable chemo-effector gradient using high absolute chemical concentrations. We have demonstrated that bacteria in such cases do not migrate up the gradient even when the chemo-effector concentration gradient is most favorable.

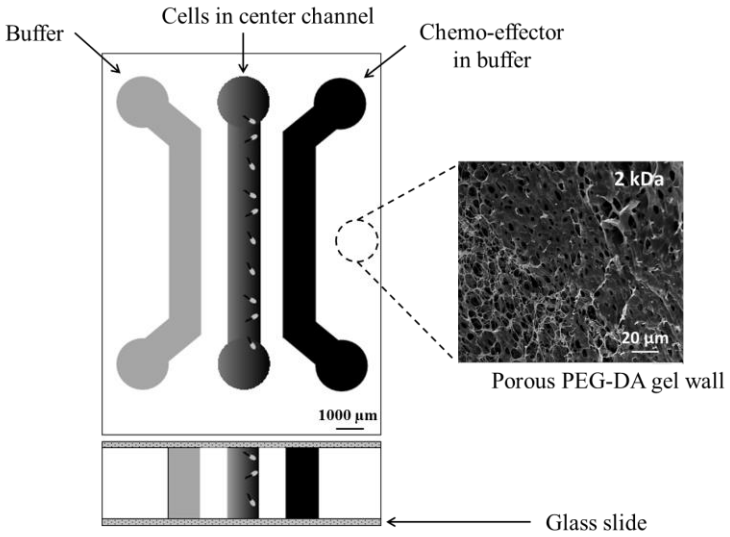

Figure 3. 2. Schematic of the microfluidic platform. The chemo-effector diffusing through the porous structure of the gel establishes a linear chemical gradient in the center channel. The scanning electron microscopy image on the right qualitatively shows the porous structure of the PEG-DA gel with 2 kDa molecular weight.

3.2 Materials and methods

a. Bacterial cell culture

The *E. coli* strain RP437 [66] was used in all chemotaxis experiments conducted in this work. To facilitate microscopy imaging, *E. coli* RP437 was transformed with a plasmid encoding GFP (pHC60; tet^R, constitutive expression of green fluorescent protein) [67]. Bacterial cultures from a single colony were incubated overnight in 10 mL of fresh T-broth [68] (10 g of tryptone, 5 g of NaCl in 1 L of H_2O) supplemented with 10 µg/mL of tetracycline in a shaking incubator (30° C, 180 rpm). A 100 µL aliquot of the overnight culture was inoculated in 10 mL of fresh T-broth supplemented with 0.04 g of the chemo-attractant (casamino acids) to promote a pronounced chemotactic response of the bacteria cells in all chemotaxis experiments [68]. A 1 mL aliquot of the liquid culture (OD_{600}=0.5) was then centrifuged at low speed (1,700 × g) for 5 minutes at room temperature and suspended in 1 mL of freshly prepared chemotactic buffer (PBS (phosphate buffered saline: 150 mM NaCl, 2 mM $Na_2HPO_4.7H_2O$, 1.9 mM KH_2PO_4, pH 7.4), 0.1 mM EDTA (pH 8.0), 0.01 mM L-methionine, and 10 mM DL-lactate) [68]. All chemicals were obtained from Fisher Scientific (Pittsburgh, PA).

b. Microfluidic platform fabrication

The microfluidic platform used to study the behavior of *E. coli* over a wide range of chemical gradients has been described in a preceding work [69]. Briefly, a solution of polyethylene glycol diacrylate (PEG-DA, MW=700 Da, 10% (v/v) in PBS) hydrogel mixed with 0.5% (w/v) of the photoinitiator Irgacure 2959 was poured within a polydimethylsiloxane (PDMS) enclosure. A three-channel pattern was transferred into the hydrogel via UV photopolymerization (365 nm,

18W/cm^2, Omnicure S1000, Vanier, Quebec) for a duration of 15 seconds, therefore producing a three-channel microfluidic setup. A controllable, steady, and linear chemical concentration gradient for the study of bacterial chemotaxis was established by continuously flowing the buffer and the chemo-effector solution in the outer channels at a flow rate of 5μL/min (PHD Ultra syringe pump, Harvard apparatus, Holliston, MA). A quasi-steady linear gradient is established in the center channel after 45 minutes as the chemo-effector diffuses through the hydrogel wall into the buffer filled center channel.

A schematic of the microfluidic device is depicted in Figure 3. 2. The diffusion coefficient of the chemo-effector (casamino acids) through the hydrogel was determined using a Franz diffusion cell [57]. The experimentally obtained diffusion coefficient was used to computationally simulate the diffusion of the chemo-attractant within the center channel of the device and design the experiments outlined below. Experimental validation of the chemical gradients generated within the center channel was conducted using a fluorescein solution; the obtained results were within 9% agreement with the computational simulation (data not shown).

c. Imaging and data analysis

Distribution of bacteria within the center channel of the microfluidic device was captured using a Zeiss AxioObserver D1 inverted microscope equipped with an AxioCam HSm camera and a 10× objective. The recorded images were converted to binary images with AxioVision software (Zeiss Microscopy, Oberkochen, Germany). The binary images were then exported in ImageJ (NIH, Bethesda, MD) to obtain the distribution of bacteria cells across the center channel. The chemotactic behavior of the bacteria was quantified using population-scale metrics of chemotaxis partition coefficient (CPC) and chemotaxis migration coefficient (CMC). These

chemotactic coefficients can be used as measures of the direction and strength of bacterial migration. The partition coefficient (CPC) is a measure of the bacteria cells population in each half of the center channel. The migration coefficient (CMC) is a measure of the distance traveled by the bacteria cells from the middle of the center channel towards the chemo-effector [44], [45], [48]. Both coefficients range between -1 and 1, with 1 indicating the strongest attraction to a chemo-effector and -1 indicating strong repellence. A coefficient value that is positive indicates that the cells respond positively to the chemo-effector present in the source channel. The coefficients can be determined using the following equations.

$$CPC = \%B_r - \%B_l \tag{3.1}$$

$$CMC = \frac{\sum[B(x) \cdot \left(x - \frac{w}{2}\right)]}{[\sum B(x)] \cdot (\frac{w}{2})} \tag{3.2}$$

Where B_r is the bacteria population in the right side of the center channel, and B_l is the bacteria population in the left side of the center channel. $B(x)$ is the bacteria population at a given position within the center channel ($x=0$ at center of the channel) and w is the width of the channel.

3.3 Results

a. Threshold chemical concentration gradient and bacterial chemotactic response

The microfluidic platform used for this study is depicted in Figure 3. 2. The platform is essentially composed of three channels separated by porous walls (PEG-DA gel). The outer channels are used to flow chemo-effectors of choice (right channel) and buffer (left channel) to establish chemical gradients in the center channel. Various linear chemical concentration gradients were generated inside the center channel of the microfluidic device to understand the chemotactic behavior of the *E. coli* strain RP437 in presence of the chemo-effector casamino acids. In a control experiment, with chemotaxis buffer continuously flowed in both outer channels, the bacteria distribution did not show any side bias over time (shown in Figure 3. 3. A).

The concentration gradient of casamino acids was then varied from 1.25×10^{-10} g/mL/mm to 2.5×10^{-2} g/mL/mm to determine the threshold chemical concentration gradient needed to promote a chemotactic response as well as the saturation concentration gradient at which chemotactic behavior is no longer observed. Both partition and migration coefficients were computed and plotted as a function of the chemical concentration gradients generated in the center channel to determine the threshold and saturation concentration gradient values (Figure 3. 3.D).

The threshold chemical concentration was found to be between $0.25\text{-}1.25\times10^{-7}$ g/mL/mm, because both the chemotactic partition coefficient (CPC) and chemotactic migration coefficient (CMC) values become positive in that range of concentration gradients. These plots also show that the CPC and CMC values increase and reach a maximum of 0.55 and 0.43, respectively, at chemical concentrations gradient of 2.5×10^{-4} g/mL/mm and 1.25×10^{-4} g/mL/mm. Figure 3. 3. B

and Figure 3. 3. C respectively illustrate the bacterial behavior in presence of the 2.5×10^{-4} g/mL/mm gradient and 2.5×10^{-2} g/mL/mm gradient. The bacteria exhibit a positive chemotactic response towards a 2.5×10^{-4} g/mL/mm gradient and a negative response towards the much higher gradient of 2.5×10^{-2} g/mL/mm.

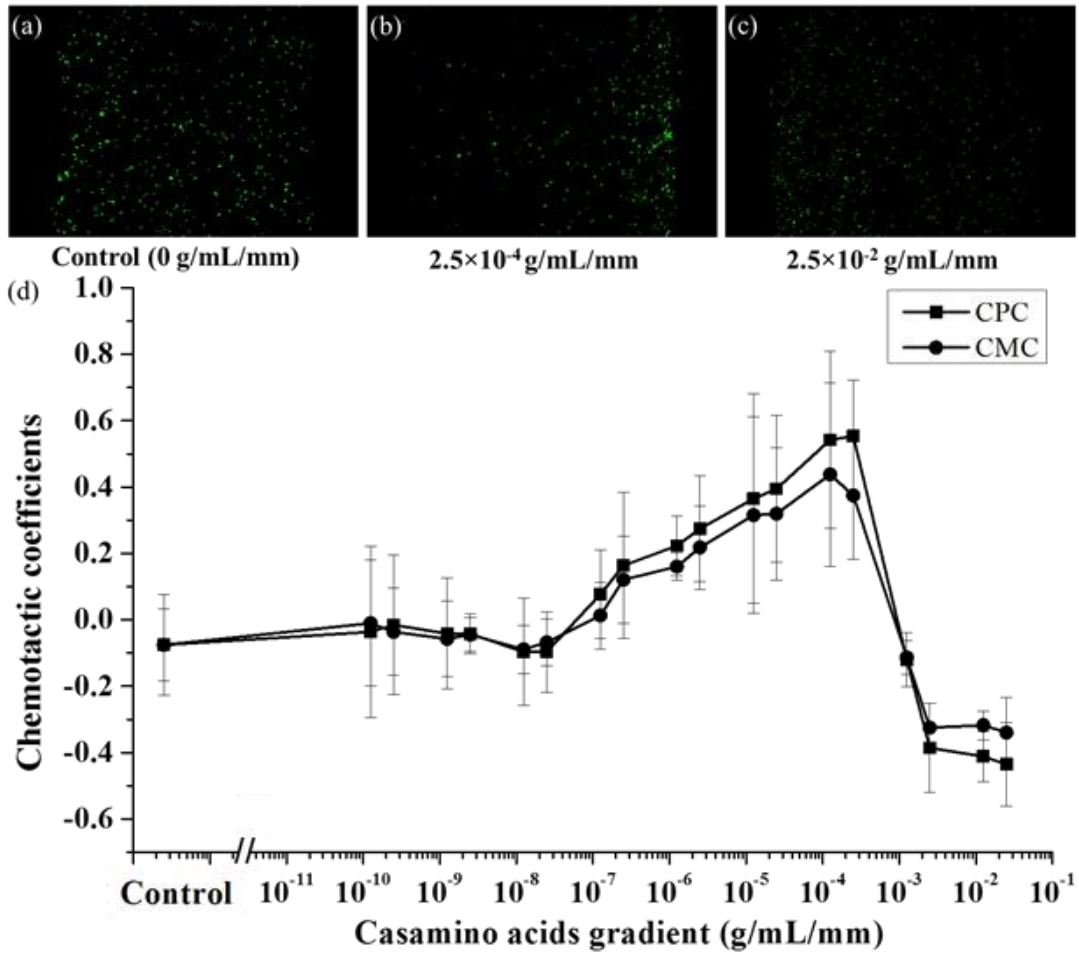

Figure 3. 3. Effect of chemical concentration gradient on the chemotactic behavior of *E. coli* RP437. Distribution of bacterial cells in the center channel in (a) absence of a gradient (control), (b) with 2.5×10^{-4} g/mL/mm chemo-effector gradient, (c) with 2.5×10^{-2} g/mL /mm chemo-effector gradient. (d) Plot showing the chemotactic partition coefficient (CPC) and the chemotactic migration coefficient (CMC) as a function of the chemo-effector gradient in the center channel.

b. The role of chemical concentration gradient and Absolute chemical concentration on the chemotactic behavior

The chemotactic coefficient curves only take into account the chemical concentration gradients in the center channel. Bacterial chemotaxis occurs not only as a result of the chemical concentration gradients in the center channel but also as a result of the absolute chemical concentration sensed. We therefore used our microfluidic platform to challenge *E. coli* with the optimum chemical concentration gradient of 2.5×10^{-4} g/mL/mm as determined earlier and with a high absolute chemo-effector concentration of 0.4 g/mL that mimics the source concentration of the high chemical concentration gradient (2.5×10^{-2} g/mL/mm) experiment. To establish the most favorable gradient of 2.5×10^{-4} g/mL/mm at this high absolute concentration, two different chemo-effector concentrations, namely 0.40000 g/mL and 0.39975 g/mL, were used. In the buffer and center channel, 0.39975 g/mL chemo-effector solution was flowed continuously for 2 hours while the 0.40000 g/mL chemo-effector solution was continuously flowed in the chemo-attractant channel. The center channel was then rinsed with blank chemotactic buffer and bacteria introduced immediately after the rinse. The concentration profile in the center channel was computationally modeled in COMSOL® given all these parameters. The plots shown in Figure 3. 4 are representatives of the chemical concentration that the bacterial cells experience in the center channel from their initial introduction (t=0) to time t = 540 seconds. As seen in Figure 3. 4, chemical concentration gradients in the center channel, observed until the quasi steady-state gradient of 2.5×10^{-4} g/mL/mm was reached (at t= 540 seconds), present very steep concentration gradients from the center of the channel to both walls of the center channel. Figure 3. 5 illustrates the behavior of bacteria in the center channel. From the initial introduction until the quasi-steady chemical gradient is established, bacteria in the center channel move away from the walls of the channel towards its middle. We observed that after the steady-state chemical

gradient has been established, bacteria in the center channel do not migrate up the chemical concentration gradient of 2.5×10^{-4} g/mL/mm, which is the most favorable gradient according to Figure 3. 3. Instead, we observe that the bacteria in the center channel end up in considerable number in the very middle of the channel after being introduced in the device. Similarly, a lack of response to the optimum concentration gradient of 2.5×10^{-4} g/mL/mm was observed using lower absolute chemical concentration values of 0.03975 g/mL and 0.04000 g/mL.

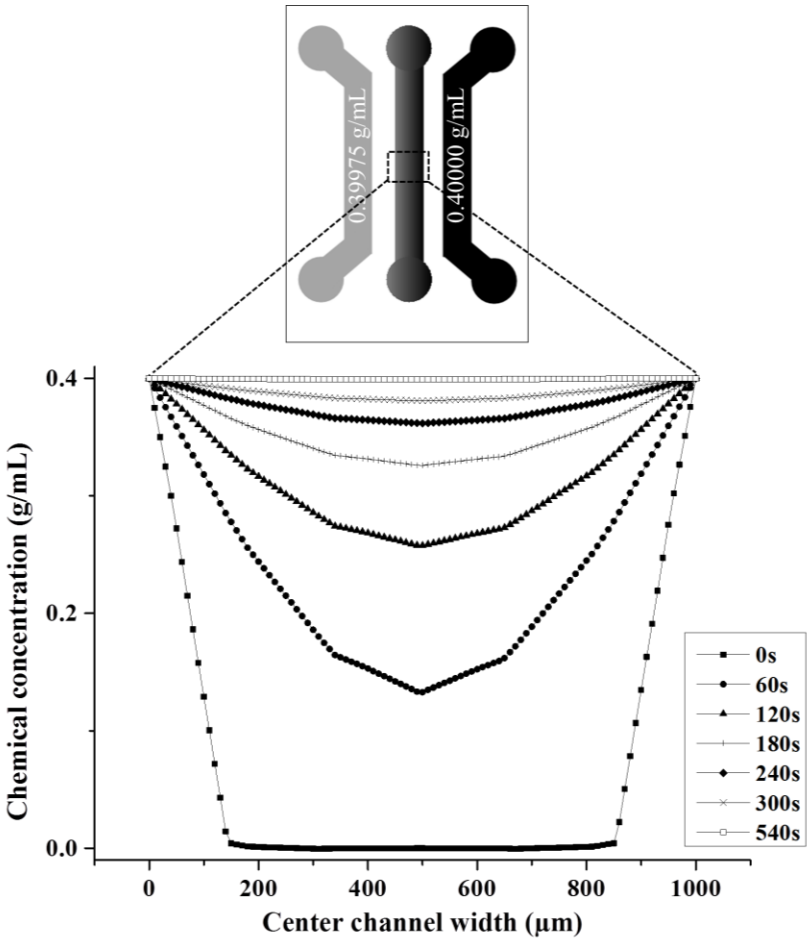

Figure 3. 4. Spatiotemporal concentration gradient profiles in the center channel of the microfluidic device. The channel to the right of the center channel is maintained at 0.4 g/mL of the chemo-effector concentration. Chemical concentration profile at time 0 s (■), Chemical concentration profile at time 60 s (●), Chemical concentration profile at time 120 s (▲), Chemical concentration profile at time 180 s (+), Chemical concentration profile at time 240 s (♦), Chemical concentration profile at time 300 s (×), Chemical concentration profile at time 540 s (□).

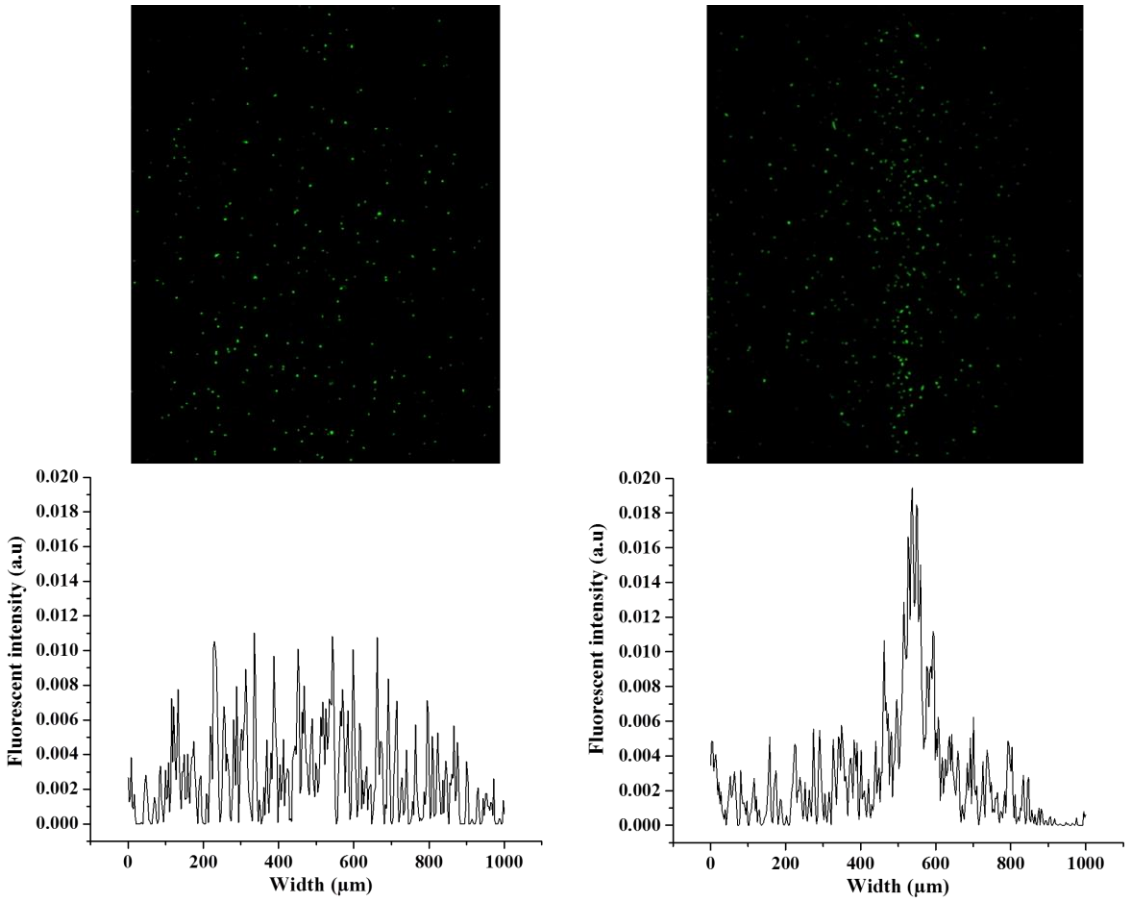

Figure 3. 5. Distribution of bacterial cells in the center channel in presence of a spatiotemporal concentration gradient at time t = 0 s (left) and time t = 1800 s (right).

3.4 Discussion

a. A chemo-attractant can act as a repellent at high concentration gradients

The trend of the data illustrated in Figure 3. 3. is in agreement with earlier works that indicate an enhanced chemotactic response with an increase in chemical concentration gradients within a certain chemical gradient range [49]. However, at concentration gradients between 2.5×10^{-4}-1.25×10^{-3} g/mL/mm, the CPC and the CMC values drastically decrease. The chemical concentration gradient at which the cells do not show a positive chemotactic response can be deduced from the CPC and CMC graphs and found to be approximately 2.5×10^{-3} g/mL/mm. This phenomenon where bacteria do not move up the gradient in a high chemical concentration environment has been discussed in previous works [70], [71]. An interesting fact however originates from the highly negative CPC and CMC values (-0.4) at high chemo-attractant concentration gradients. Previous work has shown that bacteria have the ability to sense a chemo-effector as an attractant at low chemical concentrations and as a repellent at higher chemical concentrations [45], [72]. The CPC and CMC values obtained in our experiments show for the first time that wild-type *E. coli* RP437 has a positive chemotactic response towards casamino acids for chemical concentration gradients below 1.25×10^{-3} g/mL/mm and a negative chemotactic response for gradients at or above 2.5×10^{-3} g/mL/mm.

b. Chemotaxis in bacteria is not solely dependent on the chemical gradient they sense

Spatiotemporal concentration gradients were established to investigate the effect of absolute concentrations on the chemotactic response. As seen in Figure 3. 4, the slope of the chemical concentration in the center channel is very steep near the walls of the channel until a quasi-steady

chemical gradient is established. Bacteria, homogeneously introduced in the center channel, sense the high absolute concentrations near the walls of the center channel and respond by moving away from the walls towards the center of the channel (negative chemotaxis), as shown in Figure 3. 5. As time progressed, the concentration gradient values fell in the "positive chemotaxis" range and reached a quasi-steady optimum concentration gradient value of 2.5×10^{-4} g/mL/mm (the absolute chemical concentrations were varied from 0.39975 g/mL to 0.4 g/mL and from 0.03975 g/mL to 0.04000 g/mL in two separate experiments); nevertheless, bacteria in the center channel did not migrate up the favorable chemical gradient. This observation indicates that bacterial chemotaxis is not only dependent on the chemical concentration gradients but also dependent on the absolute chemical concentration the bacteria experience at a given time.

Bacteria respond to temporal chemical concentration differences. In a stable positive linear chemical gradient, they are known to move up the gradient they experience. In this experiment, even in the presence of a favorable chemical gradient, bacteria do not exhibit positive chemotaxis towards the higher chemo-effector concentration. This phenomenon can be possibly explained by the negative effect of the high absolute chemical concentrations bacterial motility and chemotaxis, thus preventing the cells from performing chemotaxis towards the higher chemical concentration. In the event where the chemical concentrations is exceptionally high (i.e. 0.4 g/mL), cells become less motile due to the overall increase in osmotic pressure [72], [73] and as such are unable to move up the chemical gradient they are subjected to. We have conducted independent motility assays which showed cessation of bacteria motility in a 0.4 g/mL chemo-effector solution (data not shown). A similar bacteria behavior was reported previously for other chemo-effectors [74]. Considering the diminished motility of bacteria at such high concentrations of casamino acids, the experiments were repeated with absolute

chemical concentrations between 0.03975 g/mL and 0.04000 g/mL. Although bacteria were motile at these concentrations, they did not migrate up the quasi-steady favorable chemical gradient in the center channel.

In conclusion, chemotactic behavior of *E. coli* in presence of a wide range of concentration gradients (1.25×10^{-10}-2.5×10^{-2} g/mL/mm) of casamino acids was quantified. We have determined the threshold and the optimum concentration gradient values for *E. coli* chemotaxis toward casamino acids. Also, we have shown that a chemical attractant can exhibit repellent properties once the absolute chemical concentration bacteria experience is high enough to create a significant increase in osmotic pressure. Finally, we have shown that *E. coli* chemotaxis towards casamino acids is highly dependent upon the absolute chemical concentration bacteria sense, even when the chemical concentration gradient that surrounds them is most favorable.

Chapter 4: Computational and experimental study of chemotaxis of bacteria propelled micro-spherical particles[1]

Abstract

Micro-objects propelled by whole cell actuators, such as flagellated bacteria, are being increasingly studied and considered for a wide variety of applications. Here, we first present a computational model that describes the trajectory of a single bacterium in a 3D fluidic environment followed by theoretical and experimental investigations of chemotactic motility of a 10 μm diameter micro-bead propelled by an ensemble of attached flagellated bacteria. The stochastic model presented here encompasses the behavior of each individual bacterium attached to the micro-bead in a spatiotemporally varying chemo-attractant field. The computational model shows that in a chemotactic environment, the ensemble of bacteria, although constrained, propel the bead in a chemotactic manner with a 67% enhancement in displacement to distance ratio (defined as directionality) compared to non-chemotactic propulsion.

The simulation results are validated experimentally. Close agreement between theory and experiments demonstrates the possibility of using the presented model as a predictive tool for other similar bio-hybrid systems. The model developed here can be applied to particles of different sizes and possibly shapes to describe their 3D trajectory in a fluidic and semi-fluidic environment.

[1] The work discussed in this chapter was published in Physical Review E, Volume 84, Issue 6, 2011. MAT and BB designed the study. MAT conducted all the experiments and simulations. Ali Sahari, a Ph.D. candidate in our MicroN BASE laboratory contributed to the study by developing the tracking software used to record the positions of the micro-beads propelled by bacteria.

4.1 Introduction

Eukaryotic cells and unicellular prokaryotic microorganisms have been utilized as whole cell actuators for the controlled propulsion of objects of micro/nano-scale characteristic dimensions [75], [76]. Flagellated bacteria are well known for their superb swimming capabilities at speeds of up to 50 body lengths per second and their viability in a wide range of temperatures and pH. As such, they can be interfaced with microscale structures and be used as actuators [77–79]. These biotic/abiotic engineered systems, also known as bio-hybrid microrobots, are envisioned to be employed in large numbers for applications such as biosensing, transport and delivery of cargo, and minimally invasive treatment of diseases. Although the motility and taxis behavior of unicellular organisms have been extensively studied and modeled, the existing work is not readily applicable to bio-hybrid systems as very often in these systems a large number of microorganisms are configured and constrained in a specific manner. In this chapter, we present a computational stochastic model to investigate the emergent behavior of an ensemble of bacteria attached to a 10 μm spherical micro-bead in presence of a transient chemo-attractant gradient field. The stochastic model presented here encompasses the behavior of each individual bacterium attached to the micro-bead in a spatiotemporally varying chemo-attractant field. The run and tumble rate of each bacterium is adjusted according to their location and the overall force exerted on the micro-bead is calculated at every time step using matrix transformation. It is demonstrated that the constrained population of bacteria exhibits a collective chemotactic behavior evident by a 67% increase in the directionality of the micro-bead's motion in a chemo-attractant gradient field. The proposed model is experimentally validated to demonstrate that a chemo-attractant gradient can be used to autonomously control bio-hybrid microrobots effectively and at a very low cost.

4.2 Modeling

a. Materials and methods

Wild-type *S. marcescens* (ATCC 274) was grown on L-broth (1% tryptone, 0.5% yeast extract and 0.5% sodium chloride.) culture plates containing 0.65% agar (Difco Bacto agar) and 5 g/L glucose. 10 μm polystyrene micro-beads (Fisher Scientific for the 1 bacterium/7μm^2 attachment density and Sigma-Aldrich for the 1 bacterium/11 μm^2 attachment density) were washed by repetitive centrifugation in DI water and were finally suspended in motility medium (0.01 M of potassium phosphate, 0.0067 M of sodium chloride, 10^{-4} M of EDTA, 0.01 M of glucose, and 0.002% of Tween-20, pH=7.0). A 10 μL aliquot of 1% (w/v) bead suspension was pipetted behind the edge of the bacteria swarm on the plate and left at room temperature for about 5 minutes to allow bacteria to randomly interact with and adhere to the micro-beads. At the end of the 5 minutes, the bacteria and bead suspension mixture was aspirated and subsequently pipetted in 1 mL of motility medium. A volume of about 200 μL was transferred in the experiment area as shown in Figure 4. 3.a. A one-end sealed capillary filled with a 1% (w/v) casamino acid solution, a commonly used chemo-attractant is then placed at the center of the opening of the experiment area. Figure 4. 3.b, depicts a microscope image of the experiment area and the tip of the chemo-attractant capillary.

The motion of the micro-beads was captured using a Zeiss AxioObserver Z1 inverted microscope equipped with an AxioCam HSm camera at 20 frames per second. The images were analyzed using a two-dimensional (2D) particle tracking algorithm developed in MATLAB (The MathWorks, Natick, MA). Briefly, using cell segmentation and image restoration the artifacts existing in most of the captured imaged were removed. This was followed by noise removal and cell boundary recognition using a border following algorithm. Lastly, the nearest-neighbor

method was used to link segmented cells in successive frames and to determine the bacteria-propelled beads trajectories.

b. Stochastic model of a bacterium

Flagellated bacteria such as *Escherichia coli* (*E. coli*) and *Serratia marcescens* (*S. marcescens*) possess between four and ten propulsive organelles known as flagella that are 20 nm in diameter and 10 μm long. The motility of bacteria comprises of two distinct states: run and tumble. During the run state, the flagellar motors rotate counterclockwise causing the flagella to coalesce and form a bundle which then produces a propulsion force and causes the bacterium to move forward at constant speed. Each bacterium's run is followed by a tumble. Tumble occurs when one or more of the bacterium's flagellar motors rotate in the clockwise direction causing the disruption of the bundle. During a tumble, the bacterium changes its heading direction randomly to begin a new run cycle. This leads to the stochastic motion of bacteria in 3D and can be modeled as a two-state Markov chain (as shown in Figure 4. 1) with state duration distributions occurring based on an exponential distribution [80]. Therefore, the run and tumble durations can be sampled through the following exponential distribution:

$$f(t, \lambda_i) = \lambda_i e^{-\lambda_i t} \tag{4.1}$$

Where λ_t is the average rate parameter of the exponential distribution.

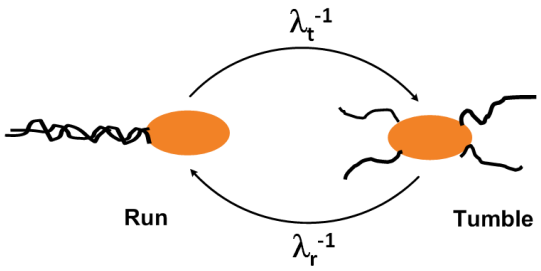

Figure 4. 1. Two-state continuous Markov chain model for a single bacterium where λ_t and λ_r are the transition rates for a tumble and a run, respectively.

The average run and tumble durations are taken to be respectively $\lambda_r \cong 0.9$ s and $\lambda_t \cong 0.1$ s in an isotropic medium (no chemical gradient) [81], [82]. However, in the presence of a positive chemo-attractant gradient, bacteria tend to extend the duration of their runs which leads to a decrease in their tumbling probability. The tumbling probability of a bacterium in a chemical attractant gradient depends on the chemical concentration at the location of the bacterium and the change in chemical concentration the bacterium is subjected to from the start to the end of a run. The tumbling probability can be computed using the following equation [83]:

$$P_t = P_0 \exp(-\sigma[\frac{\partial}{\partial t}(\frac{N_T C}{K_d + C}) + v\nabla(\frac{N_T C}{K_d + C})]) \tag{4.2}$$

where P_0 is the tumbling probability in an isotropic medium and is equal to 0.1, σ is the chemotactic sensitivity and is equal to 75,000 $\mu m^2/s$ [84], N_T is the number of homogeneous receptors and is equal to 6, K_d is the dissociation constant which is equal to 0.00014 moles, v is

the local speed of the bacterium, and C is the concentration sensed by the bacterium at any particular point in time.

At each time step, the location of each bacterium on the micro-bead with respect to a fixed reference frame is determined and subsequently, the chemical concentration sensed by each bacterium is calculated using Equation 4.3. A bacterium is set to increase its running time and therefore decrease its tumbling probability, according to Equation 4.2, when the chemical concentration it senses exceeds 3.2 nanomoles [45]. When in presence of a negative chemical gradient or in an isotropic medium, the bacterium maintains a constant tumbling probability of 0.1.

c. Chemical concentration field model

The model concentration field used in this work is based on a classic chemotaxis assay initially developed by Pfeffer and later modified by J. Adler [85]; a schematic of the setup can be seen in Figure 1. It comprises of a cylindrical capillary that contains a chemo-attractant and is placed at the entrance of an enclosure containing the bacteria-propelled micro-beads. The spatiotemporally varying chemical concentration field that is generated by diffusion of the chemo-attractant from the capillary with initial chemical attractant concentration C_0 is given by [86]:

$$C(r,t) = \frac{C_0 r_c^2}{2r\sqrt{\pi Dt}}\left[\exp\left(\frac{-r^2}{4Dt}\right) / \left(1+\frac{3r_c r}{4Dt}\right)\right] \tag{4.3}$$

Where C0 is the chemo-attractant concentration in the capillary, D is the diffusion coefficient of the chemo-attractant, t is the time from the start of the simulation, rc is the radius of the capillary, and r is the distance from the capillary to the point of interest in the experiment area. The diffusion coefficient of the chemo-attractant (1% w/v casamino acid) $D = 8.5\times10^{-10}$ m^2/s is determined according to the method described in [87].

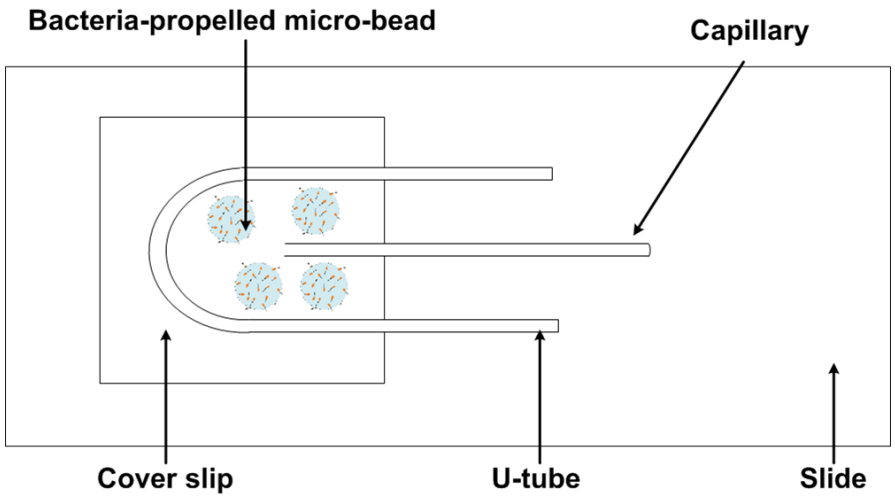

Figure 4. 2. A capillary-based chemotaxis assay was used to investigate the chemotactic behavior of bacteria-propelled micro-beads. Capillary contains the chemo-attractant solution (1% w/v casamino acids). Bacteria-propelled micro-beads are enclosed within the experiment area.

d. Stochastic model of micro-beads

The location and orientation of the bacteria attachment on the bead will serve as basis for the development of the stochastic model for dynamics of the 10 μm bead propulsion by an ensemble of attached bacteria. In this model, bacteria were assumed to be uniformly distributed over the surface of the micro-bead. The attachment density was experimentally determined to be about 1 bacterium/7μm^2 and 1 bacterium/11μm^2 in the two sets of experiments conducted. Figure 4. 3c illustrates the bacteria attachment configuration.

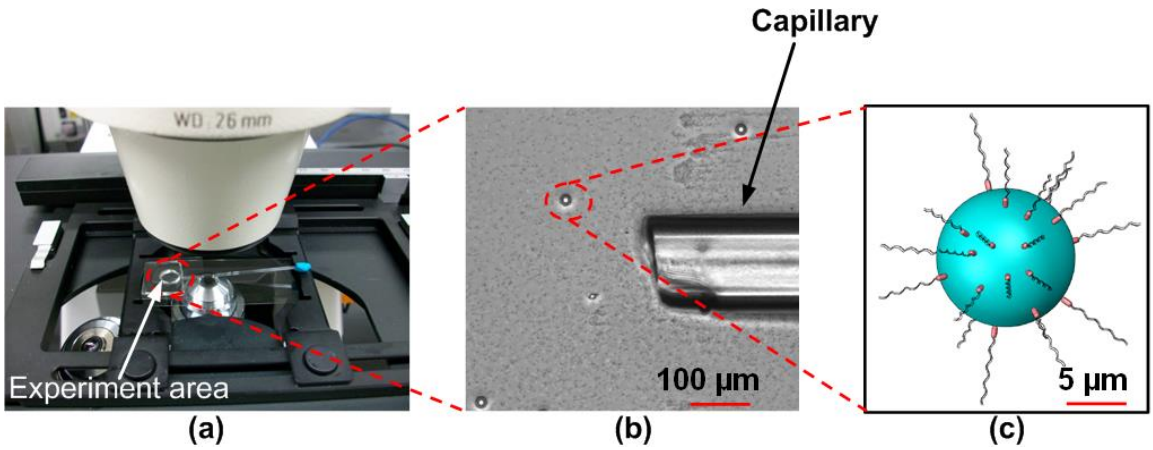

Figure 4. 3. (a) Image of the chemotaxis assay experimental setup. (b) A microscopy image of the chemotaxis assay experiment. The small particles are micro-beads propelled by an ensemble of bacteria. Chemo-attractant diffuses out from the capillary and the resulting chemo-attractant gradient field affects the dynamics of bacteria-propelled micro-beads. (c) Bacteria attach to the micro-bead at attachment densities of 1 bacterium/7 μm^2 and 1 bacterium/11 μm^2

At the start of each simulation, bacteria are randomly assigned a state of 1 (run) or 0 (tumble). A bacterium with a state of 1 will exert a force at the attachment point that equates to 0.48 pN [75]. The initial direction of the force exerted by each bacterium at the point of attachment on the surface of the bead is randomly chosen.

The dynamics of the system is assumed to be dominated by viscous effects and the inertial effects are neglected as the Reynolds number is of order of magnitude of 10^{-4}. Therefore, the overall propulsion force which results from the contributions of all the attached bacteria must equate the translational drag $\overrightarrow{F_D}$. Similarly, the overall moment the micro-bead is subjected to is equal to the rotational drag $\overrightarrow{M_D}$. This model does not take into consideration the Brownian motion, as its effect on the dynamics of the micro-bead motion is negligible when compared to

the effect of bacterial propulsion. Hence, the equations of motion governing the dynamics of the micro-bead are:

$$\overrightarrow{F_D} = 6\pi\eta r\vec{V} = \sum_b \overrightarrow{F_b} s_b \tag{4.4}$$

$$\overrightarrow{M_D} = 8\pi\eta R^3\vec{\Omega} = \sum_b \vec{r_b} \times \overrightarrow{F_b} s_b \tag{4.5}$$

Where $\vec{V}$ is the velocity of the propelled micro-bead, $\eta = 8.9\times10^{-16}$ N.s/μm^2 is the dynamic viscosity of the aqueous medium, R is the radius of the micro-bead, and $\vec{\Omega}$ is the angular velocity of the micro-bead. r_b and $\overrightarrow{F_b}$ are the position vector and propulsion force of each bacterium, respectively. s_b represents the state of each bacterium, its value is 1 when running or 0 when tumbling. Dynamics of the micro-bead were determined by taking into account the effects of all bacterial forces on the translational and rotational displacement for every time step of the simulation. The initial tumble and run time durations are assigned based on the distribution function illustrated in Equation 4.1. At the end of every time step, the change in position of each bacterium with respect to a fixed reference frame is determined. According to the change in the chemical concentration sensed by each bacterium from the start to the end of a run or tumble period, bacteria will individually sample a new run or tumble time duration. In the case of an increase of chemical concentration sensed, the bacterium will sample a new run time from the exponential distribution shown in Equation 4.1 with a higher average rate parameter λ_i. The tumble average rate parameter does not change when the chemical gradient is either null or negative.

The emergent parameters utilized to effectively characterize and compare the motion of micro-beads propelled by bacteria in both chemotactic and non-chemotactic settings are the mean velocity of the bead ($\vec{V}$), the total distance traveled by the bead (*dist*), the overall displacement value (*disp*), and the directionality. The mean velocity of every simulation run was computed by averaging the ratio of the distance traveled by the center of the bead during a time step to the duration of the time step. The mean velocity values are then averaged to determine a mean velocity value ($\vec{V}$) for the number of times the simulation was run. The total distance (*dist*) traveled by the bead is a measure of the total length traveled by the centroid of the bead from the start to the end of a single simulation, expressed as:

$$dist = \sum_{i=0}^{N} \Delta r_{bead,i} \tag{4.6}$$

These values are then averaged over the total number of simulations to obtain an average overall distance. The overall displacement (disp) is a measure of the length of the vector from the start to the end of a single simulation run, expressed as:

$$disp = \left\| \overrightarrow{r_{end} - r_{start}} \right\| \tag{4.7}$$

Its final value is obtained by averaging the displacement values over the number of times the simulation was run. The trajectories of bacteria-propelled micro-beads are of stochastic nature, therefore this parameter has not been utilized for comparison between theoretical and experimental results. In order to compare the propulsive behavior in chemotactic and non-chemotactic cases, all numerical simulations were carried out for time durations significantly

shorter than the randomization time of the micro-bead. The randomization time is the minimum time required for a system to exhibit its random walk properties and can be obtained from:

$$\tau_R^{-1} = \frac{k_B T}{8\pi\eta R^3} \tag{4.8}$$

where k_B is the Boltzmann's constant, T is the absolute temperature, η is the dynamic viscosity and R is the radius of the bead [88].

For a 10 μm diameter micro-bead, the randomization time is $\tau_R \cong 11$ minutes. Simulations with time durations of 5 seconds and longer time durations such as 30 seconds were run to observe the effect of simulation durations on the selected emergent parameters. The obtained results in both cases (5 seconds and 30 seconds) showed that the duration of the simulation has no notable effect on the velocity and the directionality. Significantly shorter time duration of 5 seconds was then chosen for the simulations mainly to compare simulations with experimental results. Most videos recorded from experiments have micro-beads in the same focal plane (minor changes in the z-direction) for short time periods that range from 5 to 10 seconds.

Both chemotactic and non-chemotactic simulations were run 400 times to identify the average stochastic behavior of the system. The 400 runs were determined to suffice as there were no major differences in the results for a larger numbers of simulation runs. The capillary radius was taken to be 100 μm and the chemical concentration in the capillary was set to C_0=0 g/mL and C_0=0.01 g/mL (w/v), respectively for the non-chemotactic and the chemotactic runs. It was assumed that the chemo-attractant concentration within the capillary remains constant throughout the simulation.

4.3 Results

a. Experimental validation of stochastic model for 10 um diameter bead

The simulation results for both chemotactic and non-chemotactic cases are presented in Table 4. 1. All four characteristic parameters are affected by the presence of the chemo-attractant concentration field. The micro-beads' mean velocity increased by about 12% from the non-chemotactic to the chemotactic environment. Over the simulation duration of 5 seconds, the directionality of the propelled micro-bead saw an increase of 67% when the micro-bead was in a chemotactic environment with an initial capillary concentration C_0=1% (w/v). A higher directionality value indicates a more directed motion of the bacteria-propelled micro-bead. The increase in the characteristic parameters is attributed to the fact that the chemical gradient sensed by the bacteria affects their tumbling probability P_t. A reduction in the tumbling probability implies an extension in the run period for each bacterium propelling the micro-bead, which will result in not only a larger overall distance but also a more directional path for the motion of the micro-bead.

In order to validate the stochastic model presented here, a chemotaxis assay for bacteria-propelled micro-beads was conducted and the experimental data was compared with the computational results.

Table 4. 1. Summary of results comparing simulations and experiments in chemotactic and non-chemotactic environments for a bacteria attachment density of 1 bacterium/7μm^2

C_0 (% w/v)	Model		Experiment	
	0	0.01	0	0.01
V(μm/s)	8.6 ± 0.6	9.6 ± 1.2	8.5 ± 1.7	9.2 ± 1.3
disp (μm)	11.3 ± 4.4	19.3 ± 3.9	13.4 ± 6.2	21.9 ± 6.4
dist (μm)	37.2 ± 2.7	41.8 ± 4.9	42.7 ± 8.3	46.1 ± 6.8
disp/dist	0.3 ± 0.1	0.5 ± 0.1	0.3 ± 0.1	0.5 ± 0.1

Table 4. 2. Summary of results comparing simulations and experiments in chemotactic and non-chemotactic environments for a bacteria attachment density of 1 bacterium/11μm^2

C_0 (% w/v)	Model		Experiment	
	0	0.01	0	0.01
V(μm/s)	8.0 ± 0.6	8.8 ± 0.8	6.4 ± 1.2	7.5 ± 1.5
disp (μm)	7.4 ± 3.3	18.6 ± 7.5	7.1 ± 4.6	22.2 ± 7.6
dist (μm)	34.2 ± 2.9	37.9 ± 3.7	38.9 ± 6.0	44.9 ± 9.4
disp/dist	0.2 ± 0.1	0.5 ± 0.2	0.2 ± 0.1	0.5 ± 0.1

The trajectory information was used to determine the average speed, distance, displacement and directionality over the 5 second duration of the experiments. Experimental results are presented in Table 4. 1 and Table 4. 2. Each data point represents an average of at least ten experiments. The trajectories of the bead do vary between experiments because of the stochastic nature of

bacteria motion. Representative examples of the bead trajectories are shown in Figure 4. 4. Addition of chemo-attractant in the environment contributes to an increase in the directionality value as well as the overall speed of the micro-bead. This can be explained by prolonged force exertion by those attached bacteria which sense an increasing chemical attractant concentration. This will result in an overall extension of the displacement of the micro-bead in a directional manner. The experimental results obtained in both chemotactic and non-chemotactic cases closely match the results obtained from the computational model. The small differences between the computational and experimental results suggest that this computational model can be used as an effective prediction tool in both chemotactic and non-chemotactic environments.

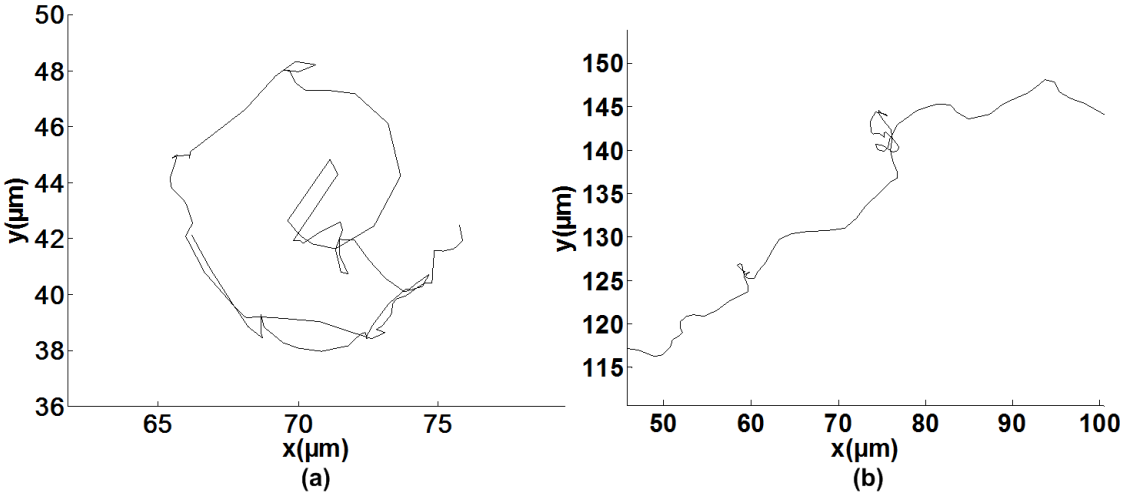

Figure 4. 4. Sample bead trajectory in (a) absence of chemo-attractant and (b) in a chemo-attractant gradient environment with 1% chemo-attractant in the capillary.

b. Effect of bacteria attachment density on micro-bead motion

The effect of the density of bacteria attachment was also explored experimentally by constructing bacteria-propelled beads at two attachment densities of: 1 bacterium/7μm^2 and 1 bacterium/11μm^2. Table 4. 1 and Table 4. 2 show the results for both bacteria attachment densities.

Reducing the bacteria attachment density results in fewer bacteria attached to the micro-bead. In the case of fewer bacteria attached to the micro-bead (no significant non-uniformity in bacteria attachment), the overall force is expected to remain unchanged or slightly reduce (based on degree of variation in attachment density). Indeed, we observe only slight variations in speed and directionality values when the bacteria attachment density is changed from 1 bacterium/7 μm^{2}to 1 bacterium/11 μm^2.

More than the number of bacteria attached to the micro-bead, the location of attachment is expected to affect the overall behavior. If the attachment density becomes significantly non-uniform, we expect to see a change in the average net resultant force and consequently observe a change in overall speed and displacement to distance ratio. In a prior work, the effect of bacteria attachment site on overall speed in an isotropic (non-chemotactic) environment was investigated [89].

c. Effect of fluid viscosity and particle size on micro-bead motion

The viscosity of the fluid will affect the speed, the displacement and the distance traveled by the micro-bead. However, the directionality will stay unchanged as long as all other parameters are kept same. This is due to the fact that the speed of the micro-bead is proportional to the net force it is subjected to. An increase in the viscosity of the fluid will result in an increase in the drag force and a decrease in the net propulsion force. This will in turn affect the distance traveled for a given period of time. Similarly, the displacement will change with the same rate the distance varies by. Therefore, when the viscosity of the media is changed, the directionality of the micro-bead stays the same while the speed decreases.

The size of the micro-bead should not have a significant effect on the displacement to distance ratio from a non-chemotactic to a chemotactic case assuming that the bacteria attachment density is kept constant. It has previously been demonstrated that for unpatterned particles the net propulsion force is linearly proportional to the radius [75], [77]. According to the Stokes equation, the drag force is also linearly proportional to the radius. Therefore, for the "same attachment density" the drag and propulsion forces change as a function of radius and the net force should not change significantly. This assertion is supported by the simulation code, which shows that the speed and the ratio of displacement to distance vary slightly when the radius of the bead is changed and the bacteria attachment density is kept intact.

4.4 Conclusions

In summary, a stochastic model for chemotactic propulsion of micro-beads is presented in this study. The model encompasses key parameters including orientation and location of the attached bacteria; spatiotemporal variations in chemo-attractant concentration field and its effect on run and tumble rates of each of the tens of the attached bacteria. This numerical model was validated experimentally and it was shown that it can effectively describe the emergent dynamics of the motion of a 10 μm micro-bead propelled by an ensemble of flagellated bacteria homogeneously attached, in both chemotactic and non-chemotactic environments. The description of the motion of the micro-bead was based on four emergent parameters of average speed, displacement, distance and directionality. It was determined that all four parameters increase from the non-chemotactic to the chemotactic case. Most notably, the results show that the presence of a chemo-attractant gradient results in 67% larger directionality values. This proves the feasibility of directed autonomous movement of bio-hybrid micro-robots through the use of chemotaxis.

This model can be easily expanded to serve as a predictive tool for other bio-hybrid systems with different whole cell actuators, non-spherical geometries, heterogeneous whole-cell actuator attachment configurations, and different spatiotemporally varying chemical concentration gradients.

Appendix B: Chemotactic model of a single bacterium in a linear chemical attractant field

We have developed a kinematic model that describes the movement of a single bacterium in a 3D fluidic milieu. This model is structured around 2 specific points:

1) Stochastic behavior of a bacterium (run and tumble behavior) as a function of the chemical field surrounding the bacterium.
2) 3D referential change that allows the tracking of the bacterium.

An aspect that is not taken into account in this kinematic model is the variation in speed of the bacterium as a function of the drag experienced during its motion. We hypothesize that the drag force experienced by a single bacterium will change as a function of the size, the location and number of nanoparticles attached to its body.

A spatially varying linear chemical concentration field was generated from a point source and the chemotactic motion of a single bacterium towards the chemical source was simulated.

The equation for the linear chemical profile is given by the following equation:

$$C(r) = 0.4 - (10^{-6}) \times \mathrm{r} \tag{4.9}$$

where r is the position of the bacterium at any given point in time. r is expressed in [µm] and C is expressed in [% g/mL].

The directionality of the bacterium's movement in 3D is evaluated using the angle formed by the ideal path vector and the displacement vector as shown in the figure below:

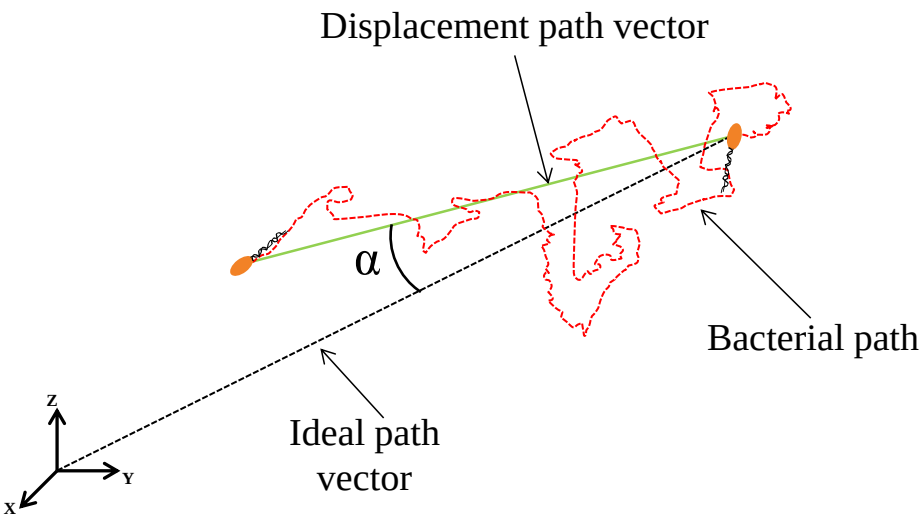

Figure 4. 5. Path of a bacterium in a 3D fluidic milieu

The directional chemotactic index can be calculated using the following equation:

$$D.C.I = \cos(\alpha) \tag{4.10}$$

The simulation results for both chemotactic and non-chemotactic cases are presented in Table 4. 1. Three characteristic parameters were used to describe the motion of a single bacterium. The trajectory information was used to determine the distance, displacement, the displacement/distance ratio and the directional chemotactic coefficient over the duration of the experiments.

Table 4. 3. Summary of simulation results comparing chemotactic and non-chemotactic environments for a single bacterium in a 3D fluidic environment.

Chemical gradient ΔC_0 (% g/mL)	Single bacterium motion	
	0	0.4
disp (µm)	3894.1 ± 650.6	1667.8 ± 691.8
dist (µm)	21435.0 ± 762.6	27421.0 ± 1159.3
disp/dist	0.18 ± 0.03	0.06 ± 0.02
D.C.I	-0.60 ± 0.14	0.32 ± 0.53

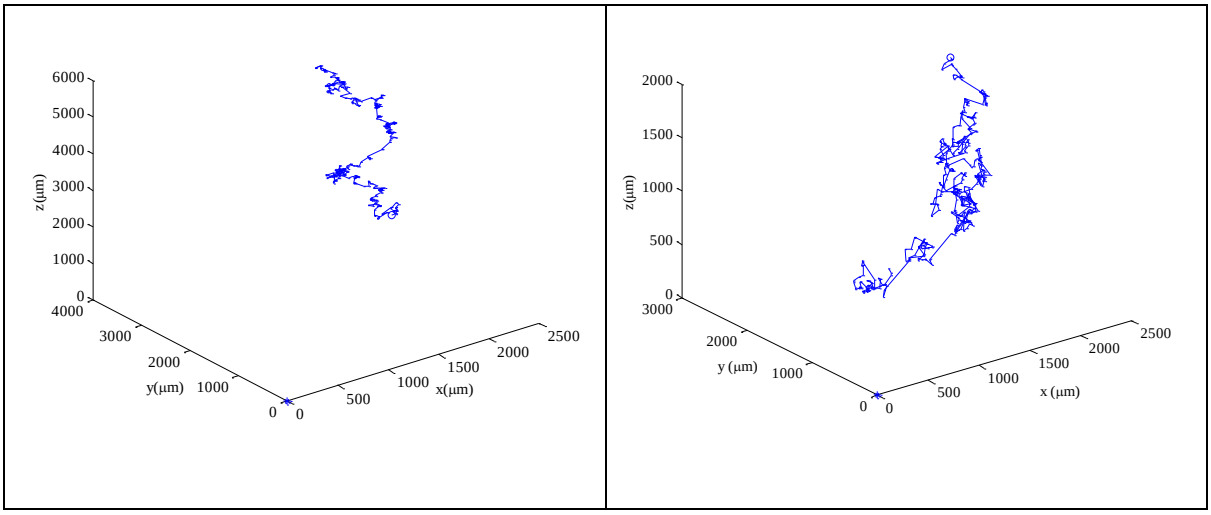

Figure 4. 6. Sample bacterial trajectory in (left) absence of chemo-attractant and (right) in a chemo-attractant gradient environment with 0.4% (w/v) chemo-attractant in the capillary. The circle on the bacterial path is representative of the starting point and the star at coordinates (0,0,0) is representative of the chemical attractant source.

Appendix C: Simulation operation details

At the beginning of the simulation, each bacterium will randomly sample a run or tumble time to execute. In the event a bacterium tumbles initially, it would then select to run for a time duration sampled from the run time exponential distribution (average of 0.9s). At the end of the run, the bacterium will tumble for a duration randomly sampled from the tumble time exponential distribution (average of 0.1s). It will then evaluate the chemical concentration it senses and compare it with the chemical concentration it sensed at the beginning of its previous run state. If the chemical concentration difference is higher than or equal to 3nM, the bacterium would elect to run with a higher run time exponential distribution (average ~ 1.3s). The simulations are conducted 400 times using different initial conditions to truly capture an average behavior from the bacteria-propelled micro-beads.

Table 4. 4. Parameters used in the simulation. The values shown here can be modified to reflect desired conditions.

Variable	Value	Description
λr_ave	0.9 s [43]	Average run time
$\lambda r'\_ave$	1.3 s	Chemotactic run time
λt_ave	0.1 s [43]	Average tumble time
$\lambda t'\_ave$	0.1 s [43]	Chemotactic tumble time
V	25 μm/s	Average speed of *S. marcescens*
dt	0.01 s	Time step
dCmin	3 nM [45]	Chemotaxis detection threshold
F_b	0.48 pN [75]	Bacteria propulsion force
χ_0	75000 $\mu m^2/s$ [84]	Chemotactic sensitivity

Chapter 5: Construction and dynamic studies of Nanoscale Bacteria Enabled Autonomous Delivery Systems (NanoBEADS)

Abstract

Bacteria are fascinating micromachines that have the natural ability to propel themselves in fluidic and porous microenvironments. This innate aptitude makes them an attractive choice for microrobotic applications. In this work, bio-hybrid microrobotic systems consisting of spherical polystyrene nanoparticles self-assembled on the body of *E. coli* bacteria are developed for drug-delivery applications. The construction and dynamics of these nanoparticle bacteria enabled autonomous drug delivery systems (NanoBEADS) are studied in isotropic fluidic environments. We show that the 3D motion of NanoBEADS is dependent upon the nanoparticle size and attachment site. These bio-based micromachines can be utilized as single agent or as a swarm in order to carry out specific tasks that have a wide range of applications.

5.1 Introduction

Recent developments in MEMS and NEMS offer tremendous hope for the use of microrobotic agents towards in-vivo diagnosis and treatment of diseases, environmental monitoring, etc. The challenges however in microrobotics are numerous; some of the issues that still remain unsurmountable despite notable advances within the field are the lack of proper power storage, locomotion and embedded intelligence [90]. Whole cell actuators, such as flagellated bacteria offer quite an incredible solution to few of the aforementioned challenges. To this end, bacteria-based bio-hybrid micro systems have been developed to address the actuation and powering challenges in microrobotics [59], [60], [76–78], [89–94]. Flagellated bacterial cells utilize chemicals already present in their native environments as source of energy [85]. Using that energy, they self-propel in fluidic and semi-solid environments by alternating run and tumble motions in a stochastic manner [81], [95]. They also have the ability to sense and respond to their microenvironment (chemical and physical cues) exceedingly well. To this date, bacteria remain the most advanced microrobotic system due to their unmatched ability to sense and react to their microenvironment and even send and receive information from the outside world. These same characteristics have motivated many researchers to use bacteria as living component of bio-hybrid microrobotic system in order to achieve specific tasks such as micro/nano-loads transport and micromanipulations [78], [92].

In this work, we utilize peritrichous bacteria *E. coli*, with all the advantages described above coupled with nanoparticles to develop bio-hybrid microrobotic agents capable of carrying nanoscale load and achieving a wide array of tasks (e.g. sensing, communication, etc.). A complete understanding of the construction (nano-loads attachment rate and location to the body of bacteria) and motile behavior (speed, drag force) of these microrobotic systems is crucial as

bacteria have been proposed as targeted drug delivery agents against solid tumors [8], [13]. Specifically in this study, we aim to examine nano-loads attachment to the body of bacteria and analyzed the kinematic behavior of the subsequent microrobotic agents in aqueous environments. This study was rendered possible by attaching nanoparticles of two different sizes to the body of a bacterium, after which, the dynamics of the system in terms of speed and drag effects on the movement of the NanoBEADS was studied in a fluidic and isotropic environment. The attachment utilizes one of the strongest non-covalent bond found in nature; the streptavidin biotin binding.

5.2 Materials and methods[2]

The bacteria *Escherichia coli* MG1655m, a derivative of *E. coli* MG1655 [96] from the K-12 family with increased motility was used in all experiments conducted in this work. Bacterial cultures from a single colony were incubated overnight in 10 mL of fresh Luria Bertani (LB) Broth (1% w/v of tryptone, 0.5% w/v of NaCl, 0.5% w/v of yeast extract) supplemented with 10 µg/mL of tetracycline in an incubator shaker (30° C, 150 rpm). A 100 µL aliquot of the overnight culture was inoculated in 10 mL of fresh LB. 1 mL aliquot of the liquid culture (OD_{600}=0.5) was then centrifuged at low speed (1,700 × g) for 5 minutes at room temperature and suspended in 1 mL of motility buffer (0.01 M potassium phosphate, 0.067 M sodium chloride, 10^{-4} M ethylene diamine tetra-acetic acid (EDTA), 0.01 M glucose, and 0.002% (v/v) Tween-20).

Bacteria were washed twice in motility buffer and incubated with 10 µg/mL of goat polyclonal anti-Lipid A LPS antibody labeled with biotin. The suspension was gyrated on a vortex shaker for one hour at 600 rpm to favor antibody attachment to the body of bacteria. The bacterial suspension was then centrifuged at low speed (1,700 × g) for 5 minutes at room temperature to remove the free antibody from the solution and was resuspended in 50 µL of motility buffer. Streptavidin-coated nanoparticles (109 nm diameter and 390 nm diameter) were agitated with biotin-covered bacteria at a desired ratio for 30 min.

Microscopy images and time-lapse videos of NanoBEADS were captured using a Zeiss AxioObserver Z1 inverted microscope equipped with an AxioCam mRM camera and a 63× oil objective. The recorded images and videos were obtained with Zen Blue 2012 software (Zeiss

[2] The NanoBEADS construction protocol was developed in collaboration with Ph.D. candidate Ali Sahari, a colleague from our MicroN BASE laboratory.

Microscopy, Oberkochen, Germany). Scanning electron micrographs of NanoBEADS were acquired using a FEI Quanta 600 FEG environmental scanning electron microscopy.

5.3 Results and discussions

Using the method described in the Materials and methods section, NanoBEADS with different nanoparticles sizes can be constructed as seen in Figure 5. 1.

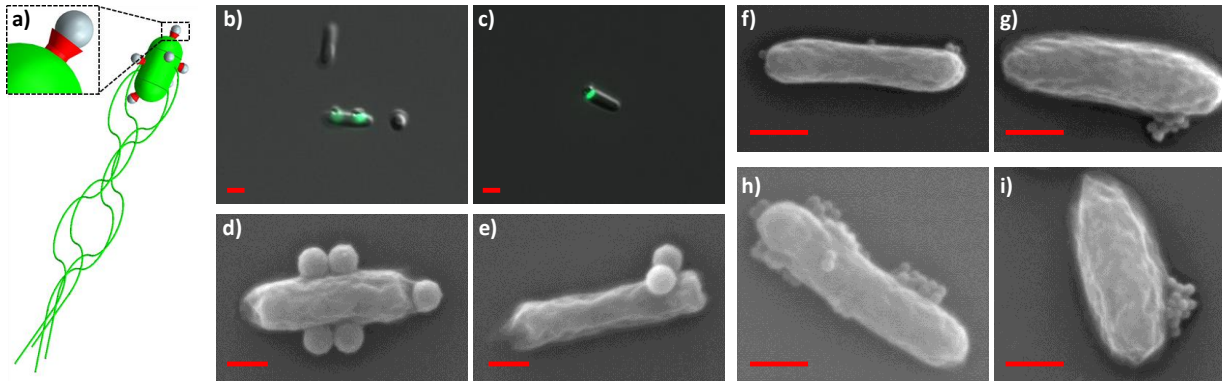

Figure 5. 1 Examples of NanoBEADS configuration, a) Schematic of construction of NanoBEADS showing streptavidin-biotin bond between a bacterium and nanoparticles, b)- c) Optical microscopy images of 390 nm particles attached to bacteria, d) and e) SEM images of 390 nm particles attached to bacteria, f)- i) SEM images of 109 nm particles attached to bacteria. All scale bars are 500 nm.

One of the principal objectives of this study was to investigate the effect of streptavidin- coated nanoparticles to bacteria ratio on NanoBEADS construction yield rate. Three ratios of nanoparticles to bacteria were investigated in this study. The attachment yield for different ratios used is illustrated in Figure 5. 2.

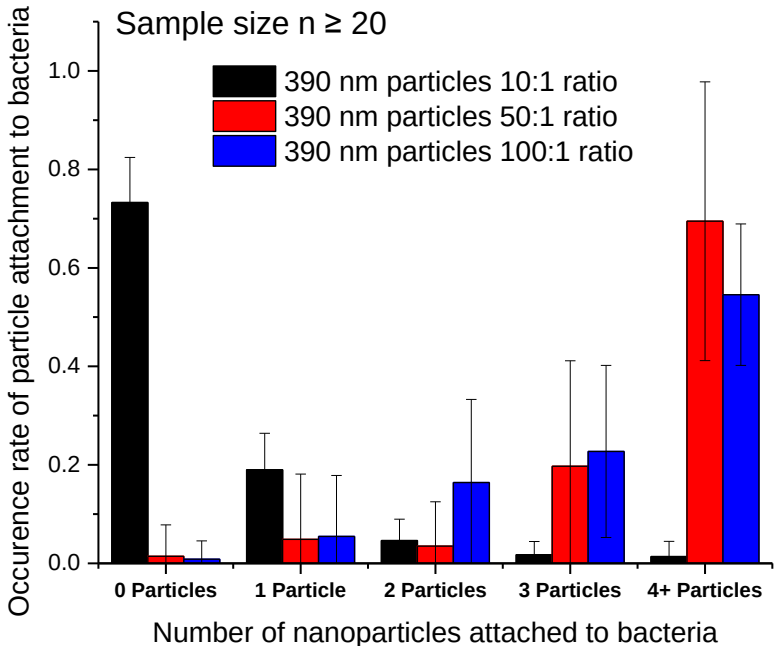

Figure 5. 2. Rate of occurrence of nanoparticles attachment to bacteria for 390 nm particles, determined experimentally.

As illustrated in Figure 5. 2, the number of bacteria carrying nanoparticles can be increased by augmenting the initial number of nanoparticles utilized during the self-assembly process. This phenomenon can be better understood through a theoretical framework developed by Smoluchowski based on aggregation kinetics [97]. Bacteria and nanoparticles are mixed under uniform and laminar shear conditions. According to the Smoluchowski theory for orthokinetic aggregation as illustrated by Eq. (5.1) and (5.2), the total number of collision can be increased by augmenting the initial number of nanoparticles and bacteria in the mixture as well as the rate coefficient. The rate coefficient and total number of collision respectively for orthokinetic collisions can be determined using the following equations:

$$k_{bp} = \frac{G}{6} \times (\mathrm{d}_b + d_p)^3 \tag{5.1}$$

$$J_{bp} = k_{bp} \times N_b \times N_p \tag{5.2}$$

Where N_b and N_p are the number concentrations of bacteria (b) and particles (p); G is the fluid shear rate (the value of G is constant throughout all experiments); d_b and d_p are respectively the diameters for bacteria (approximately 500 nm) and nanoparticles (390 nm and 109 nm in diameter).

The effects of the nanoparticle size are tremendous because larger particles have a tendency to favor higher rate coefficients of collision Eq. (5.1). This is an important parameter to take into account in the design of these microrobotic systems in order to increase the yield of NanoBEADS. For smaller nanoparticles, viscous effects that arise from the hydrodynamic interactions between bacteria and nanoparticles during orthokinetic aggregation may prevent collision [97]. Because of the low Reynolds number regime present during aggregation, particles tend to follow a curved path near the body of bacteria. This leads to larger separation distances between the nanoparticle and the body of the bacterium, thus limiting collision between the two.

The motile behavior of the NanoBEADS was studied to determine a kinematic parameter: the speed over known durations. As stated earlier, two particles sizes were employed for these studies. To ensure that the kinematics of the NanoBEADS is well captured and different from that of free swimming bacteria, NanoBEADS were constructed using a higher nanoparticle to bacteria ratio. As shown in Figure 5. 2, a higher ratio of nanoparticle to bacteria guarantees that every bacterium carries at least a particle. The kinematic parameters utilized to describe the motile behavior of the NanoBEADS do not differentiate a bacterium carrying a single

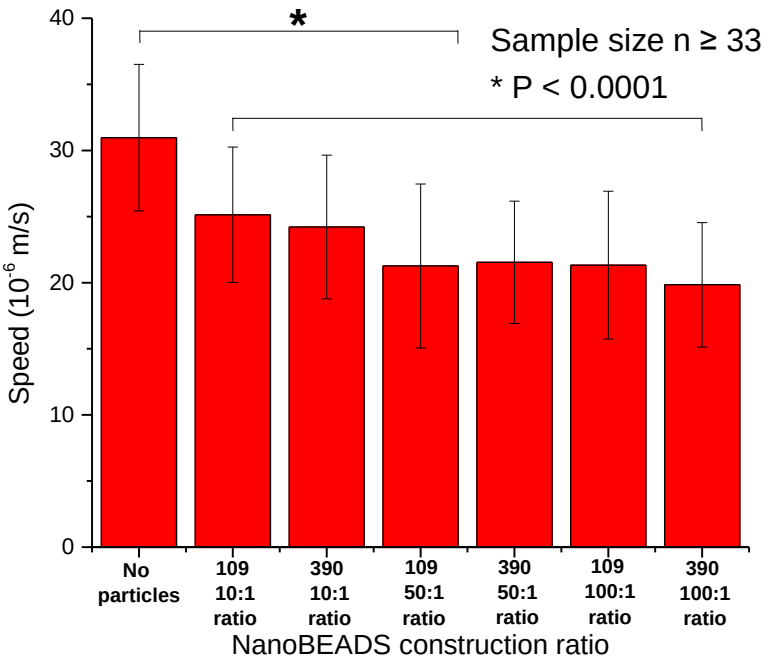

Figure 5. 3 Average speed of NanoBEADS for different construction ratios. (* P<0.0001, the speed of free swimming bacteria is higher than that of NanoBEADS.

nanoparticle from a bacterium carrying multiple. This is due to the fact that conventional microscopy does not permit a precise count of the number of nanoparticles attached to the body of a bacterium moving in an aqueous environment. The average speed and the standard deviation for free swimming bacteria, motile 109 nm NanoBEADS and motile 390 nm NanoBEADS are summarized in the Figure 5. 3.

The data shown in the graph are only taking into account NanoBEADS that are motile (about a third of the NanoBEADS have average speed above 5 μm/s). As seen, free swimming bacteria have swimming speed of approximately 30 μm/s. This average speed value is in accordance with previous speed values recorded for *E. coli* [98]. We measured a 17 % drop in average speed for NanoBEADS constructed with 109 nm and 390 nm diameter particles. The similar speeds recorded for both 50:1 and 100:1 ratio may be attributed to the clumping of 109 nm nanoparticles

during the self-assembly process. The aggregates formed have sizes that are close to larger nanoparticles (i.e. 390 nm particles), which leads to similar kinematic behavior of the NanoBEADS (Fig. 6.1 (i)-(f)). These findings imply that loading bacteria with nanoparticles has the potential to decrease their swimming capabilities. In fact, a considerable number of bacteria after nanoparticle attachment lose their motility (about 70%). This phenomenon is not only attributable to the size and number of nanoparticles attached to the body of the bacterium but is a direct effect of nanoparticle attachment location to the bacterium. *E. coli* are peritrichous bacteria with random distribution of flagella on their body as shown in Figure 5. 4.

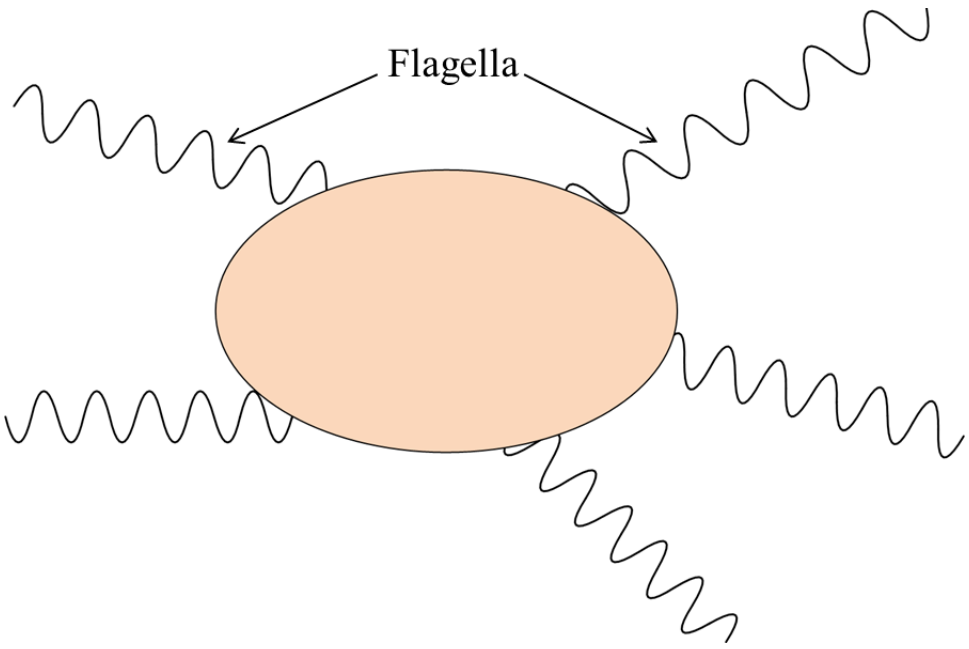

Figure 5. 4. Illustration of peritrichous bacteria, flagellar structures are randomly distributed on the bacterium's body

Given the size of the flexible hook in the flagellar assembly, it is plausible that one or more of the bacterial flagellar structures may directly interact with nanoparticles, leading to disturbance

in the flagellar bundle formation and compromised motility. Moreover, the attachment of nanoparticles to the body of a bacterium can increase the overall drag force the bacterium experiences as it moves in the fluid. To theoretically demonstrate the impact nanoparticles loading can have on the damping coefficient (defined as C) of carrier bacteria, a 3 dimensional COMSOL model of a bacterium carrying nanoparticles was developed. The damping coefficient is the ratio of the drag force of the NanoBEADS to its velocity. In this model, we first varied the location of a single nanoparticle attachment site to verify the location of maximum damping coefficient (data not shown). In the loading scenarios considered, the nanoparticle attachment location is chosen to obtain the maximum drag force on the NanoBEADS. We determined a relationship between the damping coefficient and the number of nanoparticles attached to the bacterium as illustrated in Figure 5. 5.

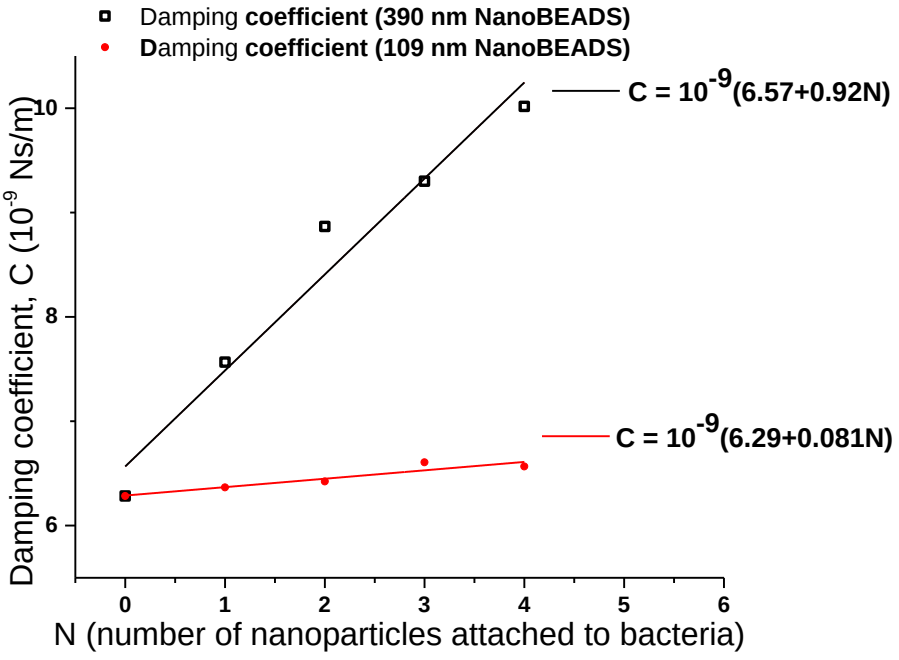

Figure 5. 5 Damping coefficients of NanoBEADS as a function of particles attached, determined using COMSOL®.

Using this relationship, we show that the drag force originating from nanoparticles attachment to bacteria can contribute to a decrease in average swimming speed of a bacterium. To illustrate this finding for the 390nm NanoBEADS' case, we determined a weighted average of the damping coefficient for each loading ratio scenarios, using the occurrence rate data from Figure 5. 2, and the damping coefficient data from Figure 5. 5. The weighted average for each loading ratio scenarios can be obtained using the equation below:

$$C_{ave} = \sum_{i=0}^{4+} Occurence\_rate_i \times damping\_coefficient_i \tag{5.3}$$

The corresponding average velocities can then be determined by using the ratio of the propulsion force of a single bacterium (0.189 pN; value determined from COMSOL model) to the average damping coefficient. Using this method only for the 390 nm NanoBEADS, the average speed values for each loading ratio scenario are found to be respectively 27.92 μm/s for the 10:1 ratio loading scenario, 19.69 μm/s for the 50:1 ratio loading scenario and 19.84 μm/s for the 100:1 ratio loading scenario. As seen in **Error! Reference source not found.** the calculated average peeds for each of the loading ratio scenario of the 390 nm NanoBEADS are in agreement with the experimental speed values shown in Figure 5. 3.

Table 5. 1. Comparison of speed data between experiment and theoretical speed data obtained from COMSOL simulations

390 nm NanoBEADS			
Loading ratio scenario	Average experimental speed (μm/s)	COMSOL theoretical speed (μm/s)	Difference (%)
10 to 1	24.21	27.92	15.33
50 to 1	21.54	19.69	8.58
100 to 1	19.85	19.84	0.03

These calculations demonstrate that nanoparticles loading on bacteria can reduce the overall speed of bacteria but not significantly as seen in **Error! Reference source not found.**. The elatively good match between experimental and theoretical speed data suggest that the COMSOL model developed is a good representation of experimental conditions and can in fact be used to predict the speed of other NanoBEADS configuration without having to resort to experiments.

5.4 Conclusion

In summary, we report the construction of NanoBEADS using one of the strongest non-covalent bonds found in nature. We were able to demonstrate that an increase in initial particle number with respect to bacteria number can contribute to a higher yield in nanoparticle attachment to bacteria attachment. In this work, we lay down the foundation to better construct hybrid microrobotic systems that use bacteria as means of locomotion. We discussed a procedure that relates the ratio between particle and bacteria number with the objective to increase the yield of NanoBEADS constructed. We have demonstrated that smaller sizes nanoparticles will not significantly deteriorate the natural transport ability of bacteria, the damping coefficient for the 109 nm NanoBEADS is only 3.1% higher than the damping coefficient experienced by a single bacterium swimming in an aqueous environment, especially if the location of nanoparticle attachment does not interfere with the flagella of the bacterium.

Appendix D: Bacterial Chemotaxis Enabled Autonomous Sorting of NanoBEADS[3]

Introduction

One major drawback in the construction of NanoBEADS using a larger nanoparticle to bacteria ratio is its direct effect on bacteria motility. As shown previously, the average speed of NanoBEADS due to nanoparticles loading decreases, and about two third of bacteria become immotile nanoparticle attachment. To circumvent this issue, we propose the utilization of motility and chemotaxis in flagellated bacteria for autonomous separation of motile NanoBEADS from non-motile ones within a microfluidic platform.

State-of-the-art robotic manipulation and assembly of micro/nanoscale objects require sophisticated hardware, computationally expensive control strategies and highly skilled users. Existing sorting methods [99] such as optical, magnetic and electrical separation often require set-ups that are costly and do not always perform well when the objects that need to be sorted are of similar size.

Therefore, new approaches are needed in order to increase micro-manipulation and assembly throughput rate and decrease the associated costs. In recent years, a paradigm shifting approach which utilizes biomotors has been proposed by a few researchers [76], [100]. Here, we introduce a bio-hybrid microrobotic approach in which the motility and chemotaxis in flagellated bacteria is harvested for autonomous sorting of NanoBEADS and possibly other micro/nanoparticles. It has been shown in the past that bacteria can be effectively used for the controlled actuation of micro/nanoscale objects [75], [77], [78], [89], [92]. Martel et al. [101] showed that microscale bricks can be manipulated and assembled into a pyramid using magnetotactic bacteria and a

[3] MAT and BB developed the design for the chemotaxis enabled sorting of NanoBEADS. Some of the experiments were conducted in collaboration with SeungBeum Chris Suh, a Ph.D. candidate in our MicroN BASE laboratory.

computer controlled external magnetic field. We have previously shown that bacteria-propelled micro-particles are capable of chemotaxis in presence of a chemo-attractant gradient [59], [102], [103].

In this work, we utilize bacteria-based propulsion combined with the concept of chemotaxis (i.e. bacteria response to chemical gradients) to sort motile NanoBEADS from non-motile ones. The use of chemical energy as power source, bacteria flagellar motor as actuators, and chemotaxis as controller makes this autonomous micro-systems sorting platform a cost-effective, compact, and fully self-contained system. This platform offers significant flexibility compared with other microfluidic based approaches such as dielectrophoresis or optical tweezers, in which particle dielectric properties or required forces can limit the applications. In contrast with probe-based systems such as atomic force microscope (AFM), the proposed platform can easily achieve parallel operation and higher throughput autonomous manipulation can be more easily achieved.

In this work, we have designed, modeled, and constructed a microfluidic workspace based on the microfluidic device discussed in Chapter 2 in which NanoBEADS are autonomously sorted using their chemotactic capability. The findings from this work will be used towards determining the requisite mechanical, physicochemical, and biological properties of such bio-hybrid manipulation and assembly workspaces.

Methodology

Design of experiment

The proposed microfluidic workspace is composed of a chemo-attractant channel, a work area and a buffer channel as shown in Figure 5. 6. The bulk of the device is made from polyethylene glycol diacrylate (MW = 700 Da). The chemo-attractant channel is filled with the chemo-attractant casamino acid at a concentration that will induce maximum chemotactic response from the bacteria. PEG-DA enables controlled and slow release of chemo-attractant such that the chemical gradient can be maintained for up to a few hours and bacterial chemotaxis can be effectively utilized for sorting during this time period. The work area contains the NanoBEADS both motile and non-motile. In presence of an appropriately designed chemo-attractant gradient, it is expected that the motile NanoBEADS will be autonomously transported towards the chemo-attractant side of the center channel while the non-motile NanoBEADS will be left behind in the center of the work area due to lack of mobility.

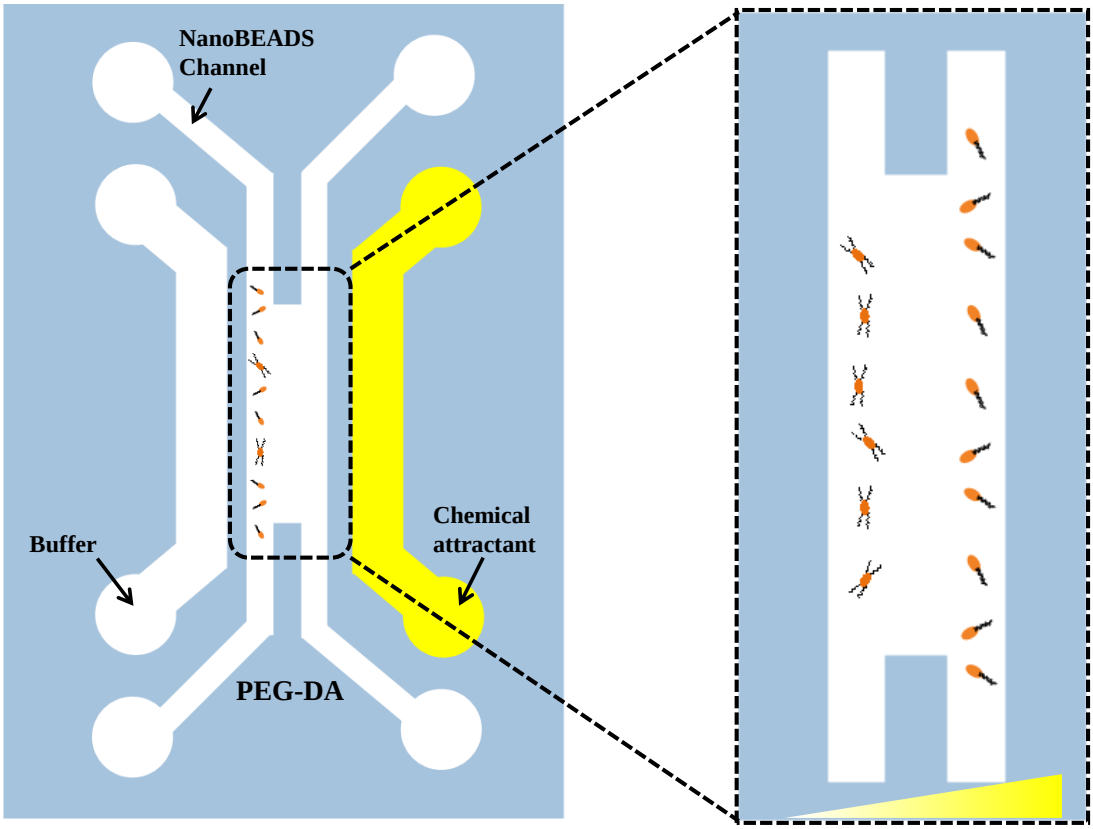

Figure 5. 6. Schematic of microfluidic platform used for autonomous sorting of NanoBEADS

Device fabrication

A one-step photolithography process was used to fabricate the microfluidic device. A rectangular PDMS enclosure of known thickness is first bonded to a glass slide using oxygen plasma (PDC-32G, Harrick Plasma, Ithaca, NY) for 30 s at 18 W. To ensure good sealing between the PEG-DA device and the underlying glass substrate, the glass surface was functionalized using a TPM (3-(Trichlorosilyl) propyl methacrylate) solution (Sigma-Aldrich, St. Louis, MO). The glass surface was first rendered hydrophilic using oxygen plasma (200 mTorr, 18 W, 5 minutes). This step is important as it removes all inorganic compounds and promotes hydroxylation of the

surface. A 1% (v/v) TPM solution dissolved in paraffin oil (Sigma-Aldrich) was prepared. The silane solution was poured in the enclosure and incubated at room temperature for 10 minutes [55], [56]. After incubation, the enclosure was thoroughly rinsed with ethanol and hard baked at 95 °C. Subsequently, the liquid PEG-DA was poured within the enclosure until it was completely filled. A glass mask was placed on the PDMS enclosure containing the liquid hydrogel. The photopolymerization was carried out by UV light exposure (365 nm, 18W/cm^2, Omnicure S1000, Vanier, Quebec) for 15 seconds. The areas of the PEG-DA solution exposed to the UV light cure due to the photopolymerization process. The non-polymerized regions are removed by rinsing the device.

Results and discussions

A mass transport simulation of casamino acid solution using finite element analysis software package COMSOL for the determined diffusion coefficient was performed as illustrated in Figure 5. 7. In this analysis, the chemo-attractant contained in one of the outermost channel will diffuse out through the gel walls into the work area.

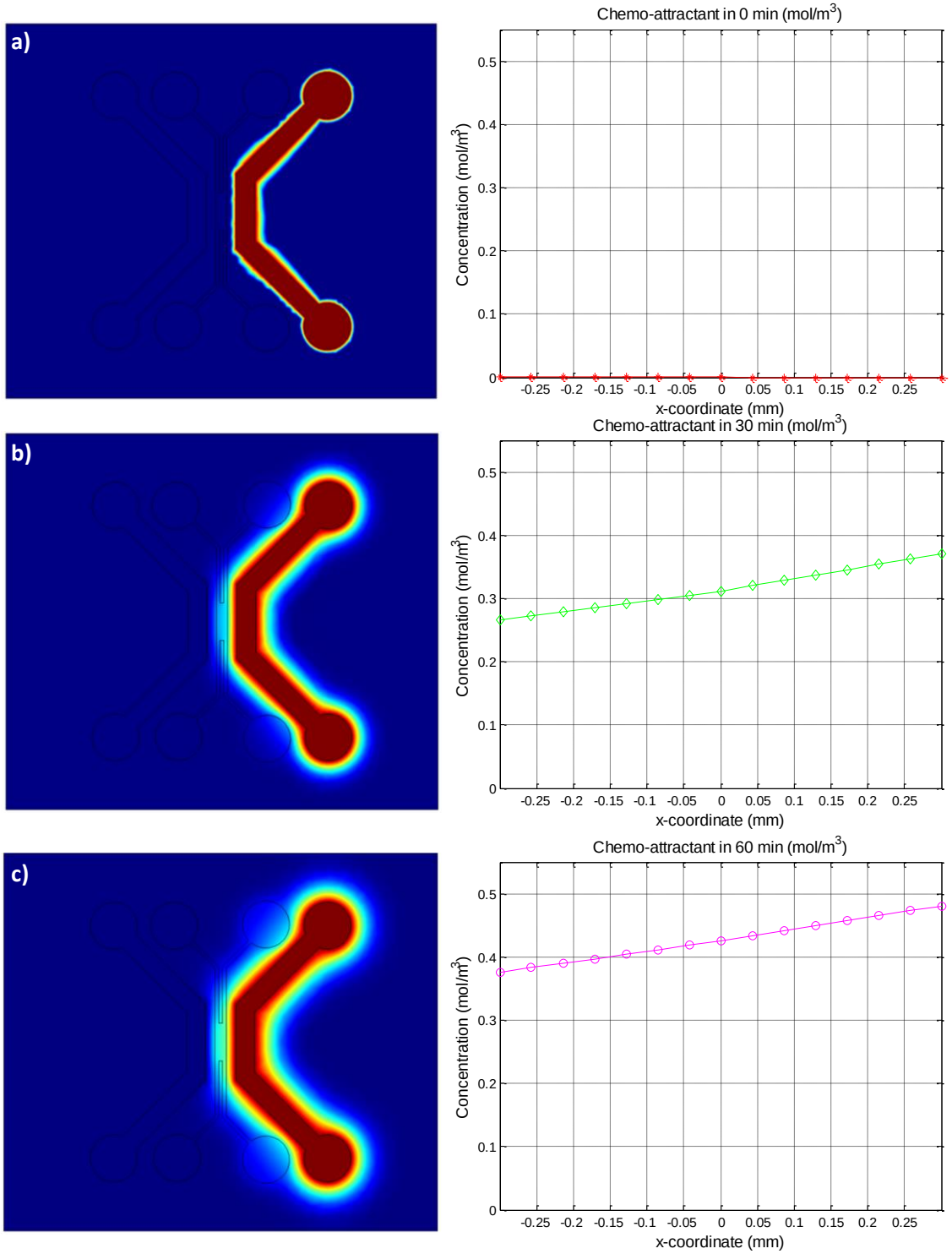

Figure 5. 7. COMSOL simulation result show the chemical concentration distribution within the micro-device at a) t =0s, b) t = 1800s and c) t =3600s

The number of NanoBEADS in the chemo-attractant side of the work area was measured as a function of time. Figure 5. 8 shows the chemotactic coefficient increase of NanoBEADS in the work area as time increases.

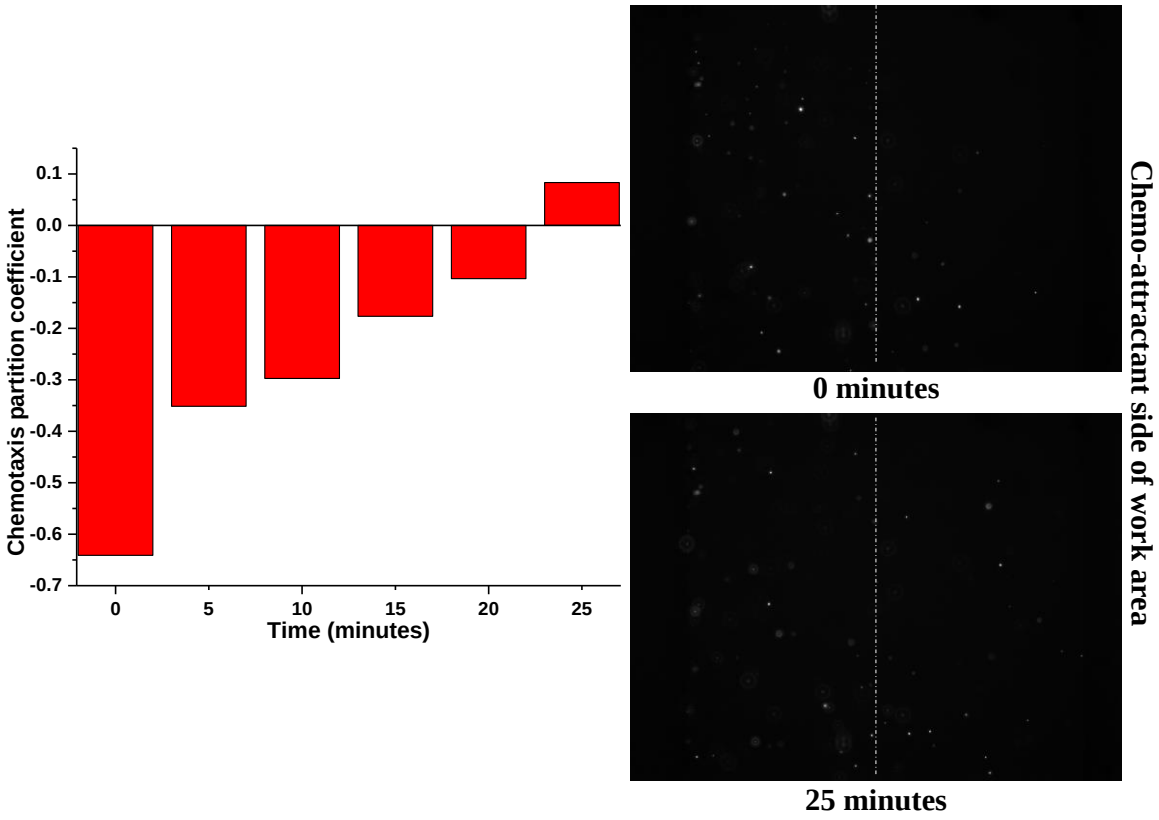

Figure 5. 8. Fluorescence microscopy images show the migration of motile NanoBEADS towards the chemoattractant side of the work area.

The strength of the method presented in this section of the chapter lies in its ability to sort smaller scale components with similar or even identical sizes and densities as long as their surface properties are different. The use of bacteria as actuators allow for selective attachment on micro-particles having different surface properties. Moreover, different bacterial strains having specific affinity to certain chemo-attractants can be used to sort more than two types of micro-

particles in terms of surface chemistries. Also, multiple sources of chemo-attractant activated in a pre-designed time controlled manner can be used to establish a spatiotemporal varying chemical gradient and achieve multi-dimensional particle manipulation.

The limitation of the proposed method includes the overall size of the work area which cannot exceed 600 μm for the single chemo-attractant design proposed here. If larger work areas are desired, additional chemo-attractant sources should be implemented to maintain a desired gradient that will continuously guide the particle to the final destination.

Conclusion

A microfluidic platform for autonomous sorting of micro-particles is introduced. Bacteria chemotaxis and motility were used to autonomously guide motile NanoBEADS from the buffer side of the work area where NanoBEADS were initially introduced to the chemo-attractant side. The number of motile NanoBEADS accumulating at the chemo-attractant side of the work area steadily increased during the duration of the experiment. The work presented here will serve as a stepping stone towards developing cost-effective, autonomous, and robust manipulation platforms which can in long-term reduce the complexity and costs associated with performance of these tasks at reduced length scales. The particularly attractive feature of the proposed system is that the biological manipulators and the microfluidic platforms used in this work can be produced cost-effectively and rapidly and are highly scalable in nature. The bio-hybrid manipulation platform as described here is not only cost-effective, but it also does not require any considerable electrical or magnetic source of power. It relies on chemical energy source for actuation and chemical signaling for steering. In future, we aspire to develop a bio-hybrid

autonomous factory for transport and delivery, sorting, or bottom-up programmed self-assembly of micron-sized objects. Successful development of such assembly and manipulation workspace could revolutionize current practices and enable high throughput and high precision bottom-up assembly strategies. In long-term, this will lead to the development of novel devices and applications in areas such as nano-electronics and advanced materials.

Chapter 6: Characterization of the transport of Nanoscale Bacteria-Enabled Autonomous Drug Delivery Systems (NanoBEADS) in tumor spheroids interstitial space

Abstract

The lack of efficacy of existing chemotherapeutic treatments of primary cancer tumors is partially attributed to the limited diffusion distance of the drug particles, which prevents successful treatment of quiescent tumor cells. For an anticancer drug to be effective against a solid primary tumor, it must be able to reach all cancerous cells within the tumor and prevent clonogenic tumor stem cells from regeneration. The low selectivity of anti-cancer drugs with respect to cancerous tissue is also problematic due to the exposure of healthy cells to anti-cancer drugs. Thus, chemotherapy can be enhanced through better anti-cancer drug carriers targeting towards cancerous cells. Several strains of attenuated bacteria including *Salmonella* Typhimurium and *Escherichia coli* have been identified to possess the innate ability to preferentially colonize tumor tissues. In this work, we demonstrate that the tumor colonizing bacteria *E. coli* and *S.* Typhimurium can be coupled with therapeutic nanoparticles to form intelligent Nanoscale Bacteria-Enabled Autonomous Drug Delivery Systems (NanoBEADS). NanoBEADS consist of an engineered abiotic component (i.e. drug-laden particles) and a living component (i.e. bacteria). The use of NanoBEADS could dramatically improve delivery of chemotherapeutic to solid primary tumors. We demonstrate that NanoBEADS can penetrate deeper within the tumor tissue when compared to passively diffusing chemotherapeutic nanoparticles.

In this work, we also investigate the transport (penetration and colonization) of an attenuated *S.* Typhimurium strain (VNP20009), and a library of its relevant mutants[4] in in-vitro tumor spheroid model. We conclude that motility and chemotaxis are not necessary for *S.*Typhimurium VNP20009 penetration and colonization of tumor spheroids.

[4] The *Salmonella* Typhimurium VNP20009 mutants described and used in this work were developed by our collaborators Katherine Broadway, Ph.D. student in Biological Sciences and her advisor Prof. Birgit Scharf.

6.1 Introduction

Current chemotherapeutics have major limitations despite the numerous technological advances in tumor-targeting [6], [20]. These limitations include the low selectivity and high systemic toxicity of drugs. Intravenous chemotherapeutic agents will circulate through the blood stream and then cross the blood vessel wall into the interstitial space [3]. However, the majority of the drug does not end up in tumor regions but rather in healthy parts of the body [6], [8]. In fact, the accumulation of administered chemotherapeutic drugs in tumors is below 5%, meaning about 95% of the drugs accumulate in other organs such as the liver, spleen and lungs [29], [30].

Another major limitation of current chemotherapeutic drugs is poor penetration once they reach the periphery of the tumors sites [3], [6], [20], [104]. This lack of penetration is essentially due to the high interstitial pressure and the dense extracellular matrix found inside solid tumors [3], [104]. The high interstitial fluid pressure works against the convective transport of macromolecules and nanoparticles whereas the dense extracellular matrix (ECM) can severely hinder the diffusion of smaller molecules inside the tumor. Finding ways to overcome these issues would tremendously impact the targeted delivery of chemotherapeutic drugs to solid cancer sites.

Pathogens (bacteria and viruses) have evolved and developed striking ways to evade the immune system and interact with target cells in the body [13], [105]. In the past two centuries, bacteria have been used either directly or indirectly for cancer therapies. In the 1900's, an American surgeon, William Coley concocted a mixture of killed bacteria that became known as the Coley toxin. In many cases, his treatment led to tumor regression after a few months of continued treatments [13]. In another more recent example, Bacillus Calmette-Guerin (BCG) vaccine, which uses the attenuated bovine tuberculosis bacterial strain (*Myobacterium bovis*) to protect

against tuberculosis, has also been utilized as one of the most successful immunotherapeutic against cancer. BCG has been used in the past 30 years to prevent cancer recurrence after endoscopic surgery of intermediate and high-risk non-muscle invasive bladder cancer. It has also proven its effectiveness against some inoperable bladder carcinoma in-situ [106].

In addition to the two examples cited above, other bacterial species have been tested for their anti-tumor effects [10], [11], [13], [14], [33], [35], [37], [106–108]. In 1998, a group of researchers was able to develop an attenuated strain of *Salmonella* Typhimurium with modified lipid A mutant (VNP20009) with suppressed virulence and showed that the new strain retained its in-vivo tumor-targeting capability [17], [109], [110]. This bacterial strain was used in a clinical trial that took place in 2001 [9]. It is a genetically stable antibiotic-sensitive strain of tumor targeting *Salmonella* Typhimurium bacteria. This strain is highly attenuated and has been shown to inhibit tumor growth. It presents excellent potential for tumor treatment due to its relative broad and high tumor specificity, its capacity to be metabolically active and its ability to replicate after systemic administration [110]. *Salmonella* auxotroph mutants have also been shown to accumulate in tumor tissues compared to healthy tissues (ratio of 1000:1) [111]. This preferential growth within tumor tissues occurs partly because *Salmonella* cells grow both under aerobic and anaerobic conditions.

In this work, we investigate the transport properties of *E. coli* NanoBEADS (developed in the previous chapter) and passively diffusing nanoparticles (i.e. the abiotic component of NanoBEADS and model drug particles) inside the interstitial space of in-vitro tumor models. Additionally, we characterize the transport properties of the attenuated *Salmonella* TyphimuriumVNP20009, and a library of its mutants in tumor spheroid models. The preferential colonization of bacteria in tumor spheroids has previously been reported in studies conducted by

other researchers [10–12], [32], [33], [107]. The mechanism through which bacteria colonize tumors is still an active topic of debate in the research community. To further our understanding of the process bacteria utilize to preferentially colonize tumors, we set out to explore bacteria transport within tumors in short timescales (30 minutes) that do not favor bacterial replication. More specifically, we wish to understand the role that bacterial motility and chemotaxis play in the initial penetration of bacteria in in-vitro tumor spheroid models.

To achieve these goals, human colon carcinoma (HT-29) cells were seeded in low-adhesion well plates to generate in-vitro tumor spheroids with microenvironment properties that resemble solid in-vivo tumors [112–116]. In the past, monolayer cell cultures have been used to assess the efficacy of anticancer drugs, however, it has become clear that these two-dimensional (2D) cell cultures are not adequate in-vitro models as they lack key attributes that are associated with 3D tumor tissue architecture. For instance, tumor tissues have mass transfer barriers and other metabolic chemical gradients present in their environment. These complex biochemical and physical properties originates from the cell-cell and cell-ECM interactions only found in 3D tumors [112], [116]. A relatively simple and reproducible model that can mimic most of the characteristics of solid in-vivo tumors are multicellular tumor spheroids (MCTS). MCTS resemble in-vivo solid tumor tissues because of the self-generated ECM components during the spheroid compaction phase, and their similarity in terms of regions of heterogeneity (necrotic core, quiescent and proliferating ring) [112], [116], [117].

6.2 Materials and methods

a. Mammalian cell cultures and tumor spheroids formation

Human colon carcinoma cells (HT-29, ATCC HTB-38) were cultured in McCoy's 5a medium supplemented with 10% fetal bovine serum (FBS, ATCC). The cells were cultured at 37 ºC with 5% CO_2 in the atmosphere. Tumor spheroids were grown in-vitro using human colon carcinoma cells (HT-29) in low adhesion round bottom 96-well plates (Corning Inc., Corning, NY, USA). Briefly, 200 µL of cell suspensions at a density of 15,000 cells are placed in each of the ultra-low attachment wells. To initiate the spheroid formation, the well plate is centrifuged at 700g for 10 minutes. This method produces a single tumor centered in each well. The plates are then incubated for at least 3 days at 37 °C, 5% CO_2 in a humidified incubator before use.

b. Bacterial cell cultures

All *Salmonella* Typhimurium strains and mutants used in this study were cultured in MSB medium (1% (w/v) tryptone, 0.5% (w/v) yeast extract, 2mM $CaCl_2$, 2mM $MgCl_2$, in 1 L of autoclaved DI water) at 37 ˚C. *Escherichia coli* strain MG1655m, a derivative of *E. coli* MG1655 [96] from the K-12 family with increased motility, was grown in Luria-Bertani (1% (w/v) tryptone, 0.5% (w/v) yeast extract, 0.5% (w/v) NaCl in 1 L of autoclaved DI water). All bacterial strains were transformed with a plasmid encoding GFP (pHC60; tet^R, constitutive expression of green fluorescent protein) [67] to facilitate fluorescence microscopy. A list of the bacterial mutants for the VNP20009 strain along with their respective functions is shown in Table 6. 1.

Table 6. 1. List of bacterial strain and relevant genotypes used in this study

Strains	Mutation	Influences	Function
***S.* Typhimurium VNP20009**	--		
	VNP20009c	Chemotaxis	Spontaneous chemotaxis mutant. Exhibits better chemotaxis compared to VNP20009
	ΔmotA	Motility	Flagella present but unable to form bundle and rotate
	ΔfliF	Motility	Flagella are not present
	ΔcheY	Chemotaxis	Bacteria are unable to respond to chemotaxis signal

c. BacteriaBots construction

Bacteria were washed twice in motility buffer and incubated in goat polyclonal anti-Lipid A LPS antibody labeled with biotin (10μg/mL). The solution was gyrated for one hour at 600 rpm to favor antibody attachment to bacterial body. The bacterial solution was then centrifuged at low speed (1,700 × g) for 5 minutes at room temperature to remove the free antibody from the solution and was resuspended in 50 μL of motility buffer. 390 nm and 500 nm diameter streptavidin coated nanoparticles were used in this study to attach nanoparticles to bacteria. Briefly, 50 μL of a known concentration of nanoparticles solution is added to 50 μL of concentrated biotin-covered bacteria. The combination is then left on a vortex shaker for mixing over 30 minutes. Using the method described above, NanoBEADS with different nanoparticles sizes can be reliably constructed.

d. Infection of tumors by bacteria, particles and NanoBEADS

Briefly, a known amount of infecting agents (5×10^7 cfu of bacteria, 1.47×10^9 of nanoparticles and 5×10^7 cfu of NanoBEADS) in McCoy's 5a were introduced in wells containing tumor spheroids with diameters between 800 µm and 1000 µm. The infected tumors were then incubated at 37 ºC with 5% CO_2 in the atmosphere for 30 minutes. After incubation the tumors were rinsed in PBS once and processed for imaging.

e. Histology, Image acquisition and data analysis

Tumors were fixed in 4% paraformaldehyde for a period of 24 hours and rinsed in phosphate buffered saline (PBS) three times. The tumors are then placed in a mold filled with embedding solution. The embedding solution consists of Tissue-Tek, OCT compound (Sakura Finetek Inc., Torrance, CA, USA) at 50% and 50% sucrose solution (60% w/v of sucrose in DI water). The mold containing the tumor was stored at -20 °C before cryosectioning.

Frozen tumor tissue sections were cut with a cryotome (HM550, Thermo Scientific, Waltham, MA, USA) at a thickness of 50 µm. A small water droplet (10 µl) is added right on top of each tumor. A thin coverslip (24×60-1, Fisher Scientific) is placed right above the tumor for imaging.

Tumor spheroid images were obtained using a Zeiss AxioObserver Z1 microscope. For analysis, slices were divided into two regions (hypoxic region and viable rim region). The hypoxic core region is composed primarily of necrotic cells and quiescent cells (cells in a state of dormancy). The viable rim is composed of mainly proliferative cells. Figure 6. 1 shows an example of a tumor slice and corresponding region limits.

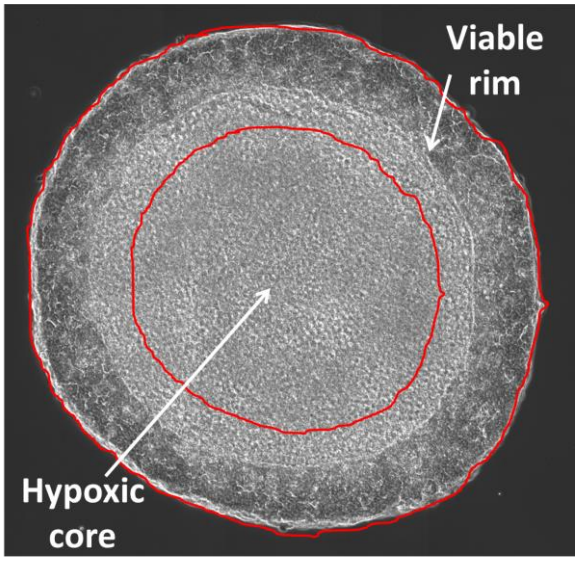

Figure 6. 1. Optical microscopy image illustrating a colon carcinoma HT-29 tumor spheroid. Viable rim primarily consists of live cells and the hypoxic core region consists of dead and quiescent cells. Scale bar is 100 µm.

f. Bacteria exposure to single HT-29 cells and bacteria/particles transport in tumors

In order to capture the behavior of single cells as they interact with different bacterial mutants for each strain, we conducted a study where single HT-29 cells were incubated with each bacterial mutant used in the study. The results (data not shown) indicate no particular morphological change in the HT-29 cells during the initial 30 minutes of incubation. This suggests that during the experiments with the in-vitro tumors, tumor cells maintain their relative morphology and by extension their microenvironment. However, the cancer cells do round up and die after longer exposure to bacteria (30 hours).

At least 4 independent bacterial cultures were used to study the transport of bacteria (VNP20009, and its respective relevant genotypes). After tumor slicing, the number of bacteria present each

slice is counted manually and then averaged over predetermined regions per culture. The percent average (number ratio of the culture averages) can then be deducted per culture sets.

6.3 Results and discussions

a. Penetration and distribution of passively diffusing nanoparticles and NanoBEADS in tumor spheroid model

In order to determine if NanoBEADS improve the transport of nanoparticles in tumor interstitium, 1.47×10^{9} of 390 nm diameter particles and 3.8×10^{8} of 500 nm diameter particles were separately incubated with a tumor spheroid at 37 ˚C and 5% CO_2 for 30 minutes. Figure 6. 2. illustrates the penetration depth of passive nanoparticles inside solid tumors.

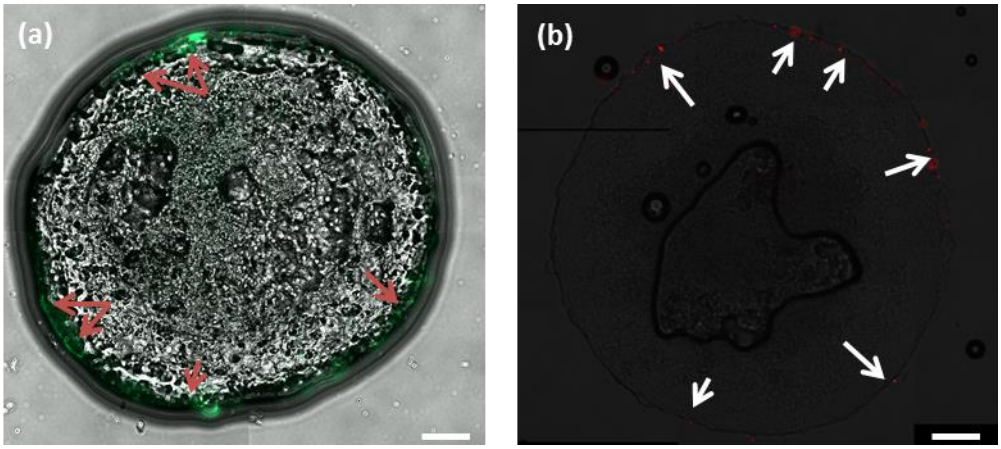

Figure 6. 2. Limited spatial distribution of 390 nm diameter particles (a) and 500 nm diameter particles (b) in tumor slices is shown by white arrows. Scale bar is 100 µm.

As seen in Figure 6. 2, the majority of nanoparticles stay in the periphery of the tumor spheroids. This lack of diffusion is mainly attributed to the highly dense extracellular matrix in tumors, tightly packed cells, and possible binding of particles to cells [104]. The transport of

passive nanoparticles in the interstitial space of tumor spheroids is dictated by diffusion. Previous research has shown that the physiological relevant collagen content (1% - 4.5%) present in tumors (in-vivo and in-vitro) alone can largely hinder the passive diffusion of nanoparticles in tumors [3]. The extremely dense ECM in tumors both in-vivo and in-vitro is responsible for the lack of particle penetration in tumors.

Bacteria can be used as an active mean of particle transport and delivery past the periphery of tumor spheroids. As such, we utilized NanoBEADS developed in the previous chapter to assess bacteria-enabled improved penetration of nanoparticles into tumor spheroid models. Approximately, 5×10^7 cfu of *E. coli* NanoBEADS were incubated at 37 ˚ C and 5% CO_2 for 30 minutes with tumor spheroids. Figure 6. 3 illustrates the improved penetration of both 390 nm and 500 nm particles deep into the tumor tissue just 30 minutes after incubation.

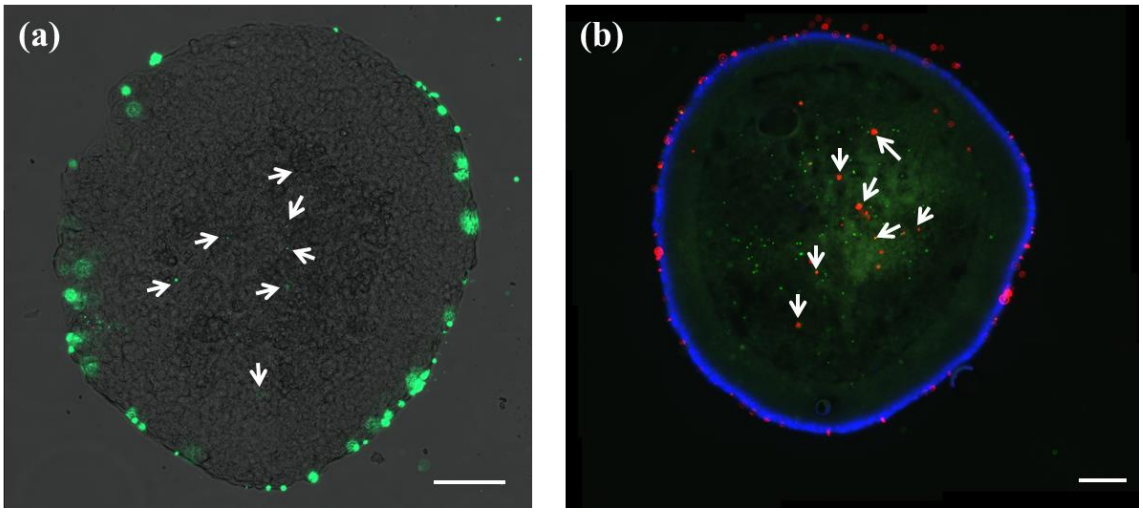

Figure 6. 3. Spatial distribution of (a) 390 nm diameter NanoBEADS and (b) 500 nm diameter NanoBEADS. All scale bars are 100 µm.

Previous research as well as this dissertation work has shown that bacteria preferentially accumulate in tumors both in-vivo and in-vitro [10], [14], [33], [35], [37], however the mechanism through which this accumulation takes place is still not well understood. In the case of NanoBEADS, deep penetration into the tissue is observed despite the fact that high nanoparticle loading may deteriorate NanoBEADS motility as discussed in the previous chapter. It is important to mention that the penetration of NanoBEADS in the tumor spheroid interstitial space is not ideal because a large number of NanoBEADS do not penetrate the interstitium of the tumor as shown in Figure 6. 3. This lack of penetration of NanoBEADS can be explained by a number of factors such as the dense ECM, which still acts as a barrier to the NanoBEADS convective transport inside the tumor spheroids and particle binding to ECM components. It is important to highlight the fact that the bond that exists between particles and bacteria is one of the strongest non-covalent bonds found in nature (value of the strength is unknown). This implies that the transport of NanoBEADS inside tumors can be potentially hindered if any of the nanoparticles attached to the bacteria bind to the ECM or the cells.

The implications of this specific study are major. Even though, particle penetration deep into the tumor tissue was achieved through NanoBEADS albeit a low rate, it is important to elucidate the mechanism through which bacteria alone are able to penetrate and colonize tumors. This added knowledge will potentially enable appropriate changes to NanoBEADS towards an improved outcome. In order to answer these questions, we investigated the role of bacterial motility and chemotaxis in tumor penetration and colonization. To achieve this goal, different bacterial mutants for the attenuated bacterial strain (*Salmonella* Typhimurium VNP20009) were used.

b. Tumor colonization by attenuated *Salmonella* Typhimurium strain VNP20009, VNP20009c, relevant non-motile genotypes (VNP20009 *ΔmotA*, VNP20009 *ΔfliF*) and non-chemotactic genotype (VNP20009 *ΔcheY*)

A total of approximately 2×10^7 cfu of *Salmonella* Typhimurium VNP20009 and its relevant mutants as described in Table 6. 1 was incubated with tumor spheroids at 37 ˚C and 5% CO_2 for 30 minutes. Figure 6. 4 illustrates representative images of transport and colonization of the bacterial strain and its relevant genotypes in tumor spheroids.

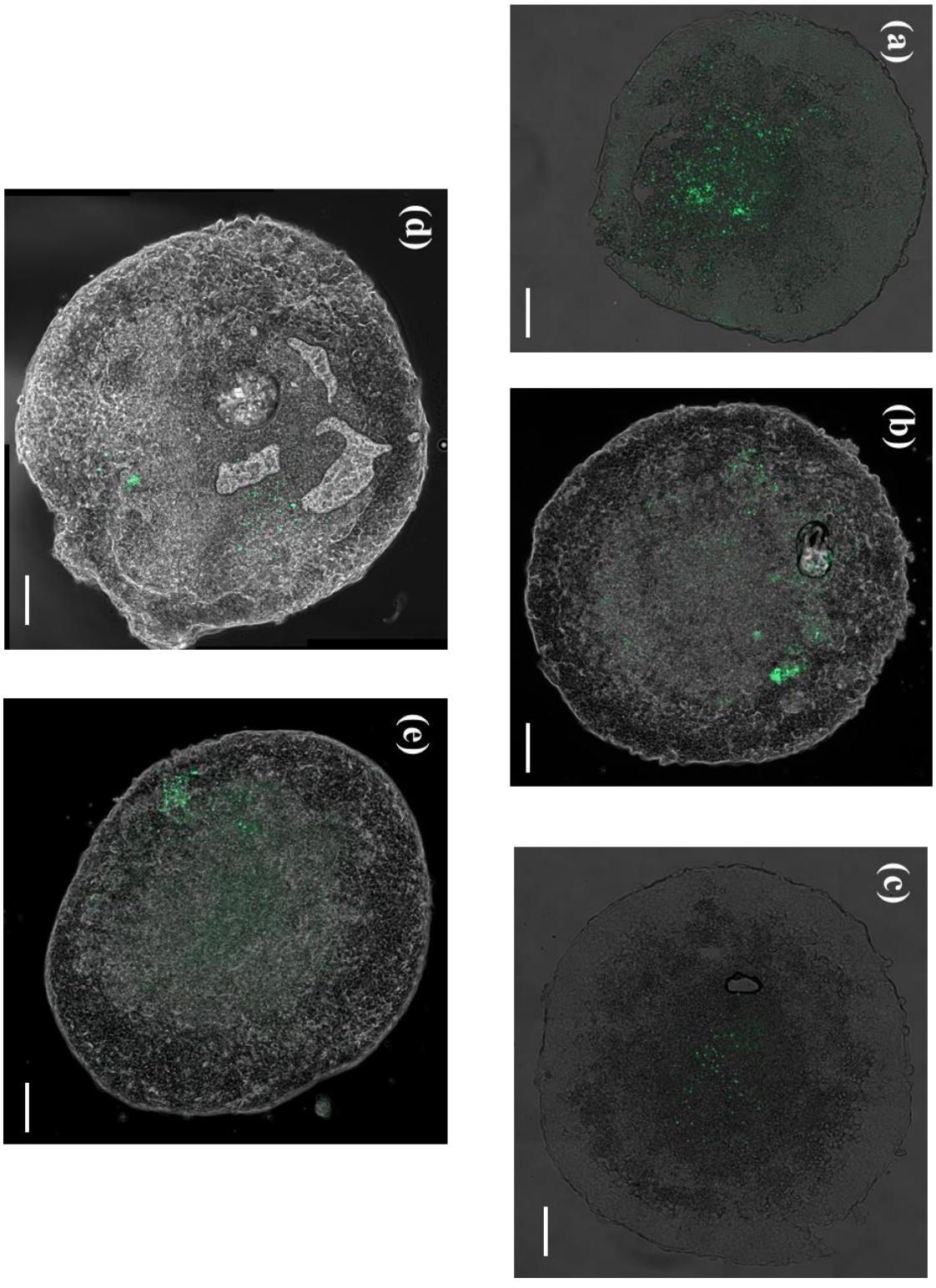

Figure 6. 4. Representative images of tumor penetration of *S*. Typhimurium (a) VNP20009, (b) VNP20009c, (c) VNP20009 *ΔmotA*, (d) VNP20009 *ΔfliF* and (e) VNP20009 *ΔcheY*. All scale bars are 100 μm.

As seen in Figure 6. 4, VNP20009 and its mutants can penetrate tumors during the 30 minute period. The transport and penetration of the bacterial strain inside the tumors was analyzed according to the method described in section e) of the materials and methods of this chapter. The distribution of the bacterial strain and its mutants in the interstitial space of the tumor spheroids is shown in Figure 6. 5. The distribution of VNP20009 and its mutant in the tumor spheroids is similar because approximately half of the bacteria in the tumor spheroids are within the hypoxic core region of the tumor spheroids, which contains most quiescent cancerous cells. Bacterial distribution within the tumors did not follow a particular trend, bacteria were found in all regions of the tumors irrespective of non-motile and non-chemotactic mutants used in all experiments.

As seen in Figure 6. 4 and Figure 6. 5, both non-motile mutants strain can penetrate tumors during the 30 minute period. These results suggest that bacterial motility is not necessary for bacterial penetration and possibly colonization of tumor spheroids. Similar results were obtained in-vivo in mouse models [107], [118] by other researchers but not in-vitro. An in-vitro study of the colonization of bacteria in tumors conducted in 2012 sought to understand the effect of bacterial motility on the accumulation and distribution of bacteria in an in-vitro tumor tissue construct established that motility is critical [12]. In that specific study, green fluorescent protein (GFP) expressing *Salmonella* SL1344, *Salmonella* Typhimurium VNP20009 (motile strain), *Escherichia coli* strains K12 MG1655 and DH5α were used. Both *Salmonella* strains were the most motile among the strains used this study, while the DH5α strain was minimally motile. The fluorescence intensity values were employed to determine the extent of bacterial penetration, growth and distribution in the tumor construct. This study evaluated the penetration and distribution of the bacterial strains used (SL1344, VNP20009, MG1655, DH5α) in deep tumor tissue construct (depth ≈ 1 mm) for time periods ranging up to 34 hours using optical microscopy

of the whole tumor. This study showed that bacterial motility was required for colonization as more motile strains were able to penetrate the tissue construct deeper. Under our experimental conditions and analysis conducted using sliced tumors, motility does not appear to be required for tumor penetration.

As seen in Figure 6. 4 and Figure 6. 5, the non-chemotaxis mutant can penetrate tumors during the 30 minute period and no particular distribution of bacteria within the tumors could be discerned. Here also, these results suggest that bacterial chemotaxis is not required for bacterial penetration and colonization of tumor spheroids. Similar results were obtained in-vivo in mouse models using *Salmonella* Typhimurium SL1344 *ΔcheY* (non-chemotactic strain) [107], [118] by other researchers. In-vitro studies that took place suggested that bacteria use their chemotaxis to sense and penetrate different regions of tumors [10], [33]. These experiments were done in-vitro using tumor cylindroids and *Salmonella* Typhimurium strains ST326 (*tsr* gene is not active), ST328 (*tar* gene is not active), ST832 (*trg* gene is not active) [10]. The authors in these studies proposed an active targeting mechanism that bacteria employ to penetrate specific regions of tumor cylindroids [10]. Briefly, bacteria penetration to the core of tumors is achieved through the following steps: 1) utilization of Tar (aspartate) receptor to first migrate towards a tumor site, 2) utilization of Tsr (serine) receptor to initiate the penetration into the tumor interstitium and 3) utilization of Trg (ribose and galactose) receptor for migration towards the core of the tumor. Under our experimental conditions however, chemotaxis is not a factor in bacterial penetration and colonization of solid tumors. Bacteria that are unable to exhibit chemotaxis behave in similarly to VNP20009c (spontaneous chemotaxis mutant of VNP20009).

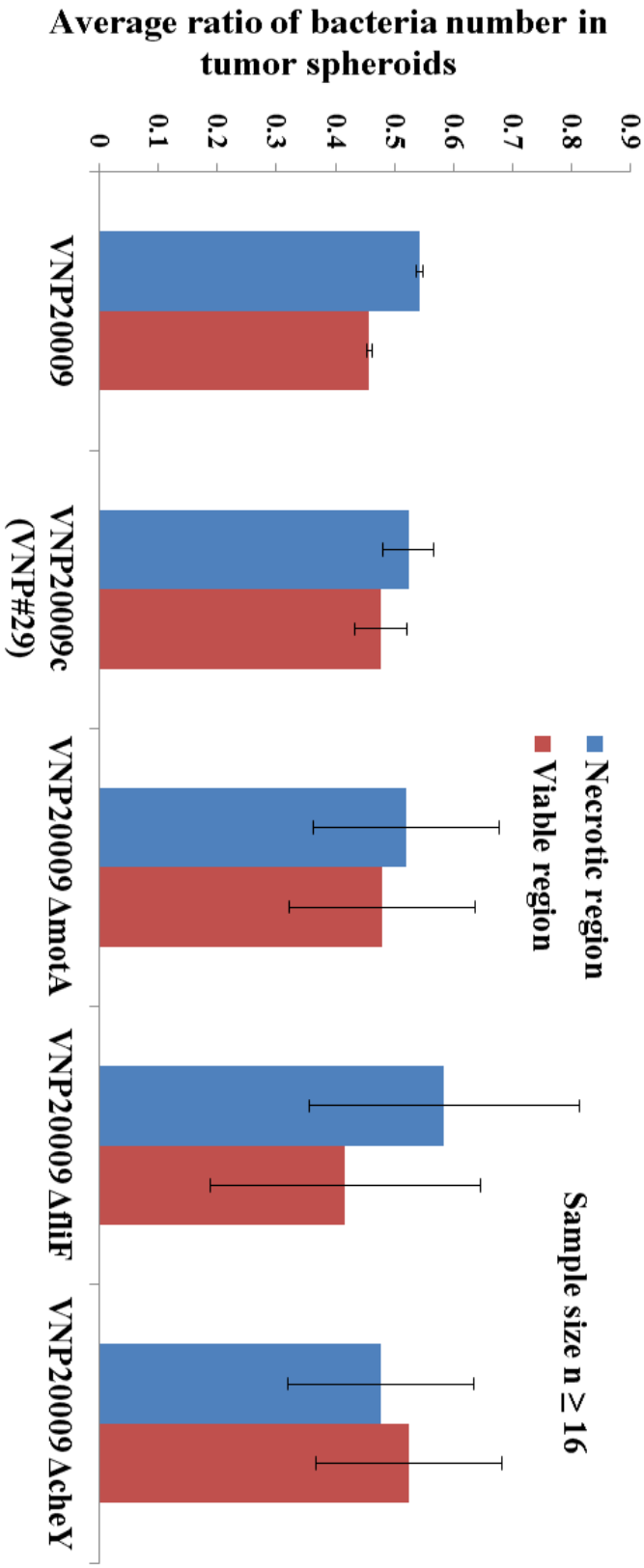

Figure 6. 5. Average ratio number of *S*. Typhimurium VNP20009 strain and relevant genotypes in tumor spheroids per regions

c. The enhanced permeability and retention effect and initial bacterial entrapment in solid tumor tissues

Blood vessels associated with in-vivo solid tumors are generally heterogeneous, dilated and tortuous in nature [3]. This contributes to wide interendothelial junctions as well as large pore sizes and higher vascular permeability [27], [29]. This phenomenon is known as the enhanced permeability and retention (EPR) effect [31] as illustrated in Figure 6. 6. Because of the EPR effect, nanoparticles can extravasate in tumor tissue from the large pores found in blood vessels near tumors [3], [4], [27], [29]. We hypothesize that bacteria whether motile or not utilize similar methods to extravasate from blood vessels into tumor tissues. Similar conditions are reproduced in-vitro through incubation of bacteria with tumor spheroid. In our experimental condition, the initial entrapment is provoked by random interaction of bacteria with the solid tumors. This is a realistic model of in-vivo conditions because of the initial and direct access bacterial cells have with tumor sites, which mimics bacteria exposure to tumor sites once they cross the blood vessel due to the EPR effect.

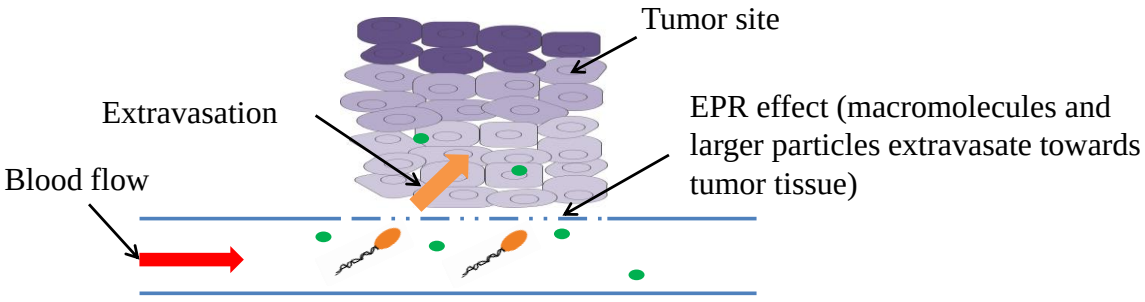

Figure 6. 6. A schematic of the enhanced permeation and retention (EPR) effect [29]

d. The mechanism of bacterial penetration in solid tumors

As shown in the results section, bacteria irrespective of motility and chemotaxis abilities are able to penetrate deep into tumor tissues and achieve colonization. A simple diffusion-based analysis can elucidate the fact that bacteria cannot diffuse through the tumor spheroids and reach the core. The diffusion length of non-motile bacteria in an aqueous environment can be obtained using the following formula: $L_d = \sqrt{6Dt}$ where D is the diffusion coefficient of the bacteria and t, the diffusion time. The diffusion coefficient of non-motile bacteria in an aqueous solution is $D=2\times10^{-13}$ m^2/s and the diffusion time considered is 30 minutes, time of bacteria exposure to tumor spheroids. The diffusion length under this condition is $L_d \approx 47$ μm. This value corresponds to the maximum distance a non-motile bacterium can displace in 30 minutes due to random diffusion. This number is simply not realistic because in the tumor environment, the diffusion coefficient of non-motile bacteria must be lower due to the gel-like structure present in tumors (ECM components) and the inherent tortuosity originating from the cell-cell interaction. The diffusion length calculated is about a tenth of the typical penetration length observed experimentally. We hypothesize that the mechanism bacteria use to penetrate deep into tumor tissues is similar to the process bacteria use in micrometer size confined spaces such as pore size filters to move about [119], coupled with growth thereafter in the rich tumor microenvironment.

The tumor microenvironment is very complex, stromal cells and proteins that make up the ECM surround tumor cells. The cell-cell junction distances encountered in such dense microenvironments are generally below a micrometer [120]. In the tight confinements found in solid tumors, a first generation of bacteria is entrapped at the periphery of the tumor spheroid. Because of the rich environment found inside tumors, growth occurs fairly rapidly and the first generation of bacteria will give rise to daughter cells, which will push themselves through the

confined interstitium that exist in the tumor spheroid. A previous study [119] of bacterial behavior in narrow channels found that cells where able to squeeze themselves through spaces that are smaller than their characteristic length (diameter in this case). This hypothesis implies that inside the tumor interstitial space, motility is irrelevant because of the pore sizes encountered. In the study referred to here, below a certain confinement pore size or width (400 nm) [119]; even motile bacteria become immotile because they are trapped and as such cannot propel forward.

The rich tumor environment [121], [122] gives rise to the division of bacteria through the many tight confinements that exist in the interstitial of the tumor. This replication could potentially explain the presence of bacteria inside the tumor spheroids all the way at its center.

This suggests that only very few bacteria initially are trapped in the periphery of the tumor spheroid, and replicate through the mechanism alluded to earlier to colonize the tumor spheroids. Presently, the initial entrapment of bacteria in the periphery of solid tumors is believed to be a random process; however additional investigation is required.

The role of bacterial chemotaxis in tumor penetration is fully dependent on bacterial motility. Bacterial cells that are non-motile are unable to exhibit chemotaxis because of the lack of motility and biased motion towards a chemical attractant source.

We therefore hypothesize that the effects of chemotaxis may not be captured in this setting because bacteria are immotile inside the dense tumor interstitial environment.

e. Safety concerns of bacteria as drug delivery agents

As seen in this work, bacteria are fascinating microorganisms that can help us better design mechanisms and drug delivery systems for cancer therapy. However, the pathogenicity of

bacteria as drug delivery agents is a major concern. The possible use of *Salmonella* Typhimurium for administration in human beings is challenging because it can induce septic shock. Numerous studies have shown that certain genetic modification in *E. coli* and *S.* Typhimurium can render the bacteria non-toxic (the TNFα induction in strains with msB^- is a third of the TNFα induction in wild-type strains) [13]. The msB gene present in wild-type strains is responsible for the lipopolysaccharide-induced septic shock in patients treated with *Salmonella*. The resulting TNFα reduction showed extremely high reductions in virulence in-vivo [13]. For instance, just 20 cfu of wild-type *Salmonella* injected intraperitoneally would cause death in mice while 2×10^7 cfu of $msbB^-$ *Salmonella* would result in negligible mortality in mice [13]. In human patients, a maximum tolerable dose of 3×10^8 cfu/m^2 of *Salmonella Typhimurium* VNP20009 bacteria was determined based on a phase I clinical trial [9]. *Salmonella* are also sensitive to antibiotics such as trimethoprim/sulfamethoxazole, ampicillin or amoxillin [123], which can permit the cessation of treatment or elimination of the bacteria after treatment [110].

Generally regarded as safe (GRAS) bacteria such as *Lactococcus lactis* could also be used in the future to synthesize and deliver proteins that are biologically active to specific sites in the body. For example, *L. lactis* has been used previously in a phase-I clinical trial, to deliver anti-inflammatory interleukin-10 (IL-10) to the intestinal mucosa to treat inflammatory bowel disease [105].

6.4 Conclusion

In conclusion, this work demonstrates that NanoBEADS can transport nanoparticles deeper into tumor tissue compared to passively diffusing drug nanoparticles. A library of *S.* Typhimurium VNP20009 and its mutants was utilized to investigate the motility and chemotaxis of *Salmonella* Typhimurium VNP20009 in tumor invasion. Our results suggest that motility and chemotaxis are not required for penetration of *S.* Typhimurium VNP20009 in tumor tissue and subsequent colonization. We hypothesize that bacteria rely on growth in constrictions (similar to the processes used in porous microenvironment (porosity ≈ 1 μm) and tight confined spaces) coupled with nutrient-rich tumor microenvironment to replicate preferentially inside the tumor spheroids over time.

Appendix E: Characterization of transport using 5 regions of a tumor slice

The tumor slices were also divided into smaller regions to possibly identify trends that are not easily identifiable using the two regions discussed above. These five regions illustrated in Figure 6. 7 are provided in this appendix to offer more insights into bacterial distribution in the tumor spheroids.

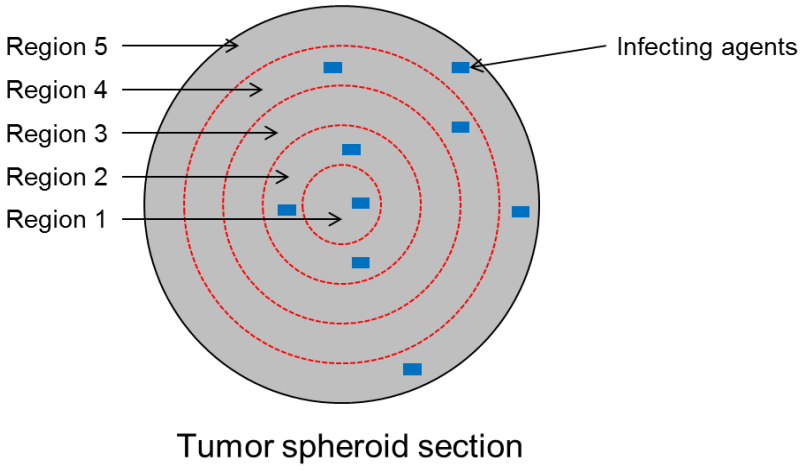

Figure 6. 7. Tumor spheroids sections divided into five regions.

The corresponding bacterial distribution in the tumor section per regions is shown in Figure 6. 8.

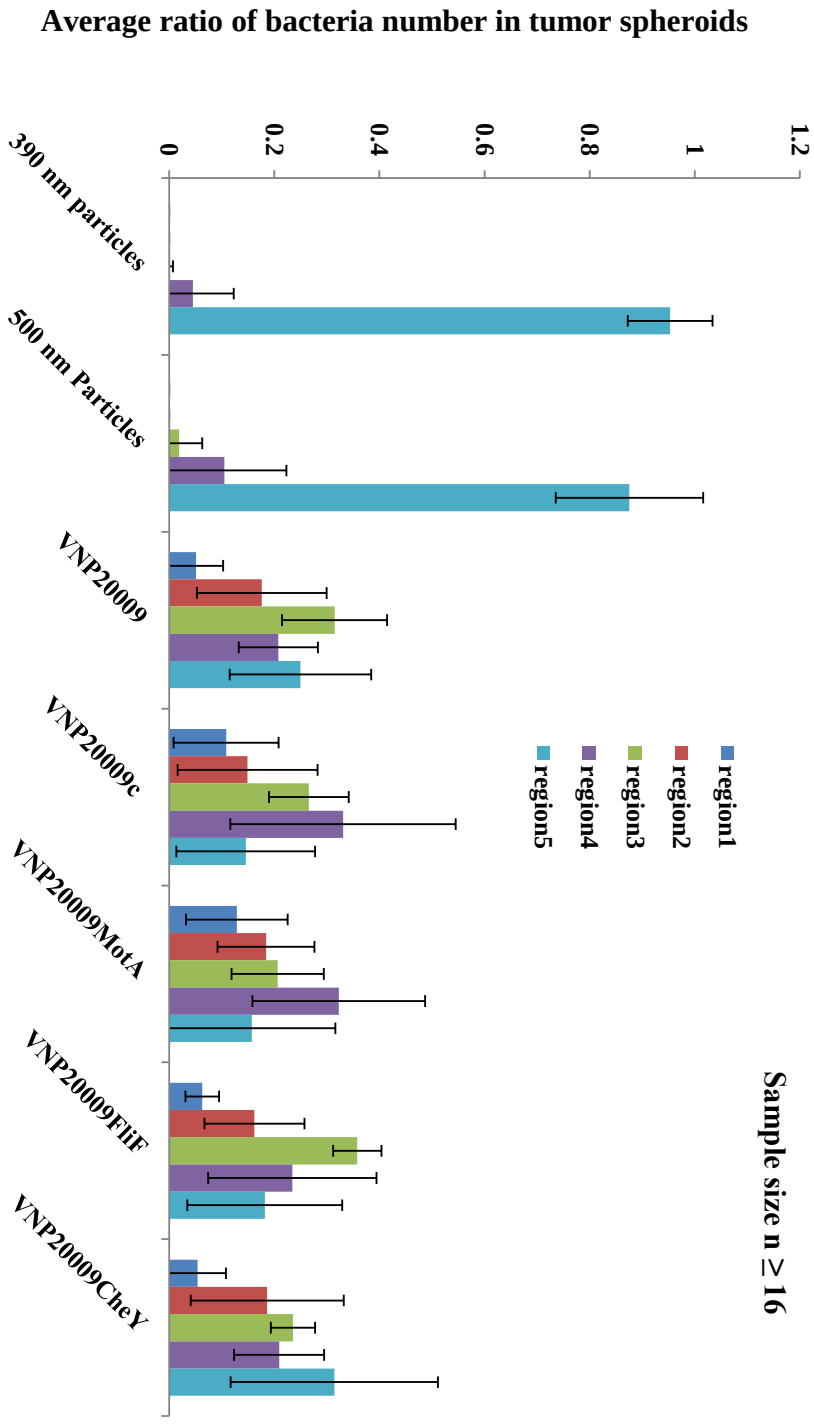

Figure 6. 8. Average ratio number of all bacterial strains and mutants used in the study in tumor spheroids per regions

Chapter 7: Conclusions and future directions

The overall objective of this dissertation work was to characterize the transport and sensing of Bacteria Enabled Autonomous Drug Delivery Systems. This was achieved through the completion of the following research tasks: 1) construction of spherical micro and nanoparticles bacteria-enabled autonomous delivery agents (Micro/NanoBEADS) by coupling living components (bacteria) with engineered micro/nanoparticles, 2) experimental and theoretical investigation of locomotion and sensing of BEADS in aqueous environments, and 3) investigation of the transport of NanoBEADS in an in-vitro tumor spheroid model. The work presented in this dissertation lays the foundation to design bacteria-carrying nanoparticles systems that can be used as individual agents or within a controllable swarm of agents in order to achieve simple and circumscribed tasks. The majority of Chapter 4 and 5 discuss these bio-hybrid microrobotic systems. The other component of the work presented in this dissertation investigates the development of relevant microenvironments to conduct appropriate observational studies of bacterial cells under known chemical concentration gradients. Chapter 2 discusses the design, fabrication and characterization of two types of microfluidic devices for bacterial and mammalian cells chemotaxis and migration studies.

7.1 Concluding remarks

Dissertation findings and original contributions

The major accomplishments of this dissertation are: (1) The design, characterization and fabrication of microfluidic platforms to study the chemotaxis behavior exhibited by bacterial and mammalian cells. The platforms discussed were developed using biomaterials such as polydimethylsiloxane (PDMS) and poly ethylene glycol diacrylate (PEG-DA), etc. (2) The development of bio-hybrid microrobotic systems that utilize bacteria as actuators and nanoparticles as inorganic components. (3) A computational model of bacteria-propelled spherical micro/nanoparticles in fluidic environments was developed an experimentally validated to understand their emergent chemotactic behavior. (4) A study of the bacterial motility and chemotaxis mutants was carried out to investigate the role of motility and chemotaxis in bacteria transport in tumor interstitium. Additionally, interstitial transport of nanoscale bacteria-enabled drug delivery agents in tumor spheroid models was carried out to demonstrate the ability of NanoBEADS to penetrate deeper in tumor tissues in contrast to passively diffusing nanoparticles. A brief summary of the work done in this dissertation is outlined below:

- **Development of microfluidic tools for cellular behavior studies**

  Microfluidic platforms using photopolymerizable hydrogel (PEG-DA) of different molecular weights were developed and characterized as engineering tools to quantitatively study the behavior of living microorganisms. The fabrication process of the PEG-DA based device requires fewer steps compared to flow-free devices, making this type of microfluidic assays unique and advantageous.

The efficacy of this platform was demonstrated by conducting a study of the chemotactic behavior of *E. coli* RP437 under (1.25×10^{-10}-2.5×10^{-2} g/mL/mm) of casamino acids gradients. This platform can generate true linear chemical gradients due to its geometrical characteristics. The channels within the platform are directly contacting non-porous surfaces and as such favor the generation of true linear chemical gradients. The chemotactic response of the bacteria was quantified for the range of chemical concentrations gradient aforementioned. The microfluidic device platforms presented here can be used to generate controllable and quasi-steady chemical concentration gradients for studying other prokaryotic or eukaryotic cells. The wide range of molecular weights of the PEG-DA polymer can enable customizable diffusive properties with respect to the specific chemical compound-cell type to be examined.

As illustrated in the appendix of Chapter 5, these microfluidic devices can be modified to accommodate various studies at the microscale and can have multiple applications.

The knowledge of the diffusion characteristics and swelling ratios of the PEG-DA gels ensures that the chemical environment can be accurately simulated and as such utilized to better explain the experimental results obtained in the study. The capability of realizing well-defined and customizable steady-state chemical gradient fields in absence of fluid flow opens many opportunities for the study of various behaviors of bacteria and mammalian cells within a controlled environment.

- **Construction and characterization of bio-hybrid Nanoscale Bacteria-Enabled Autonomous Drug Delivery Systems (NanoBEADS)**

  Bio-hybrid microrobotic systems have been developed for various applications. Nanoscale bacteria-enabled autonomous drug delivery agents were constructed, using one of the strongest non-covalent bonds found in nature, the biotin-streptavidin bond. This work showed that an increase in the nanoparticle to bacteria number ratio can contribute to a higher yield of nanoparticle attachment to the surface of bacteria. In this work, the foundation to construct hybrid microrobotic systems that use bacteria as means of locomotion is elaborated. This work also suggests that smaller size nanoparticles will not deteriorate the natural self-propulsion of bacteria especially if the location of nanoparticle attachment does not interfere with the flagella of the bacterium.

- **Separation and sorting of NanoBEADS through chemotaxis and motility**

  A microfluidic platform for autonomous sorting of micro-particles was developed. Bacteria chemotaxis and motility were used to autonomously guide motile NanoBEADS, from the buffer side of the work area where NanoBEADS were initially introduced to the chemo-attractant side. The number of motile NanoBEADS accumulating at the chemo-attractant side of the work area steadily increased during the duration of the experiment. The implications of the work presented here are multiple as this platform can serve as a stepping-stone towards the development of cost-effective, autonomous, and robust manipulation platforms. In the long-term, these types of microfluidic platform will reduce the complexity and costs associated with performance of separations of objects at reduced length scales. The particularly attractive feature of using bacteria for sorting resides in the

fact that biological manipulators and the microfluidic platforms utilized can be produced cost-effectively, rapidly and are highly scalable in nature. The bio-hybrid manipulation platform discussed is not only economical, but it also does not require any electrical or magnetic source of power. It relies on chemical energy source for actuation and chemical signaling for steering.

- **Computational modeling of bacteria-propelled spherical micro/nanoparticles in an aqueous microenvironment**

  A computational model describing the random kinematic behavior of bacteria was developed. Moreover, the collective behavior of an ensemble of bacteria constrained on a microparticle was determined. Key parameters including orientation and location of the attached bacteria; spatiotemporal variations in chemo-attractant concentration field and its effect on run and tumble rates of each of the tens of the attached bacteria are taken into account in the model developed. Experimental validation of the model was also achieved and it was shown that it can effectively describe the emergent dynamics of the motion of a 10 μm micro-bead propelled by an ensemble of flagellated bacteria homogeneously attached, in both chemotactic and non-chemotactic environments. The results obtained from this work show that the presence of a chemo-attractant gradient can result in 67% larger directionality values. This work proves the feasibility of directed autonomous movement of bio-hybrid micro-robots through the use of chemotaxis.

  This model can be easily expanded to serve as a predictive tool for other bio-hybrid systems with different whole cell actuators, non-spherical geometries, heterogeneous

whole-cell actuator attachment configurations, and different spatiotemporally varying chemical concentration gradients.

The hydrodynamic viscous effects NanoBEADS encounter as they displace in aqueous environments was captured through a COMSOL computational model. Smaller nanoparticles minimally affect the movement of bacteria because of the 3% increase in damping coefficient experienced by a bacterium swimming in an aqueous environment. In contrary, larger nanoparticles will affect the motion of bacteria due to the relatively high damping coefficient (62%) experienced by bacteria.

- **Transport characterization of bacteria and bacteria-carrying nanoparticles**

  NanoBEADS can be used as live autonomous drug delivery agents with enhanced penetration in the interstitial space of in-vitro tumor spheroid models. The transport of *Salmonella* Typhimurium VNP20009 and its relevant mutants was examined in human colon carcinoma HT-29 in-vitro tumor spheroids model. This work elucidated the fact that motility and chemotaxis are not required in the colonization of tumors by *S.* Typhimurium VNP20009.

7.2 Future directions

The work presented in this dissertation can be expanded to provide answers to existing bioengineering and biological problems. A few possible directions are outlined below:

1. **Development of an in-vitro microfluidic platform that fully mimics the physiological environment of in-vivo tumor tissues**

   Microfluidics offers considerable advantages when it comes to the design of physiologically relevant environments. Even though tumor spheroids are valid models of in-vivo tumors, physiological events that take place in-vivo are largely absent. In an effort to resolve this issue, fluidic micro-channels can be interfaced with spheroids co-culture that contain tumor cells and other cell types present in in-vivo tumor such as pericyte-like, stromal cells, etc. The fluidic channels can be designed to mimic blood vessels as well as capillaries present in-vivo. Anticancer agents such as regular chemotherapeutics and even NanoBEADS could be tested in such relevant microenvironments to evaluate their efficacy.

2. **Investigation of the mechanics of metastasis**

   What types of physical cues initiate invasive phenotypes in cancer cells? Here again, microfluidics could largely contribute to the exploration of this question. Metastatic cancer is a cancer that has spread from the primary tumor to another site and is responsible for 90% of cancer related mortalities. Metastasis occurs according to the following steps: local invasion (the cancerous cells invade healthy surrounding tissue), intravasation (the cancer cells invade and move through the lymph and blood vessel

walls), circulation (cancer cells move in the blood stream), arrest and extravasation (cancer cells eventually stop moving in capillaries and invade the capillary walls to move into nearby tissue), proliferation (cancer cells divide and multiply). Metastasis is a result of complex biological, chemical and physical interactions in-vivo, and microfluidics can help shed more light into some of the processes that take place in-vivo.

3. **Further exploration of the penetration and preferential growth of bacteria in solid tumors**

As discussed in Chapter 6, motility and chemotaxis are not requisites to observe bacterial penetration in in-vitro tumor spheroids. This prompts a very basic question around the mechanisms through which bacterial cells penetrate the tumor. The extremely rich tumor microenvironment may contribute to the accelerated growth of bacteria inside tumors. A deep understanding of this phenomenon could have major implications in cancer treatment.

Bibliography

[1] A. Jemal, R. Siegel, E. Ward, Y. Hao, J. Xu, and M. J. Thun, "Cancer statistics, 2009.," *CA: a cancer journal for clinicians a cancer journal for clinicians*, vol. 59, no. 4, pp. 225–249, 2010.

[2] A. Jemal, F. Bray, M. M. Center, J. Ferlay, E. Ward, and D. Forman, "Global cancer statistics.," *CA: a cancer journal for clinicians*, vol. 61, no. 2, pp. 69–90, 2011.

[3] R. K. Jain and T. Stylianopoulos, "Delivering nanomedicine to solid tumors.," *Nature reviews Clinical oncology*, vol. 7, no. 11, pp. 653–64, 2010.

[4] D. Peer, J. M. Karp, S. Hong, O. C. Farokhzad, R. Margalit, and R. Langer, "Nanocarriers as an emerging platform for cancer therapy," *Nature nanotechnology*, vol. 2, no. 12, pp. 751–760, Dec. 2007.

[5] O. Trédan, C. M. Galmarini, K. Patel, and I. F. Tannock, "Drug resistance and the solid tumor microenvironment.," *Journal of the National Cancer Institute*, vol. 99, no. 19, pp. 1441–54, Oct. 2007.

[6] I. F. Tannock, C. M. Lee, J. K. Tunggal, D. S. M. Cowan, and M. J. Egorin, "Limited penetration of anticancer drugs through tumor tissue: a potential cause of resistance of solid tumors to chemotherapy.," *Clinical Cancer Research*, vol. 8, no. 3, pp. 878–884, 2002.

[7] S. H. Jang, M. G. Wientjes, D. Lu, and J. L. S. Au, "Drug delivery and transport to solid tumors.," *Pharmaceutical Research*, vol. 20, no. 9, pp. 1337–1350, 2003.

[8] N. S. Forbes, “Engineering the perfect (bacterial) cancer therapy.,” *Nature Reviews Cancer*, vol. 10, no. 11, pp. 785–794, 2010.

[9] J. F. Toso, V. J. Gill, P. Hwu, F. M. Marincola, N. P. Restifo, D. J. Schwartzentruber, R. M. Sherry, S. L. Topalian, J. C. Yang, F. Stock, L. J. Freezer, K. E. Morton, C. Seipp, L. Haworth, S. Mavroukakis, D. White, S. MacDonald, J. Mao, M. Sznol, and S. A. Rosenberg, “Phase I study of the intravenous administration of attenuated Salmonella typhimurium to patients with metastatic melanoma.,” *Journal of Clinical Oncology*, vol. 20, no. 1, pp. 142–152, 2002.

[10] R. W. Kasinskas and N. S. Forbes, “Salmonella typhimurium lacking ribose chemoreceptors localize in tumor quiescence and induce apoptosis.,” *Cancer Research*, vol. 67, pp. 3201–9, Apr. 2007.

[11] H. Loessner, A. Endmann, S. Leschner, K. Westphal, M. Rohde, T. Miloud, G. Hämmerling, K. Neuhaus, and S. Weiss, “Remote control of tumour-targeted Salmonella enterica serovar Typhimurium by the use of L-arabinose as inducer of bacterial gene expression in vivo.,” *Cellular microbiology*, vol. 9, no. 6, pp. 1529–37, Jun. 2007.

[12] B. J. Toley and N. S. Forbes, “Motility is critical for effective distribution and accumulation of bacteria in tumor tissue.,” *Integrative biology quantitative biosciences from nano to macro*, vol. 4, no. 2, pp. 165–76, 2012.

[13] J. M. Pawelek, K. B. Low, and D. Bermudes, “Bacteria as tumour-targeting vectors.,” *The lancet oncology*, vol. 4, no. 9, pp. 548–556, 2003.

[14] J. Stritzker, S. Weibel, P. J. Hill, T. A. Oelschlaeger, W. Goebel, and A. A. Szalay, "Tumor-specific colonization, tissue distribution, and gene induction by probiotic Escherichia coli Nissle 1917 in live mice.," *International journal of medical microbiology IJMM*, vol. 297, no. 3, pp. 151–162, 2007.

[15] D. Morrissey, G. C. O'Sullivan, and M. Tangney, "Tumour targeting with systemically administered bacteria.," *Current Gene Therapy*, vol. 10, no. 1, pp. 3–14, 2010.

[16] C. L. Walsh, B. M. Babin, R. W. Kasinskas, J. a Foster, M. J. McGarry, and N. S. Forbes, "A multipurpose microfluidic device designed to mimic microenvironment gradients and develop targeted cancer therapeutics.," *Lab on a chip*, vol. 9, pp. 545–54, Feb. 2009.

[17] K. B. Low, M. Ittensohn, T. Le, J. Platt, S. Sodi, M. Amoss, O. Ash, E. Carmichael, A. Chakraborty, J. Fischer, S. L. Lin, X. Luo, S. I. Miller, L. Zheng, I. King, J. M. Pawelek, and D. Bermudes, "Lipid A mutant Salmonella with suppressed virulence and TNFalpha induction retain tumor-targeting in vivo.," *Nature Biotechnology*, vol. 17, no. 1, pp. 37–41, 1999.

[18] C. Facts, "Cancer Facts & Figures," *Health Policy*, vol. 1, no. 1, pp. 1–68, 2010.

[19] D. Hanahan and R. A. Weinberg, "Hallmarks of cancer: the next generation.," *Cell*, vol. 144, no. 5, pp. 646–674, 2011.

[20] A. I. Minchinton and I. F. Tannock, "Drug penetration in solid tumours," *Nature Reviews Cancer*, vol. 6, no. 8, pp. 583–592, Aug. 2006.

[21] C. Heldin, K. Rubin, K. Pietras, and A. Ostman, “High interstitial fluid pressure—an obstacle in cancer therapy,” *Nature Reviews Cancer*, vol. 4, no. 10, pp. 806–813, 2004.

[22] G. W. West, R. Weichselbaum, and J. B. Little, “Limited penetration of methotrexate into human osteosarcoma spheroids as a proposed model for solid tumor resistance to adjuvant chemotherapy.,” *Cancer research*, vol. 40, no. 10, pp. 3665–8, Oct. 1980.

[23] S. J. Lunt, A. Fyles, R. P. Hill, and M. Milosevic, “Interstitial fluid pressure in tumors: therapeutic barrier and biomarker of angiogenesis.,” *Future oncology London England*, vol. 4, no. 6, pp. 793–802, 2008.

[24] J. L. Au, S. H. Jang, J. Zheng, C. T. Chen, S. Song, L. Hu, and M. G. Wientjes, “Determinants of drug delivery and transport to solid tumors.,” *Journal of Controlled Release*, vol. 74, no. 1–3, pp. 31–46, 2001.

[25] M. Stohrer, Y. Boucher, M. Stangassinger, and R. K. Jain, “Oncotic pressure in solid tumors is elevated.,” *Cancer Research*, vol. 60, no. 15, pp. 4251–4255, 2000.

[26] P. Koumoutsakos, I. Pivkin, and F. Milde, “The Fluid Mechanics of Cancer and Its Therapy,” *Annual Review of Fluid Mechanics*, vol. 45, no. 1, pp. 325–355, Jan. 2013.

[27] L. Brannon-Peppas and J. O. Blanchette, “Nanoparticle and targeted systems for cancer therapy.,” *Advanced drug delivery reviews*, vol. 56, no. 11, pp. 1649–59, Sep. 2004.

[28] M. M. and J. Martino, *Brock Biology of Microorganisms*, 11th ed. Pearson Prentice Hall, 2006.

[29] K. P. You Han Bae, “Targeted drug delivery to tumors: Myths, reality and possibility,” *Journal of Controlled Release*, vol. 153, no. 3, pp. 198–205, 2012.

[30] K. Park, “Facing the truth about nanotechnology in drug delivery.,” *ACS nano*, vol. 7, no. 9, pp. 7442–7, Sep. 2013.

[31] A. K. Iyer, G. Khaled, J. Fang, and H. Maeda, “Exploiting the enhanced permeability and retention effect for tumor targeting.,” *Drug discovery today*, vol. 11, no. 17–18, pp. 812–8, Sep. 2006.

[32] S. Leschner, K. Westphal, N. Dietrich, N. Viegas, J. Jablonska, M. Lyszkiewicz, S. Lienenklaus, W. Falk, N. Gekara, H. Loessner, and S. Weiss, “Tumor Invasion of Salmonella enterica Serovar Typhimurium Is Accompanied by Strong Hemorrhage Promoted by TNF,” *PLoS ONE*, vol. 4, no. 8, p. 11, 2009.

[33] R. W. Kasinskas and N. S. Forbes, “Salmonella typhimurium specifically chemotax and proliferate in heterogeneous tumor tissue in vitro.,” *Biotechnology and bioengineering*, vol. 94, pp. 710–721, 2006.

[34] P. C. Maciag, S. Radulovic, and J. Rothman, “The first clinical use of a live-attenuated Listeria monocytogenes vaccine: a Phase I safety study of Lm-LLO-E7 in patients with advanced carcinoma of the cervix.,” *Vaccine*, vol. 27, no. 30, pp. 3975–83, Jun. 2009.

[35] S. Leschner and S. Weiss, “Salmonella-allies in the fight against cancer.,” *Journal of molecular medicine Berlin Germany*, vol. 88, no. 8, pp. 763–773, 2010.

[36] W. Quispe-Tintaya, D. Chandra, a. Jahangir, M. Harris, a. Casadevall, E. Dadachova, and C. Gravekamp, "Nontoxic radioactive Listeriaat is a highly effective therapy against metastatic pancreatic cancer," *Proceedings of the National Academy of Sciences*, pp. 1–6, Apr. 2013.

[37] S. Weibel, J. Stritzker, M. Eck, W. Goebel, and A. A. Szalay, "Colonization of experimental murine breast tumours by Escherichia coli K-12 significantly alters the tumour microenvironment.," *Cellular Microbiology*, vol. 10, no. 6, pp. 1235–1248, 2008.

[38] W. Pfeffer, "Locomotorische Richtungsbewegungen durch chemische Reize.," in *Unters. Bot. Inst. Tubingen*, vol. 1, 1884, pp. 363–482.

[39] J. Adler, "A method for measuring chemotaxis and use of the method to determine optimum conditions for chemotaxis by Escherichia coli.," *Journal of General Microbiology*, vol. 74, pp. 77–91, Jan. 1973.

[40] J. Adler, "Chemotaxis in bacteria.," *Annual Review of Biochemistry*, vol. 44, pp. 341–56, Jan. 1975.

[41] M. Silverman and M. Simon, "Flagellar rotation and the mechanism of bacterial motility," *Nature*, vol. 249, pp. 73–74, 1974.

[42] R. Ford, B. Phillips, J. Quinn, and D. Lauffenburger, "Measurement of bacterial random motility and chemotaxis coefficients: I. Stopped-flow diffusion chamber assay.," *Biotechnology and bioengineering*, vol. 37, pp. 647–60, Mar. 1991.

[43] H. Berg and D. Brown, “Chemotaxis in Escherichia coli analysed by three-dimensional tracking,” *Nature*, vol. 239, pp. 500–503, 1972.

[44] T. Ahmed, T. S. Shimizu, and R. Stocker, “Microfluidics for bacterial chemotaxis.,” *Integrative biology*, vol. 2, pp. 604–29, Nov. 2010.

[45] H. Mao, P. S. Cremer, and M. D. Manson, “A sensitive, versatile microfluidic assay for bacterial chemotaxis,” *Proceedings of National Academy of Sciences USA*, vol. 100, pp. 5449–5454, 2003.

[46] N. Jeon, H. Baskaran, S. Dertinger, G. Whitesides, W. Livingstone, and M. Toner, “Neutrophil chemotaxis in linear and complex gradients of interleukin-8 formed in a microfabricated device,” *Nature Biotechnology*, vol. 20, pp. 826–830, 2002.

[47] M. Yang, J. Yang, C. W. Li, and J. Zhao, “Generation of concentration gradient by controlled flow distribution and diffusive mixing in a microfluidic chip.,” *Lab on a chip*, vol. 2, pp. 158–63, Aug. 2002.

[48] U. Haessler, Y. Kalinin, M. A. Swartz, and M. Wu, “An agarose-based microfluidic platform with a gradient buffer for 3D chemotaxis studies,” *Biomedical Microdevices*, vol. 11, pp. 827–835, 2009.

[49] J. Diao, L. Young, S. Kim, E. A. Fogarty, S. M. Heilman, P. Zhou, M. L. Shuler, M. Wu, and M. P. DeLisa, “A three-channel microfluidic device for generating static linear gradients and its application to the quantitative analysis of bacterial chemotaxis,” *Lab on a chip*, vol. 6, pp. 381–388, 2006.

[50] Y. Kalinin, S. Neumann, V. Sourjik, and M. Wu, “Responses of Escherichia coli bacteria to two opposing chemoattractant gradients depend on the chemoreceptor ratio.,” *Journal of Bacteriology*, vol. 192, no. 7, pp. 1796–800, Apr. 2010.

[51] S. Cheng, S. Heilman, M. Wasserman, S. Archer, M. L. Shuler, and M. Wu, “A hydrogel-based microfluidic device for the studies of directed cell migration,” *Lab on a chip*, vol. 7, pp. 763–769, 2007.

[52] T. Ahmed, T. S. Shimizu, and R. Stocker, “Bacterial chemotaxis in linear and nonlinear steady microfluidic gradients.,” *Nano letters*, vol. 10, pp. 3379–85, Sep. 2010.

[53] G. Si, W. Yang, S. Bi, C. Luo, and Q. Ouyang, “A parallel diffusion-based microfluidic device for bacterial chemotaxis analysis.,” *Lab on a chip*, vol. 12, pp. 1389–94, Apr. 2012.

[54] S. Lin, N. Sangaj, T. Razafiarison, C. Zhang, and S. Varghese, “Influence of physical properties of biomaterials on cellular behavior,” *Pharmaceutical Research*, vol. 28, pp. 1422–1430, 2011.

[55] D. Kim, W. Lee, and W. Koh, “Micropatterning of proteins on the surface of three-dimensional poly(ethylene glycol) hydrogel microstructures.,” *Analytica Chimica Acta*, vol. 609, pp. 59–67, 2007.

[56] M. B. Mellott, K. Searcy, and M. V Pishko, “Release of protein from highly cross-linked hydrogels of poly(ethylene glycol) diacrylate fabricated by UV polymerization.,” *Biomaterials*, vol. 22, pp. 929–941, 2001.

[57] W. Liang and R. Siegel, “Theoretical and experimental exploration of rules for combining transport parameters in laminar membranes.,” *The Journal of Chemical Physics*, vol. 125, p. 44707, Jul. 2006.

[58] H. Berg, *Random walks in biology*. Princeton University Press, 1993.

[59] M. A. Traore, A. Sahari, and B. Behkam, “Computational and experimental study of chemotaxis of an ensemble of bacteria attached to a micro-bead,” *Physical Review. E*, vol. 84, pp. 61906–61908, 2011.

[60] M. A. Traore and B. Behkam, “Bacterial chemotaxis enabled autonomous sorting of micro-particles,” in *IEEE Engineering in Medicine and Biology Society*, 2012, pp. 2823–2826.

[61] L. M. Lanning, R. M. Ford, and T. Long, “Bacterial chemotaxis transverse to axial flow in a microfluidic channel.,” *Biotechnology and bioengineering*, vol. 100, pp. 653–63, Jul. 2008.

[62] T. Long and R. M. Ford, “Enhanced transverse migration of bacteria by chemotaxis in a porous T-sensor.,” *Environmental science & technology*, vol. 43, pp. 1546–52, Mar. 2009.

[63] J. Adler, “A method for measuring chemotaxis and use of the method to determine optimum conditions for chemotaxis by Escherichia coli,” *Journal of General Microbiology*, vol. 74, pp. 77–91, 1972.

[64] H. Jeon, Y. Lee, S. Jin, S. Koo, C.-S. Lee, and J. Y. Yoo, "Quantitative analysis of single bacterial chemotaxis using a linear concentration gradient microchannel.," *Biomedical Microdevices*, vol. 11, pp. 1135–43, Oct. 2009.

[65] S. A. Rice, K. S. Koh, S. Y. Queck, M. Labbate, K. W. Lam, and S. Kjelleberg, "Biofilm formation and sloughing in serratia marcescens are controlled by quorum sensing and nutrient cues biofilm formation and sloughing in serratia marcescens are controlled by quorum sensing and nutrient cues," *Journal of Bacteriology*, vol. 187, pp. 3477–3485, 2005.

[66] J. S. Parkinson and S. E. Houts, "Isolation and behavior of escherichia coli deletion mutants lacking chemotaxis functions.," *Journal of Bacteriology*, vol. 151, pp. 106–113, 1982.

[67] H. Cheng and G. C. Walker, "Succinoglycan is required for initiation and elongation of infection threads during nodulation of alfalfa by rhizobium meliloti," *Journal of Bacteriology*, vol. 180, pp. 5183–5191, 1998.

[68] D. L. Englert, M. D. Manson, and A. Jayaraman, "Investigation of bacterial chemotaxis in flow-based microfluidic devices," *Nature Protocols*, vol. 5, pp. 864–872, 2010.

[69] M. A. Traore and B. Behkam, "A PEG-DA microfluidic device for the chemotaxis study of prokaryotic and eukaryotic cells," *Journal of Micromechanics and Microengineering*, vol. 23, no. 8, p. 085014, 2013.

[70] D. E. Koshland, “Biochemistry of sensing and adaptation in a simple bacterial system.,” *Annu Rev Biochem*, vol. 50, pp. 765–82, Jan. 1981.

[71] R. Mesibov, G. W. Ordal, and J. Adler, “The range of attractant concentrations for bacterial chemotaxis and the threshold and size of response over this range. Weber law and related phenomena.,” *Journal of General Physiology*, vol. 62, pp. 203–23, Aug. 1973.

[72] C. Li, a J. Boileau, C. Kung, and J. Adler, “Osmotaxis in Escherichia coli.,” *Proceedings of National Academy of Sciences USA*, vol. 85, pp. 9451–5, Dec. 1988.

[73] A. Vaknin and H. Berg, “Osmotic stress mechanically perturbs chemoreceptors in escherichia coli.,” *Proceedings of National Academy of Sciences USA*, vol. 103, pp. 592–6, Jan. 2006.

[74] C. Li and J. Adler, “Escherichia coli shows two types of behavioral responses to osmotic upshift.,” *Journal of Bacteriology*, vol. 175, pp. 2564–7, May 1993.

[75] N. Darnton, L. Turner, K. Breuer, and H. Berg, “Moving Fluid with Bacterial Carpets,” *Biophysical journal*, vol. 86, pp. 1863–1870, Mar. 2004.

[76] D. B. Weibel, P. Garstecki, D. Ryan, W. R. DiLuzio, M. Mayer, J. E. Seto, and G. M. Whitesides, “Microoxen: Microorganisms to move microscale loads,” *Proceedings of National Academy of Sciences USA*, vol. 102, pp. 11963–11967, 2005.

[77] B. Behkam and M. Sitti, “Bacterial flagella-based propulsion and on/off motion control of microscale objects,” *Applied Physics Letters*, vol. 90, pp. 239021–239023, 2007.

[78] S. Martel, C. Tremblay, S. Ngakeng, and G. Langlois, "Controlled manipulation and actuation of micro-objects with magnetotactic bacteria," *Applied Physics Letters*, vol. 89, pp. 233904–233907, 2006.

[79] M. Kim and K. Breuer, "Use of Bacterial Carpets to Enhance Mixing in Microfluidic Systems," *Journal of fluids engineering*, vol. 129, pp. 319–324, 2007.

[80] S. Block, J. Segall, and H. Berg, "Impulse Responses in Bacterial Chemotaxis.," *CELL*, vol. 31, pp. 215–226, 1982.

[81] H. Berg, "Motile behavior of bacteria," *Physics today*, vol. 53, pp. 24–29, 2000.

[82] M. Schnitzer, "Theory of Continuum Random Wlks and Application to Chemotaxis," *Physical review. E*, vol. 48, pp. 2553–2568, 1993.

[83] D. Lauffenburger, "Quantitative Studies of Bacterial Chemotaxis and Microbial Dynamics," *Journal of microbial ecology*, vol. 22, pp. 175–185, 1991.

[84] R. Marx and M. Aitken, "Quantification of Chemotaxis to Naphtalene by Pseudomonas putida G7," *Applied and Environmental Microbiology*, vol. 65, pp. 2847–2852, 1999.

[85] J. Adler, "The sensing of chemicals by bacteria ," *American Scientist*, vol. 4, pp. 40–47, 1976.

[86] R. Futrelle and H. Berg, "Specification of gradients used for studies of chemotaxis," *Nature*, vol. 239, pp. 517–518, 1972.

[87] Y. Ma, C. Zhu, P. Ma, and T. Yu, "Studies on the Diffusion Coefficients of Amino Acids in Aqueous Solutions," *Journal of chemical and engineering data*, vol. 50, pp. 1192–1196, 2005.

[88] J. Howse, R. Jones, A. Ryan, T. Gough, R. Vafabakhsh, and R. Golestanian, "Self-Motile Colloidal Particles: From Directed Propulsion to Random Walk," *Physical Review Letters*, vol. 99, no. 4, p. 48102, Jul. 2007.

[89] B. Behkam and M. Sitti, "Effect of Quantity and Configuration of Attached Bacteria on Bacterial Propulsion of Microbeads," *Applied Physics Letters*, vol. 93, pp. 223901–223903, 2008.

[90] B. J. Nelson, I. K. Kaliakatsos, and J. J. Abbott, "Microrobots for minimally invasive medicine.," *Annual review of biomedical engineering*, vol. 12, pp. 55–85, Aug. 2010.

[91] A. Sahari, D. Headen, and B. Behkam, "Effect of body shape on the motile behavior of bacteria-powered swimming microrobots (BacteriaBots)," *Biomedical Microdevices*, vol. 14, 2012.

[92] E. Steager, C. Kim, J. Patel, S. Bith, C. Naik, L. Reber, and M. J. Kim, "Control of Microfabricated Structures Powered by Flagellated Bacteria Using Phototaxis," *Applied Physics Letters*, pp. 263901–263903, 2007.

[93] R. Fernandes, M. Zuniga, F. R. Sassine, M. Karakoy, and D. H. Gracias, "Enabling cargo-carrying bacteria via surface attachment and triggered release.," *Small (Weinheim an der Bergstrasse, Germany)*, vol. 7, no. 5, pp. 588–92, Mar. 2011.

[94] D. Akin, J. Sturgis, K. Ragheb, D. Sherman, K. Burkholder, J. P. Robinson, A. K. Bhunia, S. Mohammed, and R. Bashir, "Bacteria-mediated delivery of nanoparticles and cargo into cells.," *Nature nanotechnology*, vol. 2, no. 7, pp. 441–9, Jul. 2007.

[95] H. Berg, *Random Walk in Biology*. Princeton University Press, 1983.

[96] F. R. Blattner, "The Complete Genome Sequence of Escherichia coli K-12," *Science*, vol. 277, no. 5331, pp. 1453–1462, Sep. 1997.

[97] J. Gregory, *Particles in Water: Properties and Processes*. CRC Press, 2005.

[98] N. C. Darnton, L. Turner, S. Rojevsky, and H. C. Berg, "On torque and tumbling in swimming Escherichia coli.," *Journal of bacteriology*, vol. 189, no. 5, pp. 1756–64, Mar. 2007.

[99] R. Kersaudy-Kerhoas M. Dhariwal and M. P. Y. Desmulliez, "Recent advances in microparticle continuous separation," *The Institutution of Engineering and Technology Nanobiotechnology*, vol. 2, pp. 1–13, 2008.

[100] J. Xi, J. Schmidt, and C. Montemagno, "Self assembled microdevices driven by muscle," *Nature Material*, vol. 4, pp. 180–184, 2005.

[101] S. Martel and M. Mohammadi, "Using a Swarm of Self-propelled Natural Microrobots in the Form of Flagellated Bacteria to Perform Complex Micro-assembly Tasks," in *The 2010 IEEE International Conference on Robotics and Automation*, 2010.

[102] M. A. Traore and B. Behkam, “Autonomous Sorting of Micro-Particles Using Bacterial Chemotaxis,” in *ASME 2012 Summer Bioengineering Conference*, 2012, pp. 949–950.

[103] M. A. Traore and B. Behkam, “A stochastic model for chemotactic motion of micro-beads propelled by attached bacteria,” in *Biomedical Robotics and Biomechatronics (BioRob)*, 2010, pp. 704–709.

[104] T. T. Goodman, J. Chen, K. Matveev, and S. H. Pun, “Spatio-temporal modeling of nanoparticle delivery to multicellular tumor spheroids.,” *Biotechnology and bioengineering*, vol. 101, no. 2, pp. 388–99, Oct. 2008.

[105] J.-W. Yoo, D. J. Irvine, D. E. Discher, and S. Mitragotri, “Bio-inspired, bioengineered and biomimetic drug delivery carriers.,” *Nature reviews. Drug discovery*, vol. 10, no. 7, pp. 521–35, Jul. 2011.

[106] P. Chorobik, D. Czaplicki, K. Ossysek, and J. Bereta, “Salmonella and cancer: from pathogens to therapeutics.,” *Acta biochimica Polonica*, vol. 60, no. 3, pp. 285–97, Jan. 2013.

[107] K. Crull, D. Bumann, and S. Weiss, “Influence of infection route and virulence factors on colonization of solid tumors by Salmonella enterica serovar Typhimurium.,” *FEMS immunology and medical microbiology*, vol. 62, no. 1, pp. 75–83, Jun. 2011.

[108] E. C. Boyle, J. L. Bishop, G. A. Grassl, and B. B. Finlay, “Salmonella: from pathogenesis to therapeutics.,” *Journal of bacteriology*, vol. 189, no. 5, pp. 1489–95, Mar. 2007.

[109] J. M. Pawelek, K. B. Low, and D. Bermudes, “Tumor-targeted Salmonella as a Novel Anticancer Vector Tumor-targeted Salmonella as a Novel Anticancer Vector1,” *Cancer Research*, vol. 57, pp. 4537–4544, 1997.

[110] K. B. Low, M. Ittensohn, X. Luo, L. Zheng, I. King, J. M. Pawelek, and D. Bermudes, “Construction of VNP20009,” in *Suicide Gene Therapy Methods in Molecular Medicine™ Volume 90*, vol. 90, 2004, pp. 47–59.

[111] C. Clairmont, K. C. Lee, J. Pike, M. Ittensohn, K. B. Low, J. Pawelek, D. Bermudes, S. M. Brecher, D. Margitich, J. Turnier, Z. Li, X. Luo, I. King, and L. M. Zheng, “Biodistribution and genetic stability of the novel antitumor agent VNP20009, a genetically modified strain of Salmonella typhimurium.,” *The Journal of infectious diseases*, vol. 181, no. 6, pp. 1996–2002, Jun. 2000.

[112] G. Hamilton, “Multicellular spheroids as an in vitro tumor model.,” *Cancer letters*, vol. 131, no. 1, pp. 29–34, Sep. 1998.

[113] M. Vinci, S. Gowan, and F. Boxall, “Advances in establishment and analysis of three-dimensional tumor spheroid-based functionalassays for target validation and drug evaluation,” *BMC*, pp. 1–21, 2012.

[114] H. Hardelauf, J.-P. Frimat, J. D. Stewart, W. Schormann, Y.-Y. Chiang, P. Lampen, J. Franzke, J. G. Hengstler, C. Cadenas, L. a Kunz-Schughart, and J. West, “Microarrays for the scalable production of metabolically relevant tumour spheroids: a tool for modulating chemosensitivity traits.,” *Lab on a chip*, vol. 11, no. 3, pp. 419–28, Feb. 2011.

[115] Y. T. Phung, D. Barbone, V. C. Broaddus, and M. Ho, “Rapid generation of in vitro multicellular spheroids for the study of monoclonal antibody therapy.,” *Journal of Cancer*, vol. 2, pp. 507–14, Jan. 2011.

[116] R.-Z. Lin, R.-Z. Lin, and H.-Y. Chang, “Recent advances in three-dimensional multicellular spheroid culture for biomedical research.,” *Biotechnology journal*, vol. 3, no. 9–10, pp. 1172–84, Oct. 2008.

[117] F. Hirschhaeuser, H. Menne, C. Dittfeld, J. West, W. Mueller-Klieser, and L. a Kunz-Schughart, “Multicellular tumor spheroids: an underestimated tool is catching up again.,” *Journal of biotechnology*, vol. 148, no. 1, pp. 3–15, Jul. 2010.

[118] J. Stritzker, S. Weibel, C. Seubert, A. Götz, A. Tresch, N. van Rooijen, T. a Oelschlaeger, P. J. Hill, I. Gentschev, and A. a Szalay, “Enterobacterial tumor colonization in mice depends on bacterial metabolism and macrophages but is independent of chemotaxis and motility.,” *International journal of medical microbiology : IJMM*, vol. 300, no. 7, pp. 449–56, Nov. 2010.

[119] J. Männik, R. Driessen, P. Galajda, J. E. Keymer, and C. Dekker, “Bacterial growth and motility in sub-micron constrictions.,” *Proceedings of the National Academy of Sciences of the United States of America*, vol. 106, no. 35, pp. 14861–6, Sep. 2009.

[120] B. Alberts, D. Bray, K. Hopkin, A. Johnson, J. Lewis, M. Raff, K. Roberts, and P. Walter, *Essential Cell Biology*. 2009, pp. 1–860.

[121] M. Sznol, S. L. Lin, D. Bermudes, L. Zheng, I. King, and D. Kirn, "Use of preferentially replicating bacteria for the treatment of cancer for the treatment of cancer," *The journal of clinical investigation*, vol. 105, no. 8, pp. 1027–1030, 2000.

[122] T. Danino, J. Lo, A. Prindle, J. Hasty, and S. N. Bhatia, "In Vivo Gene Expression Dynamics of Tumor-Targeted Bacteria.," *ACS synthetic biology*, vol. 1, no. 10, pp. 465–470, Oct. 2012.

[123] *American Academy of Pediatrics. Red Book: 2012 Report of the Committee on infectious Diseases.* 2012.

[124] M. A. Traore and B. Behkam, "A PEG-DA microfluidic device for chemotaxis studies," *Journal of Micromechanics and Microengineering*, vol. 23, no. 8, p. 085014, Aug. 2013.